MECHANICALLY STABLE SOLID FREEFORM FABRICATED SCAFFOLDS WITH PERMEABILITY OPTIMIZED FOR CARTILAGE TISSUE ENGINEERING

by

Jessica Marie Kemppainen

A dissertation submitted in partial fulfillment
of the requirements for the degree of
Doctor of Philosophy
(Biomedical Engineering)
in The University of Michigan
2008

Doctoral Committee:

Professor Scott J. Hollister, Chair
Professor Paul H. Krebsbach
Associate Professor Blake J. Roessler
Assistant Professor Terri A. Zachos, Michigan State University

To my parents, who inspire me to set high goals, and to my husband who shares in the joys and sacrifices that come with reaching them.

ACKNOWLEDGEMENTS

Here I am, five years later, reflecting on all of the memories from my time in graduate school, both inside and outside of the lab. I made it through the good times and the bad: passing out in that rodent injection course during my first week, a move from G.G. Brown to the new Lurie BME building (complete with windows), a broken foot, trips down to Sequin, Texas (especially that dinner at Pappadeaux), many exciting excursions to the slaughterhouse, the "freezer incident", three major power outages during my last 3 weeks of dissertation writing, countless hours spent feeding cells, seeding scaffolds, changing media, fixing the MM2, scanning and reconstructing, watching the MTS compress scaffolds, and for the rest of my life, I don't think I will use the word "permeability" as much as I have over the past five years. Outside of the lab, I got married, moved from Ann Arbor to Plymouth to Akron, trained for a triathlon with Team in Training, watched my nephews and niece grow up, saw my brother get through law-school and my dad retire, volunteering in the Dominican Republic with Orphanage Outreach, and spent not-enough-vacations relaxing on Silver Lake and Gull Lake. And now, I have the opportunity to thank everyone who has been with me along this journey, helping to turn these events into memories.

First, I would like to thank my advisor, Dr. Scott Hollister, for offering me the opportunity to pursue my PhD in his lab when I came to him 5 years ago with no funding

and no idea what I was getting myself into. I sincerely appreciate your time (especially those occasions when you probably intended to stop into the lab for a quick minute and were bombarded with my updates and questions) and your guidance (in research, writing, and career opportunities). Thank you to my doctoral committee members, Paul Krebsbach, Blake Roessler, and Terri Zachos for you insightful questions and feedback on this work.

Thank you to all of the members of the Skeletal Tissue Engineering Group that I enjoyed sharing ideas, time, workspace, equipment, and hard-drive space with: Colleen Flanagan, Rachel Schek, Juan Taboas, Chia-Ying Lin, Eiji Saito, Alisha Diggs, Elly Liao, Darice Wong, Miller Smith, Erin Moffitt, Sara Mantila, Shelley Brown, Huina Zhang, Claire Jeong, Heesuk Kang, Annie Mitsak, Chan-Ho Park, Brandon Busuito and Alex Garnepudi. A special thanks to Rachel, for being a mentor to me during my first year, teaching me cell culture techniques, forcing me to overcome my fear of needles, and for being an inspiration to me even after you graduated. I am thankful for your guidance in the lab, and for your and Trey's friendship today. Sara and Erin, whether we were doing research, eating Qdoba, or planning weddings, it was always fun. Brandon, you were a huge asset to my research during my final year, assisting with the PCL project, helping with chondrocyte harvests, and coming in to change media during the weekends I spent in Akron. I can't thank you enough.

I am so grateful for the friendliness and generosity of people outside of our lab that helped me along the way. Thank you to everyone in the Krebsbach Lab for letting me

invade your space before we had cell culture up in LBME, especially to Wilbur Tong, for always helping me locate supplies, instruments, or chemicals. Thank you to everyone in the Spine Lab and to the Molecular Biology Core Lab (School of Dentistry, UofM) for your help with qtPCR: Chia-Ying Lin, Huina Zhang, and Tao Jincong, to Chris Strayhorn and Cynthia Zuccaro for your time and patience sectioning and staining my "not-exactly-histology" samples, to Steve Emanuel for teaching me how to machine all of those Teflon molds, to Dr. Mohamed El-Sayed for your listening ear and guidance, and to the guys at Northwest Market for always making my trips out there more fun. Thank you to the supportive BME staff, especially Maria Steele, for taking care of all of the behind-the-scenes paperwork, and for asking me if I'm there to tell her I'm pregnant every time I step into her office. Thank you to Myra Kim at CSCAR for being so brilliant and friendly. I learned so much while you helped me with the statistics for my dissertation.

Coming to grad school in Ann Arbor put me back near some old friends and introduced me to a lot of great new people. Alex, Laura, and Lindsay thanks for all of the distracting, but much needed phone conversations during my drives to and from Akron and while I was sitting here writing. Erin, I always enjoyed our chats over lunch or in the halls of LBME, and your hard work and dedication in lab while raising a family has been an inspiration to me. Annie and Nick, thank you for being such great friends, and for putting a roof over my head for my last 6 months, that somehow turned into 1 year, of grad school.

Lastly, I express my sincere gratitude to my family for their love, support and encouragement over the past five years: Mom and Dad, Amanda and Eric, Neil, Grandma Williams, and Grandma and Grandpa Hindmarsh. Also, to Joshua, Nathan and Sarah, you add so much excitement to our lives; I can't imagine what we'd do without you. Thank you to Roy, Ann and Sara Kemppainen, for welcoming me into your family and encouraging John and me in our seemingly-endless studies. Finally, to my husband, John, thank you for listening as I spent countless dinners talking about my day in the lab, and for encouraging me to work hard, but to keep things in perspective. Your perfect combination of support and impatience as we lived apart during this past year was exactly what I needed to keep going and to get done. As this chapter in our lives closes, I look forward to the new adventures we have ahead.

TABLE OF CONTENTS

LIST OF FIGURES

Figure

LIST OF TABLES

Tables

LIST OF APPENDICES

APPENDIX

ABSTRACT

Clinical treatment options for articular cartilage repair are progressing with the incorporation of synthetic matrices alongside current autologous chondrocyte implantation techniques. This work explores mechanical and mass transport design of potential matrices. Solid freeform fabrication (SFF) is used to create highly reproducible scaffolds with precise structural features in order to explore the mechanical potential of 3D designed poly(ε-caprolactone) (PCL) and poly(glycerol sebacate) (PGS) scaffolds, and to examine the effects of a designed physical property, permeability, for cartilage regeneration.

Our first aim explores the potential of PCL and PGS scaffolds to provide temporary mechanical function within a tissue defect. We find that PCL mimics the viscoelastic nature of cartilage; however its stiffness properties cannot be changed through alterations in molecular weight or melting temperature. Fabricated into the architectures explored, it has aggregate modulus (H_A) values within the correct magnitude, but higher than native cartilage. Furthermore, we demonstrate the importance of mechanically testing PCL scaffolds at physiological temperatures and we quantify their contraction in polar environments.

Poly(glycerol sebacate) has never been used for cartilage tissue engineering. We characterize how variations in the molar ratios of glycerol to sebacic acid (during pre-polymer synthesis) or variations in curing time can be used to change the stiffness of PGS, enabling fabrication of scaffolds with a wide range of architectures (designed for optimal tissue regeneration) that all support in vivo loads. Chondrocytes seeded onto PGS produce cartilaginous matrix and express cartilage specific genes similar to or better than cells cultured on PCL, showing the biocompatibility of PGS for cartilage applications for the first time.

Our second aim looks at enhancing cartilage regeneration by optimizing scaffold permeability. We show that chondrocytes prefer a lower permeable scaffold that mimics the natural environment of native tissue, producing significantly more matrix and increased expression of cartilage specific markers. Bone marrow stromal cells (BMSCs) display the opposite trend, favoring a higher permeable environment for chondrogenic differentiation, as displayed through collagen 2 to collagen 1 expression, suggesting that increased access to chondrogenic induction factors in media is more important to these cells than mimicking the low permeable environment of native tissue.

CHAPTER 1

INTRODUCTION

1.1 Problem Statement

As early as 1743 Hunter [1] observed that cartilage, "once destroyed, is not repaired." Over 250 years later, there are few methods used to repair cartilage that can restore a durable articular surface to lesions caused by trauma or evolved during the course of diseases such as osteoarthritis. Even the methods used clinically are not completely successful at restoring the native environment of cartilage over an extended period of time. In the U.S. alone, musculoskeletal conditions are estimated to cost over $300 billion annually. Musculoskeletal impairments are the number one category of reported chronic impairment and rank number one in visits to physicians' offices (102.5 million visits per year), with 36.9 million Americans (one in three) incurring a musculoskeletal injury every year. Worldwide, musculoskeletal conditions are the most common cause of physical disability and severe long-term pain.[2] It is for reasons like this that George W. Bush declared 2002-2011 as the Bone and Joint Decade.

1.2 Articular Cartilage Disease and Damage

Most all forms of disease and damage to articular cartilage result in osteoarthritis, a type II collagen disorder. Aging is the primary cause of damage to articular cartilage, where everyday use leads to flaking and formation of crevasse in its surface, commonly termed

"primary osteoarthritis". Secondary causes of osteoarthritis include obesity, trauma, congenital defects that result in abnormal joints at birth, gout, diabetes, or hormone disorders. Traumatic injury to articular cartilage can result from abnormal rotation of a joint (such as twisting injuries that usually result in anterior cruciate ligament rupture) or from forceful impact.[3] Evidence shows that each of us may have a genetic predisposition that regulates our bodies' response to these factors, determining the extent of osteoarthritis that incurs.[4]

1.3 Clinical Treatment Options

The primary reason for this tissue's dramatic inability to regenerate and repair itself stems from its isolation from the rest of the body. Cartilage lacks blood vessels, lymphatic vessels and nerves. Nutrition of cartilage relies on diffusion of nutrients from the synovial fluid that encapsulates articular joints.[5] There are a number of clinical treatment options for the repair of articular cartilage, and technology in this field is rapidly advancing. Over the past decade (1998-2008), the three most commonly performed procedures were microfracture, mosaicplasty, and autologous chondrocyte implantation (ACI). During microfracture, damaged or unstable cartilage is debrided, or cleaned away, and small holes are poked into the subchondral bone, allowing marrow elements to diffuse into the repair site. These marrow elements contain cells which can differentiate into chondrocytes, and produce a matrix that matures over time to fill the defect. Unfortunately, most of the repair tissue is fibrocartilage, which possesses a different collagen composition and, therefore, different biomechanical properties than native tissue. The microfracture technique is most effective for small articular defects (<

4cm^2), but normal cartilage composition and structure are never actually restored and tissue inevitably undergoes progressive degeneration.[6]

Mosaicplasty, or osteochondral autografting, is a treatment option that replaces damaged or missing cartilage with an osteochondral (bone + cartilage) plug taken from a non-load bearing site. Although this technique repairs the defect with already mature and healthy cartilage, it requires sacrificing healthy cartilage in one location in order to restore the damaged area. It can also be difficult for surgeons to accurately fill defects in terms of size and natural contour using mosaicplasty.[6]

Finally, there is a promising "tissue engineering" technology making its mark in the area of articular cartilage repair termed autologous chondrocyte implantation (ACI). The repair system, named Carticel®, is available through Genzyme Corporation. It is a two stage process in which a small biopsy of a patient's healthy cartilage is removed and digested. Chondrocytes extracted from the tissue during digestion are grown in culture for implantation back into the patient in the second stage. Currently, the cultured cells are simply injected under a periosteal patch that covers the defect site. These autologous cells are able to produce cartilaginous matrix, eventually replacing the articular defect with new cartilage. A clinical trial by Peterson *et al.*[7] examined the outcomes of ACI in isolated femoral condyle lesions, multiple femoral condyle lesions, including lesions of the trochlea and lesions in combination with patellar lesions (kissing lesions), osteochondritis dissecans lesions, patellar lesions, and femoral condyle lesions with anterior cruciate ligament reconstruction. All chondral defects were classified as

moderate to large (1.3-12.0 cm^2) full thickness lesions. Two to nine-year outcome measures show excellent repair in isolated femoral condyle lesions, but decreased success for those with multiple lesions or patellar lesions.

Improvements to ACI, termed "second generation" techniques, incorporate matrices to help retain cells and eliminate the need for a periosteal flap.[6-8] There are currently three "second generation" technologies being used clinically in relatively large numbers of patients: Matrix-induced autologous chondrocyte implantation (MACI®), Hyalograft C®, and Bioseed®. The scaffold materials used in these technologies are a bilaminate collagen, a hyaluronic acid-based scaffold, and a composite PLA-PGA polymer fleece, respectively. Although these treatment options show promising results, none of them have been released in the United States. NeoCart®, a bovine collagen gel/sponge 2nd generation ACI treatment, is however, entering a phase two trial in the United States that will compare its safety and efficacy versus microfracture.[9]

1.4 Tissue Engineering Improvements

Although ACI and 2nd generation ACI treatments are proving to be a promising technique and are paving the way for clinical use of *tissue engineering* treatment of articular cartilage defects, there are a number of tissue engineering principles that can still be incorporated into this repair system. Tissue engineering strategies aim to combine three components: cells, biomaterials, and growth factors, in order to repair damaged tissue. In terms of the cells used, advances can be made to utilize cells that are easier to obtain and do not require the sacrifice of healthy cartilage. Cell types currently being explored for

these purposes include bone marrow stromal cells[10-13] and pre-adipocytes.[14-18] Growth factors are also being explored for supporting chondrogenesis. These include transforming growth factor beta (TGF-β), bone morphogenetic protein (BMP), basic fibroblastic growth factor (bFGF), and insulin-like growth factor-1 (IGF-1). Their effects are being studied for multiple cell types and various conditions. [11, 19] Further advances can also be made to optimize the final component of the tissue engineering triad, the matrix (scaffold) being implanted along with the cells and growth factors. Not only should the scaffold help to retain cells and deliver growth factors, but it should provide biomimetic mechanical properties, and optimal mass transport properties to enhance cartilage tissue regeneration.

1.5 Goals of This Thesis

This thesis will focus on two primary goals for design of more advanced cartilage tissue engineering scaffolds for such repair modalities (illustrated in Figure 1.1):

1. To provide temporary mechanical function within a tissue defect through incorporating a biodegradable scaffold that initially mimics target stiffness properties of native cartilage

2. To enhance tissue regeneration through providing optimal mass transport properties within the scaffold

Goal #1: Providing Mechanical Support

Hypothesis: The mechanical properties of tissue engineering scaffolds can be controlled through biomaterial processing parameters in order to create 3D-designed scaffolds that provide adequate support to developing tissue.

Cartilage helps to distribute loads between opposing bones in a synovial joint. Due to its low friction and wear, and its compliance, it permits smooth motion and reduces contact stresses at joint surfaces. In order to do this properly, cartilage is made up of chondrocytes embedded within an extracellular matrix that is composed of collagen (~60% of the dry weight), proteoglycans (~25% dry weight), and other proteins and glycoproteins (~15% dry weight). Together, these substances maintain the proper amount of water within the matrix, and result in the unique mechanical properties of the tissue.[5]

In order to achieve the first goal, we must define the quantitative measures we wish to attain. Amongst the generally accepted requirements that an ideal tissue engineering scaffold will be biocompatible, noncytotoxic, biodegradable, able to support and hold cells, permeable, reproducible, readily available, and versatile for full and partial thickness lesions, lies the requirement that it must also be mechanically stable.[9] Here, we focus on the requirement that a scaffold should have stiffness values similar to native articular cartilage. By matching these target stiffness values, the scaffold will withstand physiological loading, produce the mechanical tension generated within the cell cytoskeleton critical for cell shape and function, and mimic stiffness values that may

affect cell to cell contacts and aggregation.[20] Furthermore, when the scaffold (with or without tissue) is implanted into a defect site, there should be no stiffness differences between healthy cartilage and regenerating tissue, which may cause fibrous tissue formation, elevated levels of strain in the adjacent cartilage, and accelerated degeneration of the tissue.[21] Functions of viscoelasticity and nonlinear elasticity, both measures of material stiffness, will be examined.

Numerous materials have been used in order to create scaffolds for tissue engineering, reviewed in depth in Chapter 3. The two materials we explore in this thesis are poly(ε-caprolactone) (PCL) and poly(glycerol-sebacate) (PGS). We explore the elastic properties of these materials using confined and unconfined compression testing, and determine if altering their processing parameters can provide initial stiffness properties of optimally designed scaffolds (goal #2) within the ranges of native articular cartilage.

Goal #2: Providing Optimal Mass Transport

Hypothesis: Mass transport properties of scaffolds affect matrix production by chondrocytes and cellular differentiation of bone marrow stromal cells.

The mass transport property that we study here is hydraulic permeability, the ease with which fluid flows through a tissue, or in this case a scaffold, when driven by a pressure gradient. Many groups have measured the permeability of bovine cartilage [22-28] in order to characterize the tissue or quantify changes due to diseases or injuries. In comparison to other musculoskeletal tissues, the permeability of cartilage is very low. And, an

increase in the permeability of osteoarthritic cartilage results in greater and more rapid deformation of tissue.[29, 30] When designing 3D scaffolds, some groups state their hypothesis that providing maximum porosity (and hence, increased permeability) will promote tissue ingrowth.[31] Though this may be true for bone tissue engineering, it must be understood that for cartilage tissue engineering, this increase in permeability contradicts the clinical finding that native healthy cartilage exhibits relatively *low* permeability.

As reviewed in Chapter 4, there are a number of studies that examine the effects of scaffold architectures on cartilage tissue regeneration, with no consensus on how the structural properties of pore size, porosity, and interconnectivity affect chondrogenesis. Li *et al.*, however, prove that none of these properties can be used individually to describe mass transport. Instead, they suggest that "one conventional physical parameter", **permeability**, be used as a description of the complicated porous structures encountered in the process of tissue engineering.[32] In this work, we will examine how the physical property of permeability, as described by Darcy's law, affects chondrocytes or bone marrow stromal cells seeded onto PCL scaffolds, cultured *in vitro*, with the hypothesis that this parameter can be used to more accurately predict the effects of scaffold architecture on chondrogenesis.

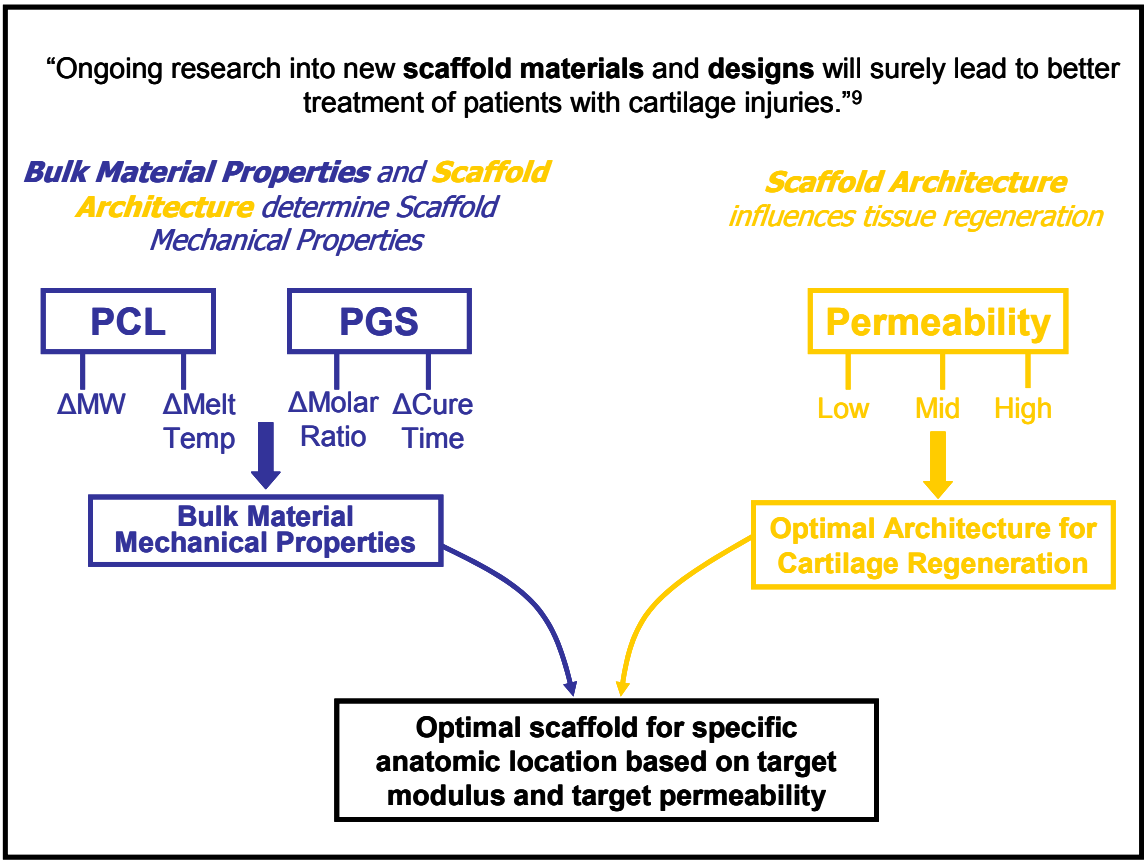

Figure 1.1 Flow diagram of dissertation goals.

"Second generation" autologous chondrocyte implantation will incorporate a scaffold, or matrix material, that will improve cell retention and provide mechanical stability, while also enhancing cartilage regeneration through physical and biochemical environmental ques. There is a wide array of scaffold components to be optimized for this repair system including the ones examined here. Research in this field will also consider surface modifications, growth factor delivery, and the ways in which degradation profiles affect tissue regeneration. Here we show that PCL and PGS scaffolds are two promising materials that can provide initial scaffold stiffness values within the ranges of articular cartilage. We then show that the permeability of a scaffold significantly affects the

differentiation of bone marrow stromal cells and cartilage matrix deposition by chondrocytes, and is an important consideration when designing scaffolds for cartilage tissue engineering.

1.6 Contents of Dissertation

Chapter two introduces the tissue we aim to repair, articular cartilage, and the structural and biomolecular components assessed in regenerated tissue. Keeping in mind our first goal, Chapter 3 introduces how biomaterials can be used to provide mechanical stability to damaged cartilage, including a review on the mechanical properties of native cartilage, materials that have been previously used for this purpose, and an introduction to Poly(ε-caprolactone) (used in Chapter 5) and Poly(glycerol-sebacate) (used in Chapter 6). The second goal of this dissertation is to enhance regeneration of cartilage through optimizing the mass transport property of *permeability*. Chapter 4 explains the rationale for studying this physical property with regards to cartilage tissue engineering. Chapter 5 characterizes the mechanical properties of melt-cast PCL for cartilage applications. Chapter 6 introduces the use of PGS in cartilage tissue engineering, characterizing mechanical properties that are adjustable through processing parameters, and showing that it is biocompatible with chondrocytes. Finally, Chapter 7 reveals that the permeability of scaffolds significantly affects GAG production by chondrocytes and differentiation of bone marrow stromal cells in 3D designed scaffolds, and should be deemed an important design consideration for cartilage tissue engineering.

References

1. Hunter W. On the structure and diseases of articulating cartilages. Philos Trans R Soc 1743;42B:514-20.

2. Anonymous. www.usbjd.org. United States Bone and Joint Decade. Accessed May 15th, 2008.

3. Shiel, William C., Jr MD. 2008;2008:.

4. Einhorn TA, O'Keefe RJ, Buckwalter JA, Eds. Orthopaedic Basic Science Foundations of Clinical Practice. Rosemont, IL: American Academy of Orthopaedic Surgeons, 2007: 465.

5. Newman AP. Articular cartilage repair. Am.J.Sports Med. 1998;26:309-24.

6. Fischgrund JS. Chapter 3: Articular Cartilage and Intervertebral Disk. In: Orthopaedic Knowledge Update. Kim HT, Yoon ST, Jarrett C, Ed. American Academy of Orthopedic Surgeons, 2008, pp: 23.

7. Peterson L, Minas T, Brittberg M, Nilsson A, Sjogren-Jansson E, Lindahl A. Two- to 9-year outcome after autologous chondrocyte transplantation of the knee. Clin.Orthop.Relat.Res. 2000;(374):212-34.

8. Anonymous. www.carticel.com. Regenerate Your Lifestyle. CARTICEL. Accessed May 23rd, 2008.

9. Safran MR, Kim H, Zaffagnini S. The use of scaffolds in the management of articular cartilage injury. J.Am.Acad.Orthop.Surg. 2008;16:306-11.

10. Caplan AI and Bruder SP. Mesenchymal stem cells: building blocks for molecular medicine in the 21st century. Trends Mol.Med. 2001;7:259-64.

11. Heng BC, Cao T, Lee EH. Directing stem cell differentiation into the chondrogenic lineage in vitro. Stem Cells 2004;22:1152-67.

12. Martin I, Padera RF, Vunjak-Novakovic G, Freed LE. In vitro differentiation of chick embryo bone marrow stromal cells into cartilaginous and bone-like tissues. J.Orthop.Res. 1998;16:181-9.

13. Yoo JU, Barthel TS, Nishimura K, Solchaga L, Caplan AI, Goldberg VM*, et al*. The chondrogenic potential of human bone-marrow-derived mesenchymal progenitor cells. J.Bone Joint Surg.Am. 1998;80:1745-57.

14. Erickson GR, Gimble JM, Franklin DM, Rice HE, Awad H, Guilak F. Chondrogenic potential of adipose tissue-derived stromal cells in vitro and in vivo. Biochem.Biophys.Res.Commun. 2002;290:763-9.

15. Im GI, Shin YW, Lee KB. Do adipose tissue-derived mesenchymal stem cells have the same osteogenic and chondrogenic potential as bone marrow-derived cells? Osteoarthritis Cartilage 2005;13:845-53.

16. Nathan S, Das De S, Thambyah A, Fen C, Goh J, Lee EH. Cell-based therapy in the repair of osteochondral defects: a novel use for adipose tissue. Tissue Eng. 2003;9:733-44.

17. Zuk PA, Zhu M, Ashjian P, De Ugarte DA, Huang JI, Mizuno H*, et al*. Human adipose tissue is a source of multipotent stem cells. Mol.Biol.Cell 2002;13:4279-95.

18. Zuk PA, Zhu M, Mizuno H, Huang J, Futrell JW, Katz AJ*, et al*. Multilineage cells from human adipose tissue: implications for cell-based therapies. Tissue Eng. 2001;7:211-28.

19. O'Connor WJ, Botti T, Khan SN, Lane JM. The use of growth factors in cartilage repair. Orthop.Clin.North Am. 2000;31:399-410.

20. Lu L, Zhu X, Valenzuela RG, Currier BL, Yaszemski MJ. Biodegradable polymer scaffolds for cartilage tissue engineering. Clin.Orthop.Relat.Res. 2001;(391 Suppl):S251-70.

21. Beaupre GS, Stevens SS, Carter DR. Mechanobiology in the development, maintenance, and degeneration of articular cartilage. J.Rehabil.Res.Dev. 2000;37:145-51.

22. Soltz MA and Ateshian GA. Interstitial fluid pressurization during confined compression cyclical loading of articular cartilage. Ann.Biomed.Eng. 2000;28:150-9.

23. Soltz MA and Ateshian GA. Experimental verification and theoretical prediction of cartilage interstitial fluid pressurization at an impermeable contact interface in confined compression. J.Biomech. 1998;31:927-34.

24. Williamson AK, Chen AC, Sah RL. Compressive properties and function-composition relationships of developing bovine articular cartilage. J.Orthop.Res. 2001;19:1113-21.

25. Ateshian GA, Warden WH, Kim JJ, Grelsamer RP, Mow VC. Finite deformation biphasic material properties of bovine articular cartilage from confined compression experiments. J.Biomech. 1997;30:1157-64.

26. Bursac PM, Obitz TW, Eisenberg SR, Stamenovic D. Confined and unconfined stress relaxation of cartilage: appropriateness of a transversely isotropic analysis. J.Biomech. 1999;32:1125-30.

27. Demarteau O, Pillet L, Inaebnit A, Borens O, Quinn TM. Biomechanical characterization and in vitro mechanical injury of elderly human femoral head cartilage: comparison to adult bovine humeral head cartilage. Osteoarthritis Cartilage 2006; 14(6):372-379.

28. Klein TJ, Chaudhry M, Bae WC, Sah RL. Depth-dependent biomechanical and biochemical properties of fetal, newborn, and tissue-engineered articular cartilage. J.Biomech. 2005; 40(1):182-190.

29. Mansour JM. Biomechanics of Cartilage. In: Kinesiology: The Mechanics and Pathomechanics of Human Movement. C. A. Oatis, Ed. Philadelphia: Lippincott Williams and Wilkins, 2003, pp: 66-79.

30. Klippel JH, Weyand CM, Crofford LJ, Stone JH, Arthritis Foundation. Primer on the rheumatic diseases. Atlanta, Ga.: Arthritis Foundation 2001.

31. Gauvin C, Azizeh Y, Reignier J, Huneault M, DiRaddo R, Fernandes J. A biomechanical approach to design and fabrication of 3D scaffolds in functional tissue engineering. (unpublished). Submitted 2005.

32. Li SH, de Wijn JR, Layrolle P, de Groot K. Accurate geometric characterization of macroporous scaffold of tissue engineering. 2003;240-2:541-5.

CHAPTER 2

ARTICULAR CARTILAGE

Articular cartilage, hyaline cartilage that covers the ends of long bones of synovial joints, is a unique and complex tissue. The intricate macromolecular structure of this tissue results in its remarkable ability to absorb everyday forces put on joints and to rebound once those forces are removed. The entire matrix that provides this function is synthesized and maintained by a sole cellular component, the chondrocyte. The matrix has an assistive counterpart, the synovial fluid it is bathed in, which provides frictionless gliding between articulating surfaces during locomotion. Together, these components make up the white, translucent, shiny tissue that coats our joint surfaces and provides our skeleton with extraordinarily durable load-bearing capacity.[1]

Although it may seem simple, one cell type that synthesizes and maintains a matrix, plus synovial fluid that nourishes it and allows it to glide against itself, cartilage is extremely difficult to repair both through the natural repair mechanisms of our body, and with the aid of modern medicine. The absence of natural repair mechanisms, as seen in other tissues, results from the tissues avascularity and hypocellularity. Cartilage receives nourishment by diffusion of nutrients from the synovial fluid, in comparison to more metabolically active tissues that are infiltrated with blood vessels supplying continual nutrients to entire organs. Furthermore, the cells responsible for synthesis and

maintenance of the tissue are rather quiescent and only comprise 1-2% of the tissue volume. Even in healthy cartilage, the turnover of extracellular matrix (ECM) components is slow, so when faced with the challenge to restore damaged tissue there is no fast mechanism to rely on. From a tissue engineering point of view, the difficulty in restoring this damaged tissue is further implicated with the heterogeneity of the tissue, which consists of superficial, middle, deep and calcified layers designated by changes in chondrocyte shape (flattened to rounded) and variations in collagen fiber thickness and orientation (thin, tangential to thick, radial bundles) throughout.

All of these intricacies lead to a wide array of qualitative and quantitative approaches to evaluating tissue engineered cartilage, including histological, biochemical, mechanical and molecular genetic measures. After introducing the embryonic development of cartilage, we review the biochemical and molecular genetic measures we will use during this work, saving intricacies of mechanical measurements for full review in Chapter 3. When regenerating articular cartilage *in vitro*, we will assess outcomes by quantifying matrix production by cells and by measuring the cellular expression of genes that relate to chondrogenic differentiation. Specifically, in this work, we measure the amount of sulfated-glycosaminoglycans (sGAGs) produced by cells seeded within a scaffold and we also quantify the cellular mRNA expression of aggrecan, collagen 1, and collagen 2. In this chapter the significance of each of these components in native tissue is explained.

2.1 Embryonic Development of Cartilage

Cartilage is formed from the *condensation* and *differentiation* of skeletal progenitor cells (cells that can form more than one skeletal cell type and tissue type in embryos and in adults). The first step in formation of cartilage-type cells is condensation of these skeletal progenitor cells. In cartilage tissue formation, the condensation consists of cells that are ALL chondrogenic and are ALL at the same stage of development, communicated via GAP junctions. At the point of cellular condensation, cartilage specific genes including heparin-sulfate and chondroitan sulfate proteoglycans are expressed, allowing differentiation between these cartilage-forming clusters and other skeletal tissue-forming groups (such as bone). Once this cellular condensation attains a critical size, genes controlling proliferation are down-regulated, and genes associated with differentiation are up-regulated. Cells differentiate based on a cocktail of growth factors and hormones that direct the cellular condensation down a chondrogenic pathway, in which the cells become chondrocytes and begin producing and maintaining cartilage. [2] One goal of this work is to differentiate bone marrow stromal cells (derived from bone marrow aspirates) down a chondrogenic lineage through culturing them in vitro in chondrogenic media on 3D-designed scaffolds. When obtained from the bone marrow stroma, these cells represent a heterogenous population of cells that can be differentiated into bone, cartilage, adipocytes and hematopoietic supporting tissues.[3] Here we focus on how differences in scaffold permeability may affect chondrogenic differentiation of bone marrow stromal cells.

2.2 Cartilage Extracellular Matrix: Glycosaminoglycans

The main matrix molecules of cartilage are proteoglycans, making up about 3-10% of the wet weight and ~25% of the dry weight of hyaline cartilage.[4] They consist of a core protein to which one or more glycosaminoglycans (GAGs) are attached (see Figure 2.1). These negatively charged aggregates attract water molecules into the tissue, giving cartilage its resistance to compression and resilience upon unloading of the tissue. The main types of GAGs found in articular cartilage are chondroitin sulfate, keratin sulfate and hyaluronic acid. The first two, being sulfated, are commonly measured through a biochemical assay in order to show the production and deposition of extracellular cartilaginous matrix. They are attached to a core protein, which is attached to a backbone of hyaluronic acid through a link protein. The type of GAG is determined by the repeating disaccharide unit labeled "A and B" in Figure 2.1. Although not depicted here, these chains are arranged on the core in pairs, called doublets, where in the case of chondroitan sulfate, the chains are separated by less than ten amino acid residues, and the doublets are separated by about thirty-five residues.[5] Proteoglycans are both synthesized and metabolized by chondrocytes, regulated such that adult cartilage maintains consistent levels of these macromolecules.

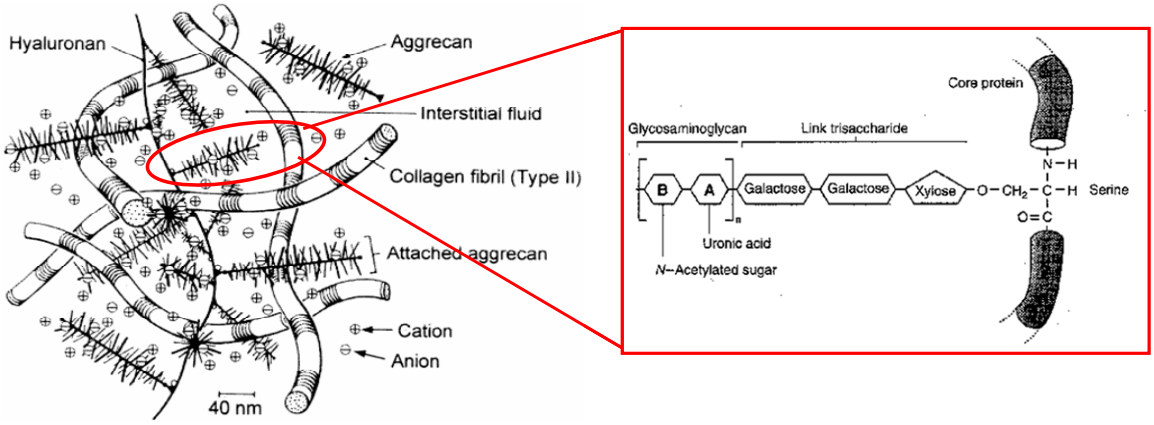

Figure 2.1 A detailed look at the glycosaminoglycans of articular cartilage[6] (portion of figure used with permission from Elsevier).

Developmentally speaking, changes in size, chemical composition and structure of proteoglycan monomers occur between fetal development and maturity of the cartilage. Proteoglycans from fetal and immature cartilage are larger, more uniform in size, and contain more chondroitin sulfate and less keratan sulfate than those of mature cartilage. Although the basis for these changes is unclear, it could help to explain the deterioration of articular cartilage during aging, and help to determine if some people are predisposed to development of osteoarthritis (OA) based on the maximum length of their proteoglycan chains during fetal development.[7]

2.3 Cartilage Gene Expression

Proteins expressed in cartilage can be measured at the transcriptional (messenger-RNA, mRNA) or translational (protein) levels. Here we measure the mRNA expression of genes that code for cartilage specific proteins (collagen 2 and aggrecan) and a gene that enables us to detect chondrogenic dedifferentiation or bone marrow stromal cell differentiation, relative to collagen 2 levels (collagen 1).

2.3.1 Aggrecan

Aggrecan is the main proteoglycan found in cartilage, and is a typical marker of differentiated chondrocytes. It is a structural proteoglycan, meaning that it helps the extracellular matrix (ECM) maintain its highly hydrated state.[2] Messenger-RNA expression of aggrecan can be detected in periosteal cells immediately before they differentiate into chondrocytes.[2] Aggrecan molecules generally exist as aggregates, made up of a central hyaluronic acid (HA) backbone with up to 100 aggrecan molecules attached by link proteins. Fully intact, these aggregates have a molecular mass of 210,000, however due to regular cleavage by aggrecanases and metalloproteinases (MTPs) they rarely exist at this length.[8] Upregulation of aggrecanases and MTPs are seen in osteoarthritis, resulting in increased cleavage of the core protein and cleavage of HA. This increase in cleavage causes a decrease in charge density of the tissue, and a decrease in aggregate size, resulting in deterioration of cartilage.[9, 10] Messenger-RNA expression of aggrecan levels (normalized to GAPDH) in native tissue vary widely, from reports on porcine cartilage explants of about 80 [8] to reports on healthy human articular cartilage ranging from .82 to 1.8.[11, 12]

2.3.2 Collagen 2

Type two collagen is the major fibrillar collagen of articular cartilage, accounting for 90-95% of the overall collagen content.[13] This gene is localized to cartilage, the vitreous of the eye, the nucleus pulposus of intervertebral discs and the embryonic chick primary corneal stroma. It provides cartilage with its tensile strength and immobilizes proteoglycans within its matrix. It can be used as a sensitive marker for chondrogenic

differentiation of precursor cells, and may coincide with an irreversible commitment to chondrogenesis. Defects in type II result in premature osteoarthritis.[2] Collagen II expression as measured by qtPCR on native tissue also shows high variation, with normalized values ranging from .2 to 94.[10, 12]

2.3.3 Collagen 1

Collagen 1, generally associated with bone, is found in small amounts in human articular cartilage and increasing amounts in fibrocartilages, presumably contributing to the functional requirements of the tissues. However, it has been reported to account for a surprisingly high 11.6% of the collagenous component of porcine cartilage.[14] Its level of expression is commonly used as a marker of chondrocyte dedifferentiation. As a ratio, the expression of collagen 2: collagen 1 is termed the "differentiation index" with a larger value correlating with a more chondrocytic genotype, and a lower value correlating with more fibroblastic gene expression.[11] Interestingly, Kosher *et al.* show that collagen 1 mRNAs are present during limb development, even when the protein is not produced in detectable amounts.[15] Osteoarthritic cartilage contains increased levels of collagen type 1, decreasing its ability to bind GAG.[2] Collagen 1 expression in native cartilage ranges from reports of none being expressed [12] to 17 (as a % of GAPDH).[10]

2.3.4 Effects of monolayer and 3D culture on gene expression

Chondrocytes are difficult to culture in monolayer, where they quickly dedifferentiate. This is shown genetically through decreases in aggrecan and collagen 2: collagen 1 expression during monolayer culture and passaging.[16-18] In 3D culture, chondrocytes

behave more favorably, where they show increased aggrecan and collagen 2: collagen 1 ratios versus cells cultured in monolayer, and increases over time.[16, 19] A report on the chondrogenic differentiation of BMSCs in pellet culture and 3D hydrogels (similar to the methods used in this work), demonstrate that aggrecan and collagen 2 expression can be maintained, or even increased under 3D conditions in chondrogenic media.[20, 21]

Although it seems useful to compare quantitative measures of these genes expressed in tissue engineered cartilage to levels found in native cartilage, upon review, these quantitative values vary quite widely. It is more accurate to compare expression levels within one study relative to time or in this case, scaffold designs. In order to relate expression levels of these genes in scaffolds to initial expression levels of the cells utilized, a sample of chondrocytes and bone marrow stromal cells were set aside just prior to cell seeding, and processed through the same methods for qtPCR as scaffolds were.

References

1. Klippel JH, Weyand CM, Crofford LJ, Stone JH, Arthritis Foundation. Primer on the rheumatic diseases. Atlanta, Ga.: Arthritis Foundation 2001.

2. Hall BK. Bones and cartilage : developmental and evolutionary skeletal biology. Australia ; San Diego, Calif.: Elsevier Academic Press 2005.

3. Krebsbach PH, Kuznetsov SA, Bianco P, Robey PG. Bone marrow stromal cells: characterization and clinical application. Crit.Rev.Oral Biol.Med. 1999;10:165-81.

4. Hall BK and Newman SA. Cartilage : molecular aspects. Boca Raton, FL: CRC Press 1991.

5. Serafini-Fracassini A and Smith JW. The structure and biochemistry of cartilage. Edinburgh: Churchill Livingstone 1974.

6. Mow VC, Ratcliffe A, Poole AR. Cartilage and diarthrodial joints as paradigms for hierarchical materials and structures. Biomaterials 1992;13:67-97.

7. Kuettner KE, Schleyerbach R, Hascall VC. Articular cartilage biochemistry. New York: Raven Press 1986.

8. Adolphe M. Biological regulation of the chondrocytes. Boca Raton, Fla.: CRC Press 1992.

9. Roughley P, Martens D, Rantakokko J, Alini M, Mwale F, Antoniou J. The involvement of aggrecan polymorphism in degeneration of human intervertebral disc and articular cartilage. Eur.Cell.Mater. 2006;11:1,7; discussion 7.

10. Fehrenbacher A, Steck E, Rickert M, Roth W, Richter W. Rapid regulation of collagen but not metalloproteinase 1, 3, 13, 14 and tissue inhibitor of metalloproteinase 1, 2, 3 expression in response to mechanical loading of cartilage explants in vitro. Arch.Biochem.Biophys. 2003;410:39-47.

11. Martin I, Jakob M, Schafer D, Dick W, Spagnoli G, Heberer M. Quantitative analysis of gene expression in human articular cartilage from normal and osteoarthritic joints. Osteoarthritis Cartilage 2001;9:112-8. doi: 10.1053/joca.2000.0366.

12. Aigner T and McKenna L. Molecular pathology and pathobiology of osteoarthritic cartilage. Cell Mol.Life Sci. 2002;59:5-18.

13. Goldberg VM and Caplan AI. Orthopedic tissue engineering : basic science and practice. New York: Marcel Dekker 2004.

14. Wardale RJ and Duance VC. Quantification and immunolocalisation of porcine articular and growth plate cartilage collagens. J.Cell.Sci. 1993;105 (Pt 4):975-84.

15. Kosher RA, Kulyk WM, Gay SW. Collagen gene expression during limb cartilage differentiation. J.Cell Biol. 1986;102:1151-6.

16. Girotto D, Urbani S, Brun P, Renier D, Barbucci R, Abatangelo G. Tissue-specific gene expression in chondrocytes grown on three-dimensional hyaluronic acid scaffolds. Biomaterials 2003;24:3265-75.

17. Barlic A, Drobnic M, Malicev E, Kregar-Velikonja N. Quantitative analysis of gene expression in human articular chondrocytes assigned for autologous implantation. J.Orthop.Res. 2008; 26(6): 847-53.

18. Salvat C, Pigenet A, Humbert L, Berenbaum F, Thirion S. Immature murine articular chondrocytes in primary culture: a new tool for investigating cartilage. Osteoarthritis Cartilage 2005;13:243-9.

19. Galois L, Hutasse S, Cortial D, Rousseau CF, Grossin L, Ronziere MC*, et al*. Bovine chondrocyte behaviour in three-dimensional type I collagen gel in terms of gel contraction, proliferation and gene expression. Biomaterials 2006;27:79-90.

20. Bosnakovski D, Mizuno M, Kim G, Takagi S, Okumur M, Fujinag T. Gene expression profile of bovine bone marrow mesenchymal stem cell during spontaneous chondrogenic differentiation in pellet culture system. Jpn.J.Vet.Res. 2006;53:127-39.

21. Bosnakovski D, Mizuno M, Kim G, Takagi S, Okumura M, Fujinaga T. Chondrogenic differentiation of bovine bone marrow mesenchymal stem cells (MSCs) in different hydrogels: influence of collagen type II extracellular matrix on MSC chondrogenesis. Biotechnol.Bioeng. 2006;93:1152-63.

CHAPTER 3

BIOMATERIAL SCAFFOLDS FOR CARTILAGE APPLICATIONS

Polymer scaffolds will play a major role in treating cartilage defects, deterioration, and damage. There are a number of natural and synthetic materials that have been used to create scaffolds for cartilage tissue engineering and a variety of fabrication methods that can be used to process these materials into scaffolds for cartilage regeneration. It is generally accepted that the requirements for the ideal scaffolds include that the construct is biocompatible, noncytotoxic, biodegradable, able to support and hold cells, permeable, mechanically stable, reproducible, readily available, and versatile for full and partial thickness lesions.[1] Here, we focus on the requirement that a scaffold should have mechanical properties, particularly stiffness values, similar to the cartilage tissue being regenerated. By matching target stiffness values of articular cartilage, the scaffold will withstand physiological loading, produce the mechanical tension generated within the cell cytoskeleton critical for cell shape and function, and mimic stiffness values that may affect cell to cell contacts and aggregation.[2] Furthermore, when the scaffold (with or without tissue) is implanted into a defect site, there should be no stiffness differences between healthy cartilage and regenerating tissue. Differences in tissue mechanical properties may cause fibrous tissue formation, elevated levels of strain in the adjacent cartilage, and acceleration of degeneration of the tissue.[3]

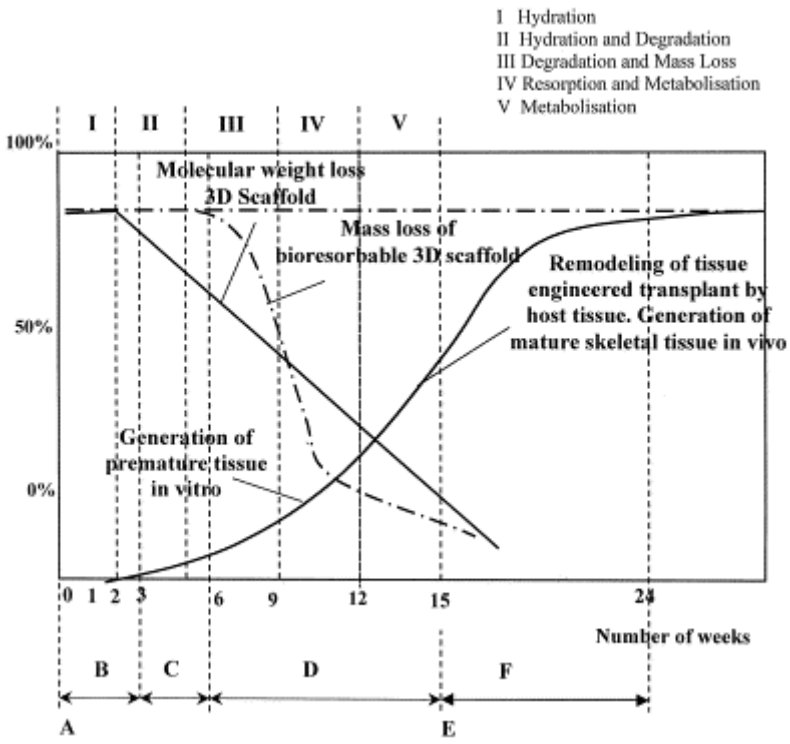

Figure 3.1. Schematic diagram[4] displaying the ideal profile for a tissue engineering scaffold, where generation of tissue compliments molecular weight and mass loss of a scaffold, resulting in mechanical properties that continually match those of native tissue (figure used with permission from Elsevier).

The repair strategy that this work aims to achieve is described by Hutmacher[4] as "strategy 1" in which "the physical scaffold structure supports the polymer/cell/tissue construct from the time of cell seeding up to the point where the tissue transplant is remodeled by the host tissue." A schematic of this strategy can be seen in Figure 3.1. Although polymer scaffold mechanical properties can be changed through variations in porosities and pore size to achieve the required initial mechanical properties, these changes also affect tissue regeneration in complicated manners. The ability to match initial properties through changes in bulk material properties is an advantageous route to pursue.

3.1 Mechanical Properties of Native Tissue

Cartilage is made up of chondrocytes embedded within an extracellular matrix that is composed of collagen (~60% of the dry weight, dw), proteoglycans (~25% dw), and other proteins and glycoproteins (~15% dw).[5] Together, these substances maintain the proper amount of water within the matrix, which confers its most significant functional property: its unique mechanical properties.[6]

Articular cartilage exhibits a viscoelastic, shock absorbing response to load. Its distinct mechanical properties stem from the biphasic nature of the tissue, in which a solid (the cartilage matrix) and a liquid (synovial fluid) have a unique interplay with one another. When loaded, the negatively charged proteoglycans in the solid matrix of cartilage are compressed together, increasing their repulsive nature to one another, and resulting in a resilient response. At the same time, when deformed, synovial fluid flows through the tissue in order to equalize pressure differences. Not only do the mechanical properties provide the proper functional abilities for load bearing, the interplay between the solid and fluid phases is also implicated in the proper development and maintenance of the tissue. The matrix acts as a signal transducer for cells, where loading creates mechanical, electrical and physiochemical signals that help direct chondrocyte synthetic and degradative activity.[7]

The mechanical property that this work focuses on matching is the equilibrium aggregate modulus (H_A) of native articular cartilage. In order to proceed with this aim, we must define the target values that we wish to achieve. The term “aggregate modulus” and

"equilibrium modulus" are synonymous, defined as the equilibrium stress divided by the equilibrium strain in stress relaxation. The term quantifies the stiffness of the tissue when all fluid flow has ceased, taking into account the interactions of fluid and solid phases affected by applied loads. The higher the aggregate modulus, the less the tissue deforms under a given load.[8] The aggregate modulus of articular cartilage depends on age, anatomic location, and mechanical testing procedures. Table 3.1 reviews the H_A values of articular cartilage as measured in confined compression. Values for human cartilage are from patients that have undergone total hip replacements due to femoral head fractures. It is important to note that higher stiffness values of these patients is most likely due to changes in the loading environment of articular cartilage that covers osteoporotic subchondral bone. The generally accepted range of H_A values for healthy articular cartilage is 0.5-1.0 MPa.

Table 3.1. Mechanical properties of articular cartilage as measured in confined compression.

Specimen	Specimen Age	Anatomical Site	Aggregate Modulus (MPa) (reported average ± stdev or range)
Bovine Articular Cartilage	fetal	Knee (femoral condyle) Knee (medial side)	0.089 ± 0.032 [9] 0.11 ± 0.03 [10]
	1-3 weeks	Knee (femoral condyle) Knee (medial side)	0.197 ± 0.021[9] 0.27 ± 0.02[10]
	3-4 weeks	Knee (patellar groove)	0.79-1.72 [11]
	6 months	Knee	0.49 ± 0.05 (in PBS)*[12] 0.64 ± 0.16 (in PVP)* [12]
	18-24 months	Hip (femoral head) Knee (medial side)	.57-1.01 [13] 0.31 ± 0.03[10]
	"Skeletally mature" "adult"	Shoulder (glenoid surface) Knee (femoral groove)	0.40 ± 0.14[14] 0.38 ± 0.12 [15]
	N/A	Hip	0.840* [16]
Human Articular Cartilage	16-85 years	Knee (patella)	0.79 ± 0.36 [17]
	24-50 years	Hip (femoral head and acetabulum)	0.679-1.816 MPa [18]
	65-90 years	Hip (femoral head)	2.22 ± 0.65[13]

PBS = phosphate buffered saline
PVP = polyvinilpyrolidone in deionized water
* dynamic mechanical analysis

3.2 Controlling Scaffold Stiffness for Cartilage Applications

A variety of natural and synthetic materials show favorable outcomes for use as scaffolds in cartilage tissue engineering. Throughout this section, the reference to "scaffolds" is not inclusive of natural material matrices such as agarose, alginate, hyaluronic acid, gelatin, fibrin glue, collagen derivative and acellular cartilage matrix, as they have been shown to have mechanical properties that are both difficult to control and too weak to support mechanical loads in an articular site. Rather, this section will focus on synthetic biomaterials, as they offer increased control and modification of scaffold properties.[19]

Synthetic polymers used for cartilage tissue engineering include polyglycolic acid (PGA), PGA+trimethylene carbonate, polycaprolactone, poly(ethylene oxide terephthalate)/poly(butylene terephthalate) (PEOT/PBT), poly(ethylene glycol) (PEG) cross-linked with polyrotaxane, silkworm and spider silk, tantalum, poly(lactic-co-glycolic acid) (PLGA), poly(3-hydroxybutyrate-co-3-hydroxyhexanoate) (PHBHHx), polylactic acid (PLLA), and poly(propylene fumarate) (PPF).[20-35] Materials reported have shown favorable outcomes as measured by GAG production by chondrocytes or differentiation of bone marrow stromal cells seeded into them and cultured in vitro or in vivo. However, long-term studies using human cells are rarely to never performed.

Many synthetic scaffolds show promising stiffness values that fall within the ranges of native cartilage tissue (.089 MPa-2.22 MPa, as seen in Table 3.1). Materials that have been fabricated into scaffolds with desirable stiffness values include PGA-PLLA meshes (0.919 MPA),[33] collagen-coated PLA microcarriers suspended in chitosan hydrogel (0.87-2.15 MPa),[34] chondroitan-sulfate-grafted PLLA (1.441 MPa),[35] PEOT/PBT 3D designed scaffolds (0.04-8.0 MPa dependant on porosity and architecture or 0.15-6.33 MPa dependant on copolymer compositions),[36, 37] PGA fiber meshes (0.138-0.199 MPa dependant on pore size),[38] fiber deposited PEGT/PBT block co-polymer scaffolds (0.05-2.5 MPa dependent on deposition parameters),[39] and photocrosslinked PEG scaffolds crosslinked with PLA (0.006MPa-0.5 MPa dependant on % macromer).[40] Synthetic scaffolds that have reported stiffness higher than desired include a blend of three copolymers of 50:50 poly(d,l)-lactide coglycolide (8.5 MPa),[41] and thermally induced phase separated PLLA, which when dry has values within the desired range (2.05 MPa),

but when wet or agarose-gel laden increases in stiffness (3.38 MPa and 5.16 MPa respectively).[42] On the other hand, there are also scaffolds reported with stiffness values below the ranges of native cartilage, including PGA unwoven meshes (.008 MPa),[43] porous polyurethane sponges (.023 MPa),[44] non-woven, coagulated, or salt leached silk fiber scaffolds (~0.05 MPa),[28] and porous PVA-PLGA scaffolds (0.087-0.102 MPa).[45] Mechanical properties pertaining to use of PCL for cartilage applications are discussed later in this chapter.

Synthetic materials offer increased control and variation over scaffold mechanical properties. Solid freeform fabrication (SFF) of scaffolds is an ideal method that can exploit this control and variability. In terms of matching mechanical properties of scaffolds to native tissue properties (goal #1), SFF grants the ability to accurately determine mechanical properties of scaffold designs through finite element analysis, simply by knowing the bulk material properties of polymers that can be used for scaffold fabrication. It is also ideal for exploring the way that mass transport will affect tissue regeneration (goal #2) as it allows for precise design and excellent reproducibility of specific architectures. Aside from the goals of this work, SFF provides many other benefits for creating scaffolds for cartilage tissue engineering. On a global scale, SFF enables design and fabrication of anatomically shaped scaffolds. For osteochondral applications, it allows the creation of biphasic scaffolds that incorporate multiple geometries into a single scaffold,[46, 47] allowing for in-growth of multiple tissues into a single structure. Particularly beneficial for articular cartilage applications, it allows the creation of different zones of organization within a single tissue compartment. Native

cartilage exhibits a superficial zone (elongated and flattened chondrocytes arranged in fascicles parallel to the surface), an intermediate zone (round chondrocytes randomly distributed), and a deep zone (chondrocytes arranged in short columns).[48] SFF allows the incorporation of distinctly designed architectural zones into a single scaffold, allowing recapitulation of this native organizational scheme. More locally, SFF allows for precise control of internal architectures, such as pore size, pore shape, interconnectivity and porosity. This increased control, over conventional methods, creates excellent reproducibility of intricate architectures, providing obvious benefits to basic science research and clinical applications. Within the field of tissue engineering research, it enables us to study how various scaffold architectures may affect cell infiltration, mass transport of nutrients and metabolic waste, and thereby influence tissue regeneration. Several authors have reviewed the advantages of SFF techniques currently in use for a wide array of other applications.[4, 49-52] In this thesis, we use SFF methods to fabricate scaffolds from two materials in order to achieve our first design goal of matching the mechanical properties of a 3D designed solid-freeform scaffolds to target modulus properties of native tissue. The two materials explored are a widely used synthetic polymer, polycaprolactone (PCL) and a more recently developed polymer, poly(glycerol sebacate) (PGS). We then use SFF to create precise, reproducible scaffolds with designed permeability in order to study the effects of this physical parameter on cartilage tissue regeneration.

3.3 Poly(ε-caprolactone)

PCL is formed when ε-caprolactone is heated and undergoes a ring-opening polymerization to form polycaprolactone, as shown in Figure 3.2. It belongs to the group of polymers called aliphatic-polyesters, which typically possess hydrolytic instability, low melting temperatures, and solubility in common organic solvents, which ironically led to the belief in the mid 1900's that these polymers were insufficient for use in practical applications, putting a halt on further studies.[53]

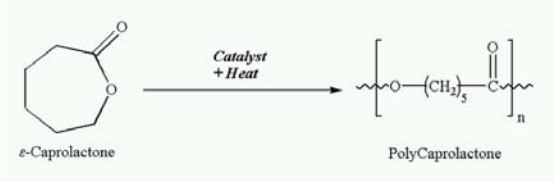

Figure 3.2. Ring opening polymerization of ε-Caprolactone to Polycaprolactone.

Now, PCL is an FDA approved, biodegradable, non-toxic polymer that is used for a variety of biomedical applications. It degrades much slower than other known biodegradable polymers through hydrolysis of its ester linkages in physiological conditions.[51] Its byproducts, caproic acid and hydroxycaproic acid, are excreted by the body without complication. In addition to being investigated as a scaffold material for tissue repair, has been used for drug delivery devices, suture, root canal filler and adhesion barrier.

Aside from the conventional methods of porogen leaching and solvent casting, there are a number of SFF techniques that have been utilized to build PCL scaffolds including fused deposition modeling,[4, 54-58] photopolymerization,[59] precision extruding deposition,[60, 61] three dimensional printing,[62] low temperature deposition,[63] multi-nozzle freeform

deposition,[64, 65] shape-deposition,[66] selective laser sintering, [67-69] drop-on-demand printing,[70] salt leaching and melt casting. In Chapter 5, we use the SFF method of melt-casting in order to create 3D-designed PCL scaffolds.

When working with PCL, there is no option of varying aspects of "prepolymerization" (as we do with PGS, discussed later) in order to alter mechanical properties. However, during the melt casting process used to fabricate scaffolds (see Figure 3.3), the molecular weight of the polymer used (see Table 3.2 for commercially available PCL) and the temperature at which the polymer is melted *can* be altered. Aside from resultant changes in mechanical properties, the molecular weight of the polymer may also affect melt casting success. During fabrication, melt-casted PCL must be liquid enough to be cast into small wax mold pores to create thin scaffold struts. However, lower molecular weight PCL, which will be more liquid, and hence easier to cast, may have inherently weaker mechanical properties. In this thesis, we choose to examine the mechanical properties of the PCL products highlighted in Table 3.2. Although all products could be used to successfully fabricate scaffolds, 14,000 Dalton PCL was quickly excluded from testing as the scaffolds were too fragile to be handled.

Table 3.2. Commercially available poly(ε-caprolactone).

Supplier/Product Number	Mean Molecular Weight	Physical Form
CAPA 6100	10,000	white solid
CAPA 6250	25,000	Pellets
CAPA 6400	37,000	Pellets
CAPA 6430	43,000	Pellets
CAPA 6500	50,000	Pellets
CAPA 6800	80,000	Pellets
CAPA 6406	33,000-38,000	Powder
CAPA 6501	50,000	Powder
CAPA 6503	50,000	Powder
CAPA 6505	50,000	Powder
CAPA 6806	80,000	Powder
CAPA 6500C		
CAPA 6506	50,000	Powder
Sigma 440752	14,000	Flakes
Sigma 181609	65,000	Pellets

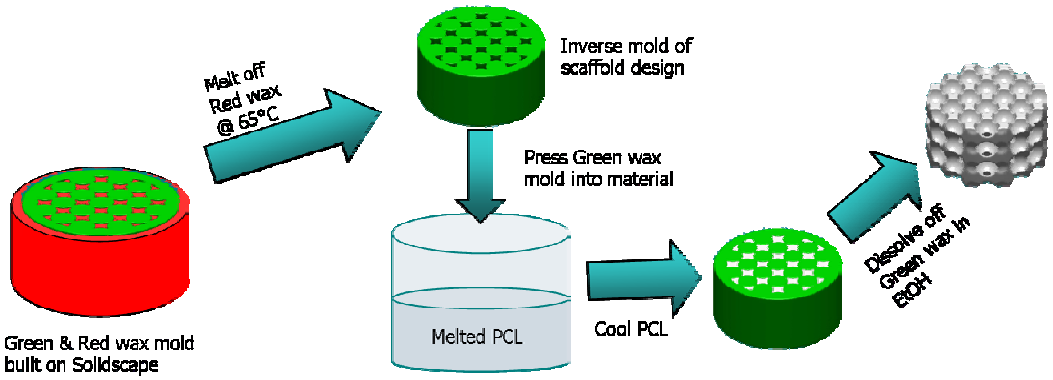

Figure 3.3. Fabrication process for melt casted PCL scaffolds includes creating a green+red wax mold, melting off red wax and then pressing the green inverse mold into melted PCL. The wax+PCL construct is then cooled before green wax is removed using 100% ethanol.

Polycaprolactone has been used for a wide range of tissue engineering applications due to its slow degradative nature, relative inert biocompatible properties, and its mechanical strength. Its extensive surge into tissue engineering applications include use for bone,

cartilage, smooth muscle, blood vessel, bladder grafting, and nerve tissue regeneration. This work will concentrate on its use for cartilage tissue repair.

The degradation of PCL has been heavily documented and shown to be much slower than other degradable polymers. Like other aliphatic-polyesters, PCL undergoes bulk hydrolysis characterized by a molecular weight loss up to 5000 due to chain scission, followed by the onset of weight loss. Its slow degradation rates are attributed to its hydrophobicity and high crystallinity that do not allow fast water penetration.[59] During its slow degradation, it does not generate an acidic environment and the byproducts that it does release (caproic acid and hydroxycaproic acid) can be naturally secreted by the body. In vitro (PBS, 37°C) PCL degradation has been characterized by weight loss of less than 2% after 42 days,[59] no apparent changes in morphology, compressive mechanical properties, and weight loss up to 45 months,[71] or no change in molecular weight (Mw) and molecular number (Mn) until at least 21 days, where-after *Sung et al.*[72] show a significant decrease in molecular number (33% at day 21 and 39% at day 28). However, Coombes *et al.*[71] show no significant changes in Mn and Mw until 12 months. PCL's degradation in vivo is faster, with studies showing complete absorption in 60 days, in which phagocytosis of small particles is observed in the final stage,[73] and more rapid changes in Mn, with a decrease of 42.6% at day 21.[72] The slow in vitro degradation profile of PCL is advantageous for studies done in Chapter 7 of this thesis. Because we look at how permeability affects chondrogenesis, it is essential to use a polymer that does not degrade throughout the in vitro culture time, thereby changing the permeability of the scaffold over time.

PCL has been shown to be compatible with a variety of cells types. Osteoblasts,[59, 67, 71] smooth muscle cells,[72] fibroblasts,[55, 74, 75] bone marrow stromal cells,[66, 76] and chondrocytes[39, 77-79] are among the cells seeded onto PCL scaffolds for skeletal tissue engineering applications. Focusing specifically on cartilage applications, studies have shown encouraging cellular infiltration, redifferentiation and proliferation of chondrocytes on PCL in vitro.[78, 80-83] Eyrich *et al.*[84] found that seeding cells into PCL scaffolds through encapsulating them in fibrin gel increased both the seeding efficiency and the homogenous matrix distribution. Furthermore, both in vitro and in vivo studies have shown abundant proteoglycans and type II collagen expression on PCL scaffolds seeded with chondrocytes, embryonic stem cells, and bone marrow-derived mesenchymal stem cells (the latter of which were induced to differentiate down a chondrogenic lineage by culture in specific differentiation medias).[30, 84-90] Oliveria *et al.*[87] report better biocompatibility compared to PGA scaffolds where they see lack of tissue in the center of scaffolds possibly due to acidic byproducts. PCL scaffolds have also been applied for use in osteochondral sites where studies show promising results in terms of bone growth, cartilage growth and integration.[91, 92] In this work, we exploit the use of PCL for studies that involve seeding of chondrocytes and bone marrow stromal cells onto scaffolds with designed permeability.

PCL is inherently hydrophobic, which can be a disadvantage for tissue engineering applications. A number of studies have demonstrated the benefits of using surface modifications to overcome this hydrophobic nature. Surface modifications of PCL

include use of acrylic acid, collagen, chitosan, NaOH, surface functionalization with NaOH, HCl, oxygen, or argon and coating with collagen 1 in order to improve cell adhesion, proliferation and function.[93-96]

PCL's array of fabrication possibilities lead to a wide range of mechanical properties for cartilage applications. Examples of PCL particle leached sponges (0.607-8.15 MPa dependant on porosity),[97] freeze-dried PCL (1.71 MPa),[30] and 3D foams of Semi-IPN PCL-PVA crosslinked with 1% glutaraldehyde (1.52-3.51 MPa with increasing PVA concentrations correlating with increase in elastic modulus)[86] have all shown properties within the ranges of native articular cartilage. Elastomeric microporous poly(L-lactide-co-epsilon-caprolactone) (PLCL) sponges created by Xie *et al.*[98] fall below these ranges (0.019 MPa), while another example of porogen leached sponges created by Izquierdo *et al.*[77] fall above these ranges (6.85 ± 1.83 MPa). All of these scaffolds, however, fall within the same magnitude of native cartilage properties, and are therefore promising for cartilage tissue engineering applications.

In this research we use the SFF process of melt casting in order to produce designed 3D scaffolds for cartilage tissue engineering. In Chapter 5, we demonstrate the importance of mechanically testing the material at 37°C for in vivo applications, quantify the contraction of melt cast PCL in ethanol (used during processing and sterilization), and characterize the effects that the processing parameters of melting temperature and polymer molecular may have on the equilibrium modulus of melt-cast PCL.

3.4 Poly(glycerol-sebacate)

Unlike PCL, Poly(glycerol sebacate) (PGS) is just recently gaining popularity within the field of tissue engineering. Synthesis and characterization of the polymer, created through a polycondensation reaction of glycerol and sebacic acid (see Figure 3.4), was first reported in literature in 1999 by Nagata *et al.*[99] In 2002, Wang *et al.*[100] began using the polymer for biotechnology and bioengineering applications. The group, out of MIT, created the polymer to provide good mechanical properties through covalent crosslinking and hydrogen bonding and rubberlike elasticity through a network of random coils with at least one trifunctional monomer. They designed the polymer with established degradation and crosslinking mechanisms optimal for tissue engineering applications. In order to satisfy tissue engineering requirements, they chose to use glycerol as the alcohol monomer and sebacic acid as the acid monomer. Along with being tougher, inexpensive and more flexible than existing biodegradable elastomers, glycerol and polymers containing sebacic acid have been approved by the US Food and Drug Administration for medical applications. To date, PGS has been used for applications in nerve guidance[101], soft tissue regeneration,[102, 103] vascular and myocardial tissue regeneration,[104-108] blood vessel reconstruction,[109, 110] drug delivery,[111] and in the replacement of photoreceptor cells.[112] PGS is a biodegradable polymer with biocompatibility and mechanical properties that make it well suited for applications such as those mentioned above and, as we show in Chapter 6, for use in cartilage tissue engineering.

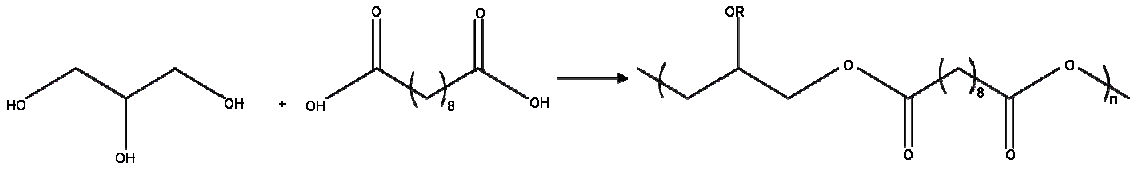

Figure 3.4. Polycondensation reaction of glycerol and sebacic acid to produce poly(glycerol sebacate) prepolymer.

PGS is processed through creating a prepolymer, and then curing this prepolymer at high temperatures to obtain a thermoset elastomeric polymer. The prepolymer form of PGS is fabricated through a polycondensation reaction. In 1997, Nagata *et al.*[99] produced a rigid, totally crosslinked polymer using a glycerol: sebacic acid ratio of 2:3 (molar ratio = 2:3). Most all literature thereafter reports use of equimolar amounts of glycerol: sebacic acid (molar ratio = 1:1), which result in a less rigid polymer. Liu *et al.* [113] also report a "two-step" method, in which they react the pre-polymer at a 1:1 molar ratio, and then continue adding sebacic acid until they reach a molar ratio of 2:2.5. This procedure creates a thermoplastic elastomer with increased strength and elongation and slower degradation than the previously reported thermoset PGS. In this thesis, using the original synthesis method outlined by Wang *et al,.*[100] we will characterize how various molar ratios of glycerol to sebacic acid (3:4, 1:1, 4:3) affect the elastic modulus of the material.

After prepolymer synthesis, the polymer must be cured at high temperatures in order to create the final product. During the curing process, micropores are created (~5-20um) through the removal of glycerol.[103] Most studies to date cure PGS at 120°C, however, in 2006 Gao *et al.*[103] show that at 150°C the transesterification reaction is far more extensive than at 120°C, creating more micropores in the resultant polymer. In 2008, Chen *et al.*[106] characterize the changes in Young's modulus, failure stress, and

degradation rate that result from a change in curing temperature (110°C v. 120°C v. 130°C). They report that the Young's modulus of PGS increases from .56MPa at 110°C to 1.2MPa at 130°C and that higher curing temperature results in lower failure stress and slower degradation. In this work, we use a consistent curing temperature of 150°C.

Since 2002, a number of groups have been processing PGS for tissue engineering applications. Most studies have fabricated the polymer through conventional methods, creating films or porogen-leached sponges. Motlagh *et al.*[109] and Crapo et al.[110] demonstrate curing the polymer into tubular sheets and films to create scaffolds for blood vessels, renal tubules, or various ducts. In this thesis, we demonstrate the ability to fabricate PGS scaffolds through SFF techniques in order to create designed pore shapes, pore sizes, porosities, and architectures. Fabrication of PGS by this means was not yet reported. Because PGS must be cured at temperatures greater than the melting temperature of ProtoBuild molds, an intermediate hydroxyapatite mold must be created and cast into the pPGS in order to create designed architectures. Details of the fabrication steps can be seen in Figure 3.5.

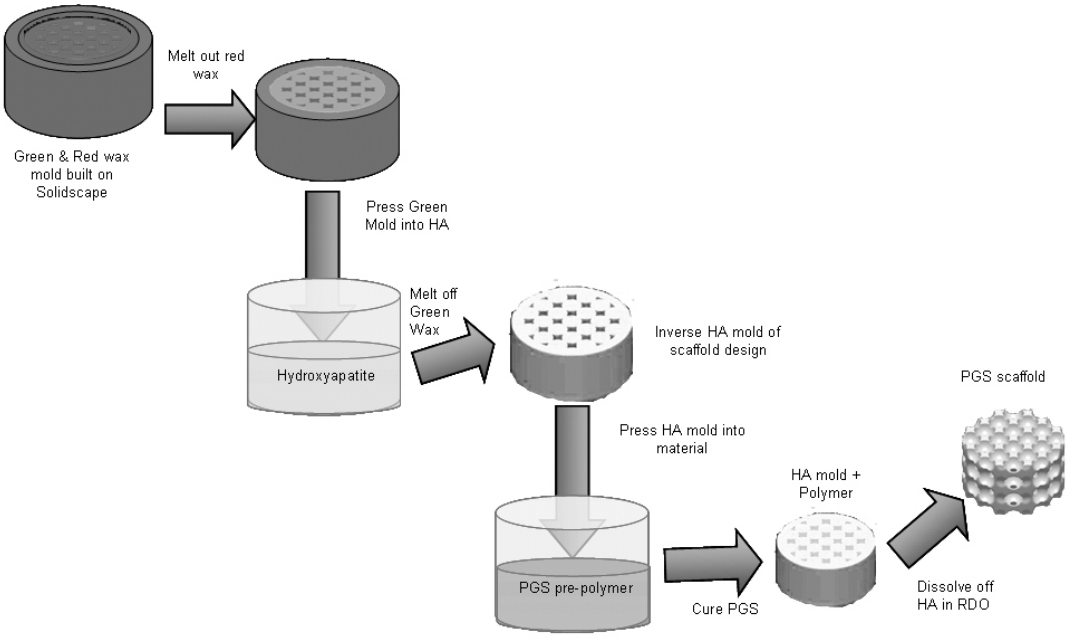

Figure 3.5. Fabrication of 3D designed PGS scaffolds involves first creating wax molds, which are cast into hydroxyapatite in order to create an inverse mold, which is then cast into PGS prepolymer and cured, resulting in a PGS scaffold.

Since 2002, the biocompatibility of PGS has been reported for a variety of bioengineering applications. In their original work, Wang *et al.* [100] demonstrate its biocompatibility with NIH 3T3 fibroblasts. They show that PGS induces little, if any, fibrous capsule formation and that it has an inflammatory response similar to that of PLGA when implanted in under the skin of rats. Positive results have also been shown for attachment, proliferation, and viability of Schwann cells (as a nerve guide),[101] human umbilical vein endothelial cells (for vascularizing TE organs),[108] platelets (for blood vessel applications) [109] , and hepatocytes (for replacement of tissue and organs).[114] The most frequent application of PGS to date has been in heart and vascular tissue. Seeding of cardiac fibroblasts on PGS show favorable levels of contraction and excitation and form layers of elongated myocytes aligned in parallel over layers of fibroblasts.[104] Endothelial progenitor cells, and smooth muscle cells adhere, proliferate and show favorable

phenotypic and morphological properties.[105] And, in 2007, PGS began being used for drug delivery by Nijst *et al*.,[111] as they demonstrated a way to mildly process the material allowing for encapsulation of temperature sensitive factors, and showed sufficient cell adhesion and proliferation of human foreskin fibroblasts. In this work, we show the biocompatibility of PGS with chondrocytes for cartilage tissue engineering applications.

One main advantages of using PGS for tissue engineering, exploited in this research, is that its mechanical properties can be tailored to match specific tissue properties simply through altering processing parameters during the prepolymer and/or curing steps. To date, most mechanical testing of PGS has been done in tension. Tensile tests on pure PGS have shown that it can be elongated repeatedly to at least three times its original length, with a tensile Young's modulus of 0.282 ± 0.0250MPa and an ultimate strength >0.5 MPa.[100] Using the two-step processing method, Liu *et al.*[113] demonstrate slightly higher elastic modulus values (.45-.55MPa), but lower tensile strain (109-236%). Using milder processing conditions for drug delivery applications, Nijst *et al.*[111] report values for Young's modulus of .05-1.38MPa, ultimate strength values of .05-.5MPa, and elongations of 42%-189%. And, in 2008, Chen *et al.*[106] demonstrate the ability to alter the mechanical properties of PGS by variation in curing temperatures, recording Young's modulus values of .056 MPa (110°C), .22MPa (120°C), and 1.2MPa (130°C), with their results for 120°C closely matching those of Wang's results for the same conditions. Compression testing done on salt leached PGS foams have resulted in lower moduli that range from ~4.5 kPa to ~7 kPa,[103] dependent on both the PGS/salt ratios and the size of the salt particles used. And, although Wang *et al.*[102] tested sheets of solid PGS in

compression to assess the materials degradation, they fail to report raw values for their compressive modulus results. Here, we test solid PGS cylinders and novel 3D-designed scaffolds in compression to determine the non-linear elastic properties of this material.

Although we will not examine the degradation of PGS in this work, it is important to note its degradative properties. PGS degrades much more quickly than does PCL. In vitro, the material loses 17% of its mass after 60 days.[100] The degradation of PGS in vivo has been shown to be much quicker than in vitro, likely due to the esterases associated with macrophages shown to degrade polyesters.[111] As a direct comparison, after 60 days in vivo, the material is totally absorbed. In vivo, PGS undergoes surface erosion, resulting in a number of benefits for tissue engineering applications including a linear degradation profile of mass, preservation of geometry, and retention of mechanical strength. There are a number of factors that contribute to changes in degradation. Liu *et al.*[115] report that thermoplastic-PGS (TMPGS) degrades more slowly than PGS, and show that the prepolymer molecular weight affects degradation speed, but not mechanism. Lowering of the curing temperature causes PGS to degrade more quickly (in PBS)[106] as does cell seeding onto the material.[107] And, although not studied here, it is likely that the degradation profile of PGS could also be altered through variations in prepolymer molar ratios or curing time.

An additional benefit of PGS in tissue engineering applications is its lack of swelling in water. When cured at 120°C, Wang *et al.*[100] and Chen *et al.*[106] show low swelling values, 2% and 4% respectively. Chen *et al*.[106] also report that swelling is decreased

with increasing curing temperature (2.5% at 130°C). Solid cylinders used for our studies, cured at 150°C, showed no significant swelling.

Here, we use this novel material to create 3D designed scaffolds for cartilage tissue engineering applications. Although the material exhibits a purely elastic response, in comparison to the viscoelastic response of native cartilage, matching this to cartilage equilibrium modulus is a good first step, as there is no data that indicates how critical it is to match all cartilage properties exactly to achieve adequate function and superior tissue regeneration. We show that the elastic modulus of PGS can be tailored through variations in prepolymer molar ratios and changes in curing time. With an established database of mechanical properties for different processing parameters, we can match the mechanical properties of a wide range of scaffold architectures to the properties of native tissue. As proof of concept, we show that chondrocytes can be seeded into the scaffolds, and cultured in vitro to produce quantities of sGAG and expression of cartilage specific markers comparable to or higher than values produced on relatively inert PCL.

References

1. Safran MR, Kim H, Zaffagnini S. The use of scaffolds in the management of articular cartilage injury. J.Am.Acad.Orthop.Surg. 2008;16:306-11.

2. Lu L, Zhu X, Valenzuela RG, Currier BL, Yaszemski MJ. Biodegradable polymer scaffolds for cartilage tissue engineering. Clin.Orthop.Relat.Res. 2001;(391 Suppl):S251-70.

3. Beaupre GS, Stevens SS, Carter DR. Mechanobiology in the development, maintenance, and degeneration of articular cartilage. J.Rehabil.Res.Dev. 2000;37:145-51.

4. Hutmacher DW. Scaffolds in tissue engineering bone and cartilage. Biomaterials 2000;21:2529-43.

5. Freed LE, Hollander AP, Martin I, Barry JR, Langer R, Vunjak-Novakovic G. Chondrogenesis in a cell-polymer-bioreactor system. Exp.Cell Res. 1998;240:58-65.

6. Newman AP. Articular cartilage repair. Am.J.Sports Med. 1998;26:309-24.

7. Klippel JH, Weyand CM, Crofford LJ, Stone JH, Arthritis Foundation. Primer on the rheumatic diseases. Atlanta, Ga.: Arthritis Foundation 2001.

8. Mansour JM. Biomechanics of Cartilage. In: Kinesiology: The Mechanics and Pathomechanics of Human Movement. C. A. Oatis, Ed. Philadelphia: Lippincott Williams and Wilkins, 2003, pp: 66-79.

9. Klein TJ, Chaudhry M, Bae WC, Sah RL. Depth-dependent biomechanical and biochemical properties of fetal, newborn, and tissue-engineered articular cartilage. J.Biomech. 2007; 40(1):182-90.

10. Williamson AK, Chen AC, Sah RL. Compressive properties and function-composition relationships of developing bovine articular cartilage. J.Orthop.Res. 2001;19:1113-21.

11. Bursac PM, Obitz TW, Eisenberg SR, Stamenovic D. Confined and unconfined stress relaxation of cartilage: appropriateness of a transversely isotropic analysis. J.Biomech. 1999;32:1125-30.

12. Moroni L, Poort G, Van Keulen F, de Wijn JR, van Blitterswijk CA. Dynamic mechanical properties of 3D fiber-deposited PEOT/PBT scaffolds: an experimental and numerical analysis. J.Biomed.Mater.Res.A. 2006;78:605-14.

13. Demarteau O, Pillet L, Inaebnit A, Borens O, Quinn TM. Biomechanical characterization and in vitro mechanical injury of elderly human femoral head cartilage:

comparison to adult bovine humeral head cartilage. Osteoarthritis Cartilage 2006;14(6):589-96.

14. Ateshian GA, Warden WH, Kim JJ, Grelsamer RP, Mow VC. Finite deformation biphasic material properties of bovine articular cartilage from confined compression experiments. J.Biomech. 1997;30:1157-64.

15. Schinagl RM, Gurskis D, Chen AC, Sah RL. Depth-dependent confined compression modulus of full-thickness bovine articular cartilage. J.Orthop.Res. 1997;15:499-506.

16. Schwartz CJ and Bahadur S. Investigation of articular cartilage and counterface compliance in multi-directional sliding as in orthopedic implants. Wear 2007;262:1315-20.

17. Armstrong CG and Mow VC. Variations in the intrinsic mechanical properties of human articular cartilage with age, degeneration, and water content. J.Bone Joint Surg.Am. 1982;64:88-94.

18. Athanasiou KA, Agarwal A, Dzida FJ. Comparative study of the intrinsic mechanical properties of the human acetabular and femoral head cartilage. J.Orthop.Res. 1994;12:340-9.

19. Raghunath J, Rollo J, Sales KM, Butler PE, Seifalian AM. Biomaterials and scaffold design: key to tissue-engineering cartilage. Biotechnol.Appl.Biochem. 2007;46:73-84.

20. Jansen EJ, Pieper J, Gijbels MJ, Guldemond NA, Riesle J, Van Rhijn LW*, et al*. PEOT/PBT based scaffolds with low mechanical properties improve cartilage repair tissue formation in osteochondral defects. J.Biomed.Mater.Res.A. 2008; Apr 22, Epub ahead of print.

21. Schmal H, Mehlhorn AT, Kurze C, Zwingmann J, Niemeyer P, Finkenzeller G*, et al*. In vitro study on the influence of fibrin in cartilage contructs based on PGA fleece materials. Orthopade 2008;37:424-34.

22. Mardones RM, Reinholz GG, Fitzsimmons JS, Zobitz ME, An KN, Lewallen DG*, et al*. Development of a biologic prosthetic composite for cartilage repair. Tissue Eng. 2005;11:1368-78.

23. Wang Y, Bian YZ, Wu Q, Chen GQ. Evaluation of three-dimensional scaffolds prepared from poly(3-hydroxybutyrate-co-3-hydroxyhexanoate) for growth of allogeneic chondrocytes for cartilage repair in rabbits. Biomaterials 2008;29:2858-68.

24. Janjanin S, Li WJ, Morgan MT, Shanti RM, Tuan RS. Mold-Shaped, Nanofiber Scaffold-Based Cartilage Engineering Using Human Mesenchymal Stem Cells and Bioreactor. J.Surg.Res. 2008; Jan 28, Epub ahead of print.

25. Munirah S, Kim SH, Ruszymah BH, Khang G. The use of fibrin and poly(lactic-co-glycolic acid) hybrid scaffold for articular cartilage tissue engineering: an in vivo analysis. Eur.Cell.Mater. 2008;15:41-52.

26. Uebersax L, Merkle HP, Meinel L. Insulin-like growth factor I releasing silk fibroin scaffolds induce chondrogenic differentiation of human mesenchymal stem cells. J.Control.Release 2008;127:12-21.

27. Mukherjee DP, Smith DF, Rogers SH, Emmanual JE, Jadin KD, Hayes BK. Effect of 3D-microstructure of bioabsorbable PGA:TMC scaffolds on the growth of chondrogenic cells. J.Biomed.Mater.Res.B.Appl.Biomater. 2008; Jun 10, Epub ahead of print.

28. Gellynck K, Verdonk PC, Van Nimmen E, Almqvist KF, Gheysens T, Schoukens G*, et al*. Silkworm and spider silk scaffolds for chondrocyte support. J.Mater.Sci.Mater.Med. 2008; Jun 11, Epub ahead of print.

29. Kim GH. Electrospun PCL nanofibers with anisotropic mechanical properties as a biomedical scaffold. Biomed.Mater. 2008;3:25010.

30. Lin CH, Su JM, Hsu SH. Evaluation of type II collagen scaffolds reinforced by poly(epsilon-caprolactone) as tissue-engineered trachea. Tissue Eng.Part C.Methods 2008;14:69-77.

31. Emin N, Koc A, Durkut S, Elcin AE, Elcin YM. Engineering of rat articular cartilage on porous sponges: effects of tgf-beta 1 and microgravity bioreactor culture. Artif.Cells Blood Substit.Immobil.Biotechnol. 2008;36:123-37.

32. Sha'ban M, Kim SH, Idrus RB, Khang G. Fibrin and poly(lactic-co-glycolic acid) hybrid scaffold promotes early chondrogenesis of articular chondrocytes: an in vitro study. J.Orthop.Surg. 2008;3:17.

33. Beatty MW, Ojha AK, Cook JL, Alberts LR, Mahanna GK, Iwasaki LR*, et al*. Small intestinal submucosa versus salt-extracted polyglycolic acid-poly-L-lactic acid: a comparison of neocartilage formed in two scaffold materials. Tissue Eng. 2002;8:955-68.

34. Hong Y, Gong Y, Gao C, Shen J. Collagen-coated polylactide microcarriers/chitosan hydrogel composite: injectable scaffold for cartilage regeneration. J.Biomed.Mater.Res.A. 2008;85:628-37.

35. Lee CT, Huang CP, Lee YD. Biomimetic porous scaffolds made from poly(L-lactide)-g-chondroitin sulfate blend with poly(L-lactide) for cartilage tissue engineering. Biomacromolecules 2006;7:2200-9.

36. Moroni L, de Wijn JR, van Blitterswijk CA. 3D fiber-deposited scaffolds for tissue engineering: Influence of pores geometry and architecture on dynamic mechanical properties. Biomaterials 2005; 27(7): 974-85.

37. Moroni L, de Wijn JR, van Blitterswijk CA. 3D fiber-deposited scaffolds for tissue engineering: influence of pores geometry and architecture on dynamic mechanical properties. Biomaterials 2006;27:974-85.

38. Moutos FT, Freed LE, Guilak F. A biomimetic three-dimensional woven composite scaffold for functional tissue engineering of cartilage. Nat.Mater. 2007;6:162-7.

39. Woodfield TB, Malda J, de Wijn J, Peters F, Riesle J, van Blitterswijk CA. Design of porous scaffolds for cartilage tissue engineering using a three-dimensional fiber-deposition technique. Biomaterials 2004;25:4149-61.

40. Bryant SJ, Bender RJ, Durand KL, Anseth KS. Encapsulating chondrocytes in degrading PEG hydrogels with high modulus: engineering gel structural changes to facilitate cartilaginous tissue production. Biotechnol.Bioeng. 2004;86:747-55.

41. Spain TL, Agrawal CM, Athanasiou KA. New technique to extend the useful life of a biodegradable cartilage implant. Tissue Eng. 1998;4:343-52.

42. Gong Y, He L, Li J, Zhou Q, Ma Z, Gao C*, et al*. Hydrogel-filled polylactide porous scaffolds for cartilage tissue engineering. J.Biomed.Mater.Res.B.Appl.Biomater. 2007;82:192-204.

43. Hu JC and Athanasiou KA. Low-density cultures of bovine chondrocytes: effects of scaffold material and culture system. Biomaterials 2005;26:2001-12.

44. Grad S, Kupcsik L, Gorna K, Gogolewski S, Alini M. The use of biodegradable polyurethane scaffolds for cartilage tissue engineering: potential and limitations. Biomaterials 2003;24:5163-71.

45. Charlton DC, Peterson MG, Spiller K, Lowman A, Torzilli PA, Maher SA. Semi-degradable scaffold for articular cartilage replacement. Tissue Eng.Part A. 2008;14:207-13.

46. Taboas JM, Maddox RD, Krebsbach PH, Hollister SJ. Indirect solid free form fabrication of local and global porous, biomimetic and composite 3D polymer-ceramic scaffolds. Biomaterials 2003;24:181-94.

47. Schek RM, Taboas JM, Segvich SJ, Hollister SJ, Krebsbach PH. Engineered osteochondral grafts using biphasic composite solid free-form fabricated scaffolds. Tissue Eng. 2004;10:1376-85.

48. Ross MH and Pawlina W. Histology : a text and atlas : with correlated cell and molecular biology. Baltimore, MD: Lippincott Williams & Wilkins 2006.

49. Landers R, Hubner U, Schmelzeisen R, Mulhaupt R. Rapid prototyping of scaffolds derived from thermoreversible hydrogels and tailored for applications in tissue engineering. Biomaterials 2002;23:4437-47.

50. Sachlos E and Czernuszka JT. Making tissue engineering scaffolds work. Review: the application of solid freeform fabrication technology to the production of tissue engineering scaffolds. Eur.Cell.Mater. 2003;5:29,39; discussion 39-40.

51. Sun H, Mei L, Song C, Cui X, Wang P. The in vivo degradation, absorption and excretion of PCL-based implant. Biomaterials 2006;27:1735-40.

52. Sun W, Starly B, Darling A, Gomez C. Computer-aided tissue engineering: application to biomimetic modelling and design of tissue scaffolds. Biotechnol.Appl.Biochem. 2004;39:49-58.

53. Duda A and Penczek S. Mechanisms of Aliphatic Polyester Formation. In: Biopolymers. Weinheim; Chichester: Wiley-VCH, 2001.

54. Hutmacher DW. Scaffold design and fabrication technologies for engineering tissues--state of the art and future perspectives. J.Biomater.Sci.Polym.Ed. 2001;12:107-24.

55. Hutmacher DW, Schantz T, Zein I, Ng KW, Teoh SH, Tan KC. Mechanical properties and cell cultural response of polycaprolactone scaffolds designed and fabricated via fused deposition modeling. J.Biomed.Mater.Res. 2001;55:203-16.

56. Rohner D, Hutmacher DW, Cheng TK, Oberholzer M, Hammer B. In vivo efficacy of bone-marrow-coated polycaprolactone scaffolds for the reconstruction of orbital defects in the pig. J.Biomed.Mater.Res.B.Appl.Biomater. 2003;66:574-80.

57. Zein I, Hutmacher DW, Tan KC, Teoh SH. Fused deposition modeling of novel scaffold architectures for tissue engineering applications. Biomaterials 2002;23:1169-85.

58. Ramanath HS, Chua CK, Leong KF, Shah KD. Melt flow behaviour of poly-epsilon-caprolactone in fused deposition modelling. J.Mater.Sci.Mater.Med. 2008;19:2541-50.

59. Kweon H, Yoo MK, Park IK, Kim TH, Lee HC, Lee HS*, et al*. A novel degradable polycaprolactone networks for tissue engineering. Biomaterials 2003;24:801-8.

60. Hoque ME, Hutmacher DW, Feng W, Li S, Huang MH, Vert M*, et al*. Fabrication using a rapid prototyping system and in vitro characterization of PEG-PCL-PLA scaffolds for tissue engineering. J.Biomater.Sci.Polym.Ed. 2005;16:1595-610.

61. Wang F, Shor L, Darling A, Sun W, Guceri S, Lau A. Precision extruding deposition and characterization of cellular poly-e-caprolactone tissue scaffolds. Solid Freeform Fabrication Symposium. 2003.

62. Wu BM, Borland SW, Giordano RA, Cima LG, Sachs EM, Cima MJ. Solid free-form fabrication of drug delivery devices. J Controlled Release 1996;40:77,78-87.

63. Xiong Z, Yan Y, Wang S, Zhang R, Zhang C. Fabrication of porous scaffolds for bone tissue engineering via low-temperature deposition. Scripta Materialia 2002;46:771,772-776.

64. Sun W, Darling A, Starly B, Nam J. Computer-aided tissue engineering: overview, scope and challenges. Biotechnol.Appl.Biochem. 2004;39:29-47.

65. Sun W and Lal P. Recent development on computer aided tissue engineering--a review. Comput.Methods Programs Biomed. 2002;67:85-103.

66. Marra KG, Szem JW, Kumta PN, DiMilla PA, Weiss LE. In vitro analysis of biodegradable polymer blend/hydroxyapatite composites for bone tissue engineering. J.Biomed.Mater.Res. 1999;47:324-35.

67. Williams JM, Adewunmi A, Schek RM, Flanagan CL, Krebsbach PH, Feinberg SE*, et al*. Bone tissue engineering using polycaprolactone scaffolds fabricated via selective laser sintering. Biomaterials 2005;26:4817-27.

68. Wiria FE, Leong KF, Chua CK, Liu Y. Poly-epsilon-caprolactone/hydroxyapatite for tissue engineering scaffold fabrication via selective laser sintering. Acta Biomater. 2007;3:1-12.

69. Tan KH, Chua CK, Leong KF, Cheah CM, Gui WS, Tan WS*, et al*. Selective laser sintering of biocompatible polymers for applications in tissue engineering. Biomed.Mater.Eng. 2005;15:113-24.

70. Mondrinos MJ, Dembzynski R, Lu L, Byrapogu VK, Wootton DM, Lelkes PI*, et al*. Porogen-based solid freeform fabrication of polycaprolactone-calcium phosphate scaffolds for tissue engineering. Biomaterials 2006;27:4399-408.

71. Coombes AG, Rizzi SC, Williamson M, Barralet JE, Downes S, Wallace WA. Precipitation casting of polycaprolactone for applications in tissue engineering and drug delivery. Biomaterials 2004;25:315-25.

72. Sung HJ, Meredith C, Johnson C, Galis ZS. The effect of scaffold degradation rate on three-dimensional cell growth and angiogenesis. Biomaterials 2004;25:5735-42.

73. Chen J, Huang C, Chen Z. Study on the biocompatibility and toxicology of biomaterials--poly(epsilon-caprolactone). Sheng Wu Yi Xue Gong Cheng Xue Za Zhi 2000;17:380-2.

74. Tang ZG and Hunt JA. The effect of PLGA doping of polycaprolactone films on the control of osteoblast adhesion and proliferation in vitro. Biomaterials 2006;27:4409-18.

75. Oh SH, Park IK, Kim JM, Lee JH. In vitro and in vivo characteristics of PCL scaffolds with pore size gradient fabricated by a centrifugation method. Biomaterials 2007;28:1664-71.

76. Li WJ, Tuli R, Okafor C, Derfoul A, Danielson KG, Hall DJ*, et al*. A three-dimensional nanofibrous scaffold for cartilage tissue engineering using human mesenchymal stem cells. Biomaterials 2005;26:599-609.

77. Izquierdo R, Garcia-Giralt N, Rodriguez MT, Caceres E, Garcia SJ, Gomez Ribelles JL*, et al*. Biodegradable PCL scaffolds with an interconnected spherical pore network for tissue engineering. J.Biomed.Mater.Res.A. 2008;85:25-35.

78. Garcia-Giralt N, Izquierdo R, Nogues X, Perez-Olmedilla M, Benito P, Gomez-Ribelles JL*, et al*. A porous PCL scaffold promotes the human chondrocytes redifferentiation and hyaline-specific extracellular matrix protein synthesis. J.Biomed.Mater.Res.A. 2008;85:1082-9.

79. Li WJ, Danielson KG, Alexander PG, Tuan RS. Biological response of chondrocytes cultured in three-dimensional nanofibrous poly(epsilon-caprolactone) scaffolds. J.Biomed.Mater.Res.A. 2003;67:1105-14.

80. Thorvaldsson A, Stenhamre H, Gatenholm P, Walkenstrom P. Electrospinning of highly porous scaffolds for cartilage regeneration. Biomacromolecules 2008;9:1044-9.

81. Li WJ, Cooper JA,Jr, Mauck RL, Tuan RS. Fabrication and characterization of six electrospun poly(alpha-hydroxy ester)-based fibrous scaffolds for tissue engineering applications. Acta Biomater. 2006;2:377-85.

82. Tsai WB and Wang MC. Effects of an avidin-biotin binding system on chondrocyte adhesion and growth on biodegradable polymers. Macromol.Biosci. 2005;5:214-21.

83. Lee JW, Kim YH, Park KD, Jee KS, Shin JW, Hahn SB. Importance of integrin beta1-mediated cell adhesion on biodegradable polymers under serum depletion in mesenchymal stem cells and chondrocytes. Biomaterials 2004;25:1901-9.

84. Eyrich D, Wiese H, Maier G, Skodacek D, Appel B, Sarhan H*, et al*. In vitro and in vivo cartilage engineering using a combination of chondrocyte-seeded long-term stable fibrin gels and polycaprolactone-based polyurethane scaffolds. Tissue Eng. 2007;13:2207-18.

85. Fecek C, Yao D, Kacorri A, Vasquez A, Iqbal S, Sheikh H*, et al*. Chondrogenic Derivatives of Embryonic Stem Cells Seeded into 3D Polycaprolactone Scaffolds Generated Cartilage Tissue In Vivo. Tissue Eng.Part A. 2008; May 7th, Epub ahead of print.

86. Mohan N and Nair PD. Polyvinyl alcohol-poly(caprolactone) semi IPN scaffold with implication for cartilage tissue engineering. J.Biomed.Mater.Res.B.Appl.Biomater. 2008;84:584-94.

87. Oliveira JM, Rodrigues MT, Silva SS, Malafaya PB, Gomes ME, Viegas CA*, et al*. Novel hydroxyapatite/chitosan bilayered scaffold for osteochondral tissue-engineering applications: Scaffold design and its performance when seeded with goat bone marrow stromal cells. Biomaterials 2006;27:6123-37.

88. Li WJ, Tuli R, Huang X, Laquerriere P, Tuan RS. Multilineage differentiation of human mesenchymal stem cells in a three-dimensional nanofibrous scaffold. Biomaterials 2005;26:5158-66.

89. Huang Q, Goh JC, Hutmacher DW, Lee EH. In vivo mesenchymal cell recruitment by a scaffold loaded with transforming growth factor beta1 and the potential for in situ chondrogenesis. Tissue Eng. 2002;8:469-82.

90. Bunaprasert T, Thongmarongsri N, Thanakit V, Ruangvejvorachai P, Buranapraditkul S, Maneesri S*, et al*. Tissue engineering of cartilage with porous polycarprolactone--alginate scaffold: the first report of tissue engineering in Thailand. J.Med.Assoc.Thai. 2006;89 Suppl 3:S108-14.

91. Shao X, Goh JC, Hutmacher DW, Lee EH, Zigang G. Repair of large articular osteochondral defects using hybrid scaffolds and bone marrow-derived mesenchymal stem cells in a rabbit model. Tissue Eng. 2006;12:1539-51.

92. Cao T, Ho KH, Teoh SH. Scaffold design and in vitro study of osteochondral coculture in a three-dimensional porous polycaprolactone scaffold fabricated by fused deposition modeling. Tissue Eng. 2003;9 Suppl 1:S103-12.

93. Serrano MC, Portoles MT, Vallet-Regi M, Izquierdo I, Galletti L, Comas JV*, et al*. Vascular endothelial and smooth muscle cell culture on NaOH-treated poly(epsilon-caprolactone) films: a preliminary study for vascular graft development. Macromol.Biosci. 2005;5:415-23.

94. Perego G, Preda P, Pasquinelli G, Curti T, Freyrie A, Cenni E. Functionalization of poly-(L-lactic-co-epsilon-caprolactone): effects of surface modification on endothelial cell proliferation and hemocompatibility [corrected]. J.Biomater.Sci.Polym.Ed. 2003;14:1057-75.

95. Mei N, Chen G, Zhou P, Chen X, Shao ZZ, Pan LF*, et al*. Biocompatibility of Poly(epsilon-caprolactone) scaffold modified by chitosan--the fibroblasts proliferation in vitro. J.Biomater.Appl. 2005;19:323-39.

96. Cheng Z and Teoh SH. Surface modification of ultra thin poly (epsilon-caprolactone) films using acrylic acid and collagen. Biomaterials 2004;25:1991-2001.

97. Lebourg M, Sabater Serra R, Mas Estelles J, Hernandez Sanchez F, Gomez Ribelles JL, Suay Anton J. Biodegradable polycaprolactone scaffold with controlled porosity obtained by modified particle-leaching technique. J.Mater.Sci.Mater.Med. 2008;19:2047-53.

98. Xie J, Ihara M, Jung Y, Kwon IK, Kim SH, Kim YH*, et al*. Mechano-active scaffold design based on microporous poly(L-lactide-co-epsilon-caprolactone) for articular cartilage tissue engineering: dependence of porosity on compression force-applied mechanical behaviors. Tissue Eng. 2006;12:449-58.

99. Nagata M, Machida T, Sakai W, Tsutsumi N. Synthesis, characterization, and enzymatic degradation of network aliphatic copolyesters. 1999;37:2005-11.

100. Wang Y, Ameer GA, Sheppard BJ, Langer R. A tough biodegradable elastomer. Nat.Biotechnol. 2002;20:602-6.

101. Sundback CA, Shyu JY, Wang Y, Faquin WC, Langer RS, Vacanti JP*, et al*. Biocompatibility analysis of poly(glycerol sebacate) as a nerve guide material. Biomaterials 2005;26:5454-64.

102. Wang Y, Kim YM, Langer R. In vivo degradation characteristics of poly(glycerol sebacate). J.Biomed.Mater.Res.A. 2003;66:192-7.

103. Gao J, Crapo PM, Wang Y. Macroporous elastomeric scaffolds with extensive micropores for soft tissue engineering. Tissue Eng. 2006;12:917-25.

104. Radisic M, Park H, Martens TP, Salazar-Lazaro JE, Geng W, Wang Y*, et al*. Pre-treatment of synthetic elastomeric scaffolds by cardiac fibroblasts improves engineered heart tissue. J.Biomed.Mater.Res.A. 2007; 86(3): 713-24.

105. Gao J, Ensley AE, Nerem RM, Wang Y. Poly(glycerol sebacate) supports the proliferation and phenotypic protein expression of primary baboon vascular cells. J.Biomed.Mater.Res.A. 2007;83:1070-5.

106. Chen QZ, Bismarck A, Hansen U, Junaid S, Tran MQ, Harding SE*, et al*. Characterisation of a soft elastomer poly(glycerol sebacate) designed to match the mechanical properties of myocardial tissue. Biomaterials 2008;29:47-57.

107. Sales VL, Engelmayr GC,Jr, Johnson JA,Jr, Gao J, Wang Y, Sacks MS*, et al*. Protein precoating of elastomeric tissue-engineering scaffolds increased cellularity, enhanced extracellular matrix protein production, and differentially regulated the phenotypes of circulating endothelial progenitor cells. Circulation 2007;116:I55-63.

108. Fidkowski C, Kaazempur-Mofrad MR, Borenstein J, Vacanti JP, Langer R, Wang Y. Endothelialized microvasculature based on a biodegradable elastomer. Tissue Eng. 2005;11:302-9.

109. Motlagh D, Yang J, Lui KY, Webb AR, Ameer GA. Hemocompatibility evaluation of poly(glycerol-sebacate) in vitro for vascular tissue engineering. Biomaterials 2006;27:4315-24.

110. Crapo PM, Gao J, Wang Y. Seamless tubular poly(glycerol sebacate) scaffolds: High-yield fabrication and potential applications. J.Biomed.Mater.Res.A. 2007; 86(3): 354-63.

111. Nijst CL, Bruggeman JP, Karp JM, Ferreira L, Zumbuehl A, Bettinger CJ*, et al*. Synthesis and characterization of photocurable elastomers from poly(glycerol-co-sebacate). Biomacromolecules 2007;8:3067-73.

112. Neeley WL, Redenti S, Klassen H, Tao S, Desai T, Young MJ*, et al*. A microfabricated scaffold for retinal progenitor cell grafting. Biomaterials 2008;29:418-26.

113. Liu QY, Tian M, Ding T, Shi R, Feng YX, Zhang LQ*, et al*. Preparation and characterization of a thermoplastic poly(glycerol sebacate) elastomer by two-step method. J Appl Polym Sci 2007;103:1412-9.

114. Bettinger CJ, Orrick B, Misra A, Langer R, Borenstein JT. Microfabrication of poly (glycerol-sebacate) for contact guidance applications. Biomaterials 2006;27:2558-65.

115. Liu QY, Tian M, Shi R, Zhang LQ, Chen DF, Tian W. Structure and properties of thermoplastic poly(glycerol sebacate) elastomers originating from prepolymers with different molecular weights. J Appl Polym Sci 2007;104:1131-7.

CHAPTER 4

DESIGNED SCAFFOLD PERMEABILITY FOR CARTILAGE REGENERATION

In designing 3D cartilage scaffolds, the hope would be that there is an optimum window of structural feature sizes that both mimic the mechanical properties of articular cartilage and allow for optimal tissue in growth. Some groups state their hypothesis that providing maximum porosity will promote tissue in growth.[1] Though this may be true for bone tissue engineering, it must be understood that for cartilage tissue engineering this increase in porosity correlates with an increase in permeability, contradicting a number of findings. Clinically, healthy cartilage has relatively *low* permeability, and increases in permeability are correlated with disease and deterioration. Basic science has shown that decreases in permeability with tissue depth correlates with a rise in proteoglycan content.[2] And in tissue engineering studies, cartilage grows in anaerobic conditions where oxygen diffusion is *low*.[3-5]

Many groups have measured the permeability of bovine cartilage in order to characterize the tissue or quantify changes due to diseases or injuries.[6-13] Compared to the permeability of hard tissues, such as cancellous bone (.002 – 2 x 10^{-8} m^4/Ns) or

cortical bone (.79 – 9 x 10^{-12} m^4/Ns), soft tissues including intervertebral disc (1.2-1.9 x 10^{-15} m^4/Ns), meniscus (0.6 x 10^{-15} m^4/Ns), ligament (1-6 x 10^{-16} m^4/Ns), and articular cartilage (0.1 – 2.0 x 10^{-15} m^4/Ns) exhibit relatively low permeability.[14] In reference to disease and damage, an increase in permeability of articular cartilage results in greater and more rapid deformation of tissue.[15, 16] Alexopoulos *et al.*[17] developed a finite element model to show that lower permeability in the pericellular matrix of healthy cartilage reduces local fluid fluxes that are increased in osteoarthritic tissue. They suggest that chondrocytes are sensitive to these changes in the pericellular matrix. Changes in fluid movement, as governed by tissue permeability, affect nutrient transport, hydrodynamic lubrication, mechanical signaling, and cellular level shear stresses. This finding is not only important for clinicians studying disease state, but is also relevant to the design of tissue engineering scaffolds.

4.1 TISSUE ENGINEERING AND PERMEABILITY

Reproducible fabrication of specific scaffold designs through SFF enables us to study how structural features can influence cartilage regeneration. Most studies to date have examined the effects that pore size, pore shape, or interconnectivity have on tissue production by chondrocytes in vitro. Some studies show that a larger pore size, higher porosity, or increased connectivity (all presumably related to increased permeability) support better migration and higher proliferation of cells, greater amounts of GAG-deposition, and increased collagen II content.[18-20] One study that reports improved chondrocyte proliferation, higher metabolic activity and more overall GAG with increasing pore size, also shows that when this increased GAG is normalized to DNA

content, there is no significant difference, suggesting that the increased GAG content per construct is most likely just due to increased cellularity.[18] Another study reports that although increased pore size results in higher GAG/DNA content on a more hydrophilic polymer composition, this is not seen in more hydrophobic scaffolds.[19] Additionally, Malda *et al*.[21] show no effect of pore size on GAG content in vitro, but demonstrate that in vivo an increased pore size produces greater amounts of GAG. The studied effects of these structural properties on chondrogenically-pulsed mesenchymal stem cells seeded into nonwoven fibrous meshes, shows that an increase in porosity and pore size (resulting in a measured increase in gas permeability) supports more rapid proliferation, and greater synthesis and retention of GAG.[22]

In contrast, there is evidence showing that structural properties that would presumably decrease permeability show more favorable results for chondrogenesis. Beginning in 1973, Reddi and Huggins show that closed tubes (versus open tubes) favor chondrogenesis over osteogenesis, concluding that higher oxygen and nutrient supply favor the latter.[23] Yoon *et al.*[24] show that chondrocytes seeded in denser alginate gels produce more collagen II and IGF-1 mRNA expression. They hypothesize that this could be due to an increase in the diffusional resistance of soluble molecules. Pore size effects on chondrogenesis show that a smaller pore size is most favorable, with one study showing increases in the percentage of cells that remain spherical in shape and increases in GAG/DNA on a 20μm pore size.[25] And, although another study shows that their smallest pore size of 13μm produces a thicker layer of cartilage and greater amounts of GAG, the sGAG content per DNA is not different, nor was the amount of collagen

accumulated per cell.[4] Finally, Kuboki *et al*. suggested that smaller pores are more favorable for chondrogenesis when they saw endochondral ossification on 90-120 μm pores and direct bone formation on 350 μm pores.[26]

Taken together, these studies demonstrate that there is no consensus on how the structural properties of pore size, porosity, and interconnectivity affect chondrogenesis. Li *et al.*, however, prove that none of these properties (also including pore distribution, fenestration size and distribution, and orientation of pores) can be used individually to describe mass transport. Instead, they suggest that "one conventional physical parameter", permeability, be used as a description of the complicated porous structures encountered in the process of tissue engineering.[27] In this work, we examine how the physical property of permeability, as described by Darcy's law, affects chondrocytes or bone marrow stromal cells seeded onto PCL scaffolds and cultured *in vitro*, with the hypothesis that this parameter can be used to more accurately predict the effects of scaffold architecture on chondrogenesis.

4.2 ONE EXPLANATION: OXYGEN TENSION

One explanation for the effects that scaffold permeability has on cartilage tissue regeneration is described by its correlation with oxygen tension. In native tissue, oxygen tensions follow the same trend as permeability, where embryonic cartilage exhibits low oxygen levels (5-10%) [5, 28, 29] in contrast to bone (~25%).[30] In normal conditions, chondrocytes are living in an environment with low oxygen supply. And, it is proposed that increases in oxygen levels (hyperoxia) may result in the disturbance of chondrocytic

metabolism. In their review on the effects of oxygen tension on cartilage tissue, Malda *et al.*[5] conclude that "low oxygen induces production of cartilage specific components and structure of the extracellular matrix, whereas hyperoxia disturbs chondrocyte metabolism and inhibits production of proteoglycans." This statement, however, is surrounded by much scientific controversy.

In response to variations in partial oxygen pressure chondrocytes produce abnormal levels of reactive oxygen species (ROS), including nitric oxide (NO) and superoxide anion (0_2^-). These ROS, and the derivative radicals that they generate, have effects on intracellular signaling, chondrocyte apoptosis, and matrix synthesis and breakdown. In normal cartilage ROS are produced at low levels in response to a low oxygen environment, where they are positively involved in the control of cellular functions. Equilibrium between ROS production and intracellular antioxidants is modulated, in part, by oxygen tension in the tissue. In joint diseases, such as osteoarthritis and rheumatoid arthritis, ROS are produced in greater amounts, resulting in oxidative stresses that cause degradation of cellular membranes, nucleic acids, proteoglycans and collagens, resulting in deterioration of the tissue.[31]

Herontin *et al*.[31] explain that the exposure of chondrocytes to H_2O_2 (a ROS derivative) inhibits proteoglycan and DNA synthesis. However, there is evidence of both inhibitory and stimulatory oxygen effects on chondrocyte maintenance or redifferentiation of chondrocytes in monolayer and 3D in vitro environments. Oxygen tensions in these studies are imposed through variations in overall oxygen supply to the in vitro

environment, from .1%, 1% or 5% (low oxygen conditions, similar to that of healthy cartilage) to 20 or 21% (high oxygen conditions).

De-differentiated chondrocytes favor low oxygen supply for redifferentiation in 3D culture, where studies show increased proteoglycan synthesis, upregulation of collagen 2 and aggrecan, and down-regulation of collagen 1.[32-35] However, these effects are not seen with the same cells cultured in monolayer. [33, 35] There are conflicting effects of oxygen tensions on differentiated chondrocytes in 3D and monolayer culture. Most studies support the hypothesis that decreased oxygen levels mimic natural cartilage, showing increases in collagen 2, better shape, cellular distribution, tissue smoothness, proteoglycan content, and decreased collagen 1 expression.[36-41] However, there are a couple of studies that contradict these findings, showing decreases in collagen 2 and matrix production at low oxygen levels, and increases in GAG in response to high oxygen levels.[42-45] Also of note are studies that show no chondrogenic differences in response to changes in oxygen tension, suggesting that these cells are insensitive to these variations.[46, 47] In support of our hypothesis that lower permeability will enhance matrix production by chondrocytes, Malda *et al.*[5] state that "low oxygen conditions *in vitro* mimic the *in vivo* cartilage environment, and are thus likely to be a specific stimulus, decreasing dedifferentiation during expansion and enhancing redifferentiation of chondrocytes *in vitro*."

A number of studies have also looked at the effects of imposed oxygen tensions on differentiation of BMSCs down a chondrogenic lineage. Kanichai *et al.*[48] report

increased collagen 2 and proteoglycan deposition in response to low oxygen tension. Robins *et al.*[49] support this finding in 3D, reporting an increase in sox 9, collagen 2, and aggrecan, and furthermore, revealing that these upregulations are accompanied by an increase in nuclear accumulation of a hypoxia-inducible factor (HIF-1α).

Oxygen tension in 3D-designed scaffolds is inherently varied through designed changes in permeability. However, nobody has studied the effects of controlled scaffold permeability on chondrogenesis by chondrocytes or bone marrow stromal cells as seen in Chapter 7. In Chapter 7, differences in matrix production and cartilage-specific gene expression by chondrocytes and BMSCs, seen in relation to changes in permeability, may be explained in part by correlating variations in oxygen tension caused by the designed changes in permeability of these scaffolds.

References

1. Gauvin C, Azizeh Y, Reignier J, Huneault M, DiRaddo R, Fernandes J. A biomechanical approach to design and fabrication of 3D scaffolds in functional tissue engineering. (unpublished), submitted 2005.

2. Maroudas . Permeability of articular cartilage. 1968;219:1260.

3. Yoo JU, Barthel TS, Nishimura K, Solchaga L, Caplan AI, Goldberg VM*, et al*. The chondrogenic potential of human bone-marrow-derived mesenchymal progenitor cells. J.Bone Joint Surg.Am. 1998;80:1745-57.

4. Bhardwaj T, Pilliar RM, Grynpas MD, Kandel RA. Effect of material geometry on cartilagenous tissue formation in vitro. J.Biomed.Mater.Res. 2001;57:190-9.

5. Malda J, Martens DE, Tramper J, van Blitterswijk CA, Riesle J. Cartilage tissue engineering: controversy in the effect of oxygen. Crit.Rev.Biotechnol. 2003;23:175-94.

6. Soltz MA and Ateshian GA. Interstitial fluid pressurization during confined compression cyclical loading of articular cartilage. Ann.Biomed.Eng. 2000;28:150-9.

7. Soltz MA and Ateshian GA. Experimental verification and theoretical prediction of cartilage interstitial fluid pressurization at an impermeable contact interface in confined compression. J.Biomech. 1998;31:927-34.

8. Williamson AK, Chen AC, Sah RL. Compressive properties and function-composition relationships of developing bovine articular cartilage. J.Orthop.Res. 2001;19:1113-21.

9. Ateshian GA, Warden WH, Kim JJ, Grelsamer RP, Mow VC. Finite deformation biphasic material properties of bovine articular cartilage from confined compression experiments. J.Biomech. 1997;30:1157-64.

10. Bursac PM, Obitz TW, Eisenberg SR, Stamenovic D. Confined and unconfined stress relaxation of cartilage: appropriateness of a transversely isotropic analysis. J.Biomech. 1999;32:1125-30.

11. Demarteau O, Pillet L, Inaebnit A, Borens O, Quinn TM. Biomechanical characterization and in vitro mechanical injury of elderly human femoral head cartilage: comparison to adult bovine humeral head cartilage. Osteoarthritis Cartilage 2006; 14(6): 589-96.

12. Klein TJ, Chaudhry M, Bae WC, Sah RL. Depth-dependent biomechanical and biochemical properties of fetal, newborn, and tissue-engineered articular cartilage. J.Biomech. 2005; 40(1): 182-90.

13. Mow VC, Ratcliffe A, Poole AR. Cartilage and diarthrodial joints as paradigms for hierarchical materials and structures. Biomaterials 1992;13:67-97.

14. Sander EA and Nauman EA. Permeability of musculoskeletal tissues and scaffolding materials: experimental results and theoretical predictions. Crit.Rev.Biomed.Eng. 2003;31:1-26.

15. Klippel JH, Weyand CM, Crofford LJ, Stone JH, Arthritis Foundation. Primer on the rheumatic diseases. Atlanta, Ga.: Arthritis Foundation 2001.

16. Mansour JM. Biomechanics of Cartilage. In: Kinesiology: The Mechanics and Pathomechanics of Human Movement. C. A. Oatis, Ed. Philadelphia: Lippincott Williams and Wilkins, 2003, pp: 66-79.

17. Alexopoulos LG, Setton LA, Guilak F. The biomechanical role of the chondrocyte pericellular matrix in articular cartilage. Acta Biomater. 2005;1:317-25.

18. Griffon DJ, Sedighi MR, Schaeffer DV, Eurell JA, Johnson AL. Chitosan scaffolds: interconnective pore size and cartilage engineering. Acta Biomater. 2006;2:313-20.

19. Miot S, Woodfield T, Daniels AU, Suetterlin R, Peterschmitt I, Heberer M*, et al*. Effects of scaffold composition and architecture on human nasal chondrocyte redifferentiation and cartilaginous matrix deposition. Biomaterials 2005;26:2479-89.

20. Freed LE, Marquis JC, Nohria A, Emmanual J, Mikos AG, Langer R. Neocartilage formation in vitro and in vivo using cells cultured on synthetic biodegradable polymers. J.Biomed.Mater.Res. 1993;27:11-23.

21. Malda J, Woodfield TB, van der Vloodt F, Wilson C, Martens DE, Tramper J*, et al*. The effect of PEGT/PBT scaffold architecture on the composition of tissue engineered cartilage. Biomaterials 2005;26:63-72.

22. Mukherjee DP, Smith DF, Rogers SH, Emmanual JE, Jadin KD, Hayes BK. Effect of 3D-microstructure of bioabsorbable PGA:TMC scaffolds on the growth of chondrogenic cells. J.Biomed.Mater.Res.B.Appl.Biomater. 2008; Jun 10, Epub ahead of print.

23. Reddi AH and Huggins CB. Influence of geometry of transplanted tooth and bone on transformation of fibroblasts. Proc.Soc.Exp.Biol.Med. 1973;143:634-7.

24. Yoon DM, Hawkins EC, Francke-Carroll S, Fisher JP. Effect of construct properties on encapsulated chondrocyte expression of insulin-like growth factor-1. Biomaterials 2007;28:299-306.

25. Nehrer S, Breinan HA, Ramappa A, Young G, Shortkroff S, Louie LK*, et al*. Matrix collagen type and pore size influence behaviour of seeded canine chondrocytes. Biomaterials 1997;18:769-76.

26. Kuboki Y, Jin Q, Kikuchi M, Mamood J, Takita H. Geometry of artificial ECM: sizes of pores controlling phenotype expression in BMP-induced osteogenesis and chondrogenesis. Connect.Tissue Res. 2002;43:529-34.

27. Li SH, de Wijn JR, Layrolle P, de Groot K. Accurate geometric characterization of macroporous scaffold of tissue engineering. 2003;240-2:541-5.

28. Lund-Olesen K. Oxygen tension in synovial fluids. Arthritis Rheum. 1970;13:769-76.

29. Falchuk KH, Goetzl EJ, Kulka JP. Respiratory gases of synovial fluids. An approach to synovial tissue circulatory-metabolic imbalance in rheumatoid arthritis. Am.J.Med. 1970;49:223-31.

30. Woodhouse CF. An Instrument for the Measurement of Oxygen Tension in Bone - a Preliminary Report. 1961;43:819-28.

31. Henrotin YE, Bruckner P, Pujol JP. The role of reactive oxygen species in homeostasis and degradation of cartilage. Osteoarthritis Cartilage 2003;11:747-55.

32. Malda J, van Blitterswijk CA, van Geffen M, Martens DE, Tramper J, Riesle J. Low oxygen tension stimulates the redifferentiation of dedifferentiated adult human nasal chondrocytes. Osteoarthritis Cartilage 2004;12:306-13.

33. Kurz B, Domm C, Jin M, Sellckau R, Schunke M. Tissue engineering of articular cartilage under the influence of collagen I/III membranes and low oxygen tension. Tissue Eng. 2004;10:1277-86.

34. Murphy CL and Sambanis A. Effect of oxygen tension and alginate encapsulation on restoration of the differentiated phenotype of passaged chondrocytes. Tissue Eng. 2001;7:791-803.

35. Domm C, Schunke M, Christesen K, Kurz B. Redifferentiation of dedifferentiated bovine articular chondrocytes in alginate culture under low oxygen tension. Osteoarthritis Cartilage 2002;10:13-22.

36. Hansen U, Schunke M, Domm C, Ioannidis N, Hassenpflug J, Gehrke T*, et al*. Combination of reduced oxygen tension and intermittent hydrostatic pressure: a useful tool in articular cartilage tissue engineering. J.Biomech. 2001;34:941-9.

37. Nagel-Heyer S, Goepfert C, Adamietz P, Meenen NM, Portner R. Cultivation of three-dimensional cartilage-carrier-constructs under reduced oxygen tension. J.Biotechnol. 2006;121:486-97.

38. Saini S and Wick TM. Effect of low oxygen tension on tissue-engineered cartilage construct development in the concentric cylinder bioreactor. Tissue Eng. 2004;10:825-32.

39. Schneider N, Lejeune JP, Deby C, Deby-Dupont GP, Serteyn D. Viability of equine articular chondrocytes in alginate beads exposed to different oxygen tensions. Vet.J. 2004;168:167-73.

40. Wernike E, Li Z, Alini M, Grad S. Effect of reduced oxygen tension and long-term mechanical stimulation on chondrocyte-polymer constructs. Cell Tissue Res. 2008;331: 473-83.

41. Pawelek JM. Effects of thyroxine and low oxygen tension on chondrogenic expression in cell culture. Dev.Biol. 1969;19:52-72.

42. Grimshaw MJ and Mason RM. Modulation of bovine articular chondrocyte gene expression in vitro by oxygen tension. Osteoarthritis Cartilage 2001;9:357-64.

43. Grimshaw MJ and Mason RM. Bovine articular chondrocyte function in vitro depends upon oxygen tension. Osteoarthritis Cartilage 2000;8:386-92.

44. Murphy CL and Sambanis A. Effect of oxygen tension on chondrocyte extracellular matrix accumulation. Connect.Tissue Res. 2001;42:87-96.

45. Clark CC, Tolin BS, Brighton CT. The effect of oxygen tension on proteoglycan synthesis and aggregation in mammalian growth plate chondrocytes. J.Orthop.Res. 1991;9:477-84.

46. Malda J, van den Brink P, Meeuwse P, Grojec M, Martens DE, Tramper J*, et al*. Effect of oxygen tension on adult articular chondrocytes in microcarrier bioreactor culture. Tissue Eng. 2004;10:987-94.

47. Schneider N, Mouithys-Mickalad A, Lejeune JP, Duyckaerts C, Sluse F, Deby-Dupont G*, et al*. Oxygen consumption of equine articular chondrocytes: Influence of applied oxygen tension and glucose concentration during culture. Cell Biol.Int. 2007;31:878-86.

48. Kanichai M, Ferguson D, Prendergast PJ, Campbell VA. Hypoxia promotes chondrogenesis in rat mesenchymal stem cells: a role for AKT and hypoxia-inducible factor (HIF)-1alpha. J.Cell.Physiol. 2008;216:708-15.

49. Robins JC, Akeno N, Mukherjee A, Dalal RR, Aronow BJ, Koopman P*, et al*. Hypoxia induces chondrocyte-specific gene expression in mesenchymal cells in association with transcriptional activation of Sox9. Bone 2005;37:313-22.

CHAPTER 5

CHARACTERIZATION OF 3D-DESIGNED MELT CAST POLY(ε-CAPROLACTONE) SCAFFOLDS FOR CARTILAGE TISSUE ENGINEERING

5.1 Introduction

Polycaprolactone (PCL), an FDA approved, biodegradable, nontoxic polymer has gained popularity in the field of tissue engineering over the past decade. PCL's slow degradation profile coupled with its strong mechanical properties make it ideal for applications in bone and drug delivery, where it has commonly been applied. Recently, this material is being used in a wider range of applications, including osteochondral repair, spinal cord regeneration, bone, cartilage, smooth muscle, blood vessel, and bladder grafting. Here, we concentrate on its applications for cartilage tissue engineering.

Commercially available PCL is being fabricated in a variety of ways for tissue engineering applications. Methods include fused deposition modeling,[1-6] photopolymerization,[7] precision extruding deposition,[8, 9] three dimensional printing,[10] low temperature deposition,[11] multi-nozzle freeform deposition,[12, 13] shape-deposition,[14] selective laser sintering,[15-17] drop-on-demand printing,[18] salt leaching and melt casting. Each fabrication process has unique advantages and disadvantages, along with unique

material properties that are often reported as being solely dependent on scaffold design (pore size, porosity, fiber size) for each fabrication method.

When applying any of the aforementioned fabrication it is desirable to create scaffolds that have mechanical properties similar to the tissue being regenerated. Here we focus on matching the equilibrium aggregate modulus (H_A) of a scaffold to that of native articular cartilage. By matching target H_A values of articular cartilage, the scaffold will withstand physiological loading, produce the mechanical tension generated within the cell cytoskeleton critical for cell shape and function, and mimic stiffness values that may affect cell to cell contacts and aggregation.[19] Furthermore, when the scaffold (with or without tissue) is implanted into a defect site, there should ideally be no stiffness differences between healthy cartilage and regenerating tissue. Differences in tissue mechanical properties may cause fibrous tissue formation, elevated levels of strain in the adjacent cartilage, and acceleration of degeneration of the tissue.[20] There are two components that determine the final effective scaffold stiffness: 1) the base material stiffness and 2) the scaffold pore architecture. Since pore geometry may be restricted by tissue in growth requirements, it would be advantageous to also alter effective scaffold stiffness by altering the base material stiffness. With a specific focus on the fabrication method of melt casting, here we characterize how the processing parameters of molecular weight and melt-casting temperature may be used to alter the H_A of PCL scaffolds for cartilage applications. We also demonstrate the importance of mechanically testing PCL at physiological temperatures in order to obtain accurate H_A values for in vivo applications.

Integration of image-based design and analysis (IBEA) techniques{{318 Hollister,S.J. 2000; 301 Hollister,S.J. 2005}} with solid freeform fabrication (SFF) of scaffolds is advantageous as an engineering choice that can exploit the control and variability of mechanical properties of synthetic polymers. When matching mechanical properties of scaffolds to native tissue properties, IBEA-SFF grants us the ability to accurately determine mechanical properties of scaffold designs through finite element analysis (FEA), simply by knowing the bulk material properties polymers that can be used for scaffold fabrication. Here we show that we can use the aggregate modulus values of solid PCL cylinders in order to accurately predict that aggregate modulus values of various scaffold designs from the computational design phase through the actual fabricated scaffold.

It is also important to fully characterize 3D designed scaffolds in terms of their structural properties before carrying these fabrication processes into clinical applications. Here we characterize the contraction of melt-cast PCL caused by post-processing of the scaffolds in ethanol. When designing custom scaffolds modeled from MRI or CT images of specific patient defects, it is important to compensate for any change un structural dimensions that may be altered during processing, such as swelling or contraction of the material.

The importance of fully and accurately characterizing the mechanical and structural properties of 3D designed scaffolds, and determining means by which these properties

can be altered for specific clinical applications is evident. Here we show that the aggregate modulus values of melt-cast PCL scaffolds are not significantly altered through changes in molecular weight (within the ranges of 25 kDa to 50 kDa) or melt-casting temperature (with the ranges of 110°C to 150°C). However, in carrying out these experiments, we demonstrate the importance of performing these mechanical tests at physiological temperatures, characterize the contraction of this material in ethanol, and provide support for the use of FEA programs in order to non-destructively predict the mechanical properties of SFF scaffolds.

5.2 Materials and Methods

Fabrication of solid PCL cylinders

Solid PCL cylinders (approximately 3 mm height, 6.35mm diameter, n=15 per group, total = 180 cylinders) were made by placing PCL pellets (25, 37, 43 kDa) (Solvay Caprolactones, Warrington, Cheshire, UK, product #s 6250, 6400, 6430), or PCL powder (50kDa) (Polysciences Inc., Warrington, PA. CAT# 19561) into a Teflon mold which was then melted (110°C, 130°C, or 150°C, 1 Torr, 5 hours). Preliminary work done melting PCL at 90°C showed that at this lower temperature, the PCL did not fully settle, and as shown through μCT imaging, air bubbles were present throughout the cylinder. This group was therefore excluded from further study. After melting, the Teflon mold was removed from the oven and allowed to cool at room temperature for 24 hours. For accurate mechanical testing, two parallel surfaces were created using a Polycut machine (Leica, Inc., Deerfield, IL). Cylinders were then soaked in 70% EtOH

for 24 hours followed by soaking in phosphate buffered saline (ph 7.4, GIBCO) for 12 hours prior to mechanical testing.

A second series of solid PCL cylinders were fabricated with the same polymer molecular weight and melting parameters as scaffold fabrication (37kDa, 115°C, 1 Torr, 120 minutes). The bulk mechanical properties from these cylinders were used for finite element analysis calculations described below.

Fabrication of 3D Designed Scaffolds

Three-dimensional (3D)-designed scaffolds (3mm height, 6.85mm diameter, 1mm spherical pores) were designed using custom Interactive Data Language™ programs (IDL; Research Systems, Inc., Boulder, CO). Scaffolds were designed with 100% interconnected, 1mm, spherical pores with variations in throat size between pores that resulted in three design porosities (54%, 63%, 70%) Inverse wax molds of the designs were built on a Solidscape MM2 3D printer (SolidScape Inc., Merrimack, NH). Scaffolds were made by pressing inverse wax molds directly into melted 37kDa polycaprolactone (CAPA 6400, Solvay Caprolactones, Warrington, Cheshire, UK). Briefly, PCL pellets were placed into a Teflon mold, and melted (115°C, 1 Torr, 120 minutes). After melting and air bubble removal, the Teflon mold was pulled from the oven, and allowed to cool for 270 seconds at room temperature until it reached 80°C (just below the melting temperature of the wax molds). At this time, inverse wax molds were pressed into the melted PCL, and the entire construct was cooled overnight. The wax was then dissolved from the PCL using 100% EtOH. A schematic of this process was shown in Figure 3.3.

Scaffolds were designed for future studies on the effects of permeability on tissue regeneration, and are therefore referred to as a "low, mid and high" permeability designs.

Although it is necessary to heat PCL to higher temperatures in order to eliminate air bubbles, by allowing melted PCL to cool to 80°C before casting the wax mold into the material, we eliminate the need for production of a secondary hydroxyapatite scaffold previously used to manufacture these scaffolds in our lab. [22]

Mechanical Testing of Solid cylinders and 3D designed scaffolds

Stress relaxation testing was performed in confined compression using an MTS Alliance RT30 electromechanical test frame (MTS Systems Corp., MN), following a protocol established by Guilak *et al.*[23] and used extensively in the field by others.[24, 25] Following a preload (0.67 N (solid cylinders) or .22 N (scaffolds), 600s hold) the crosshead was lowered to 10% strain at .25μm/s, and then held at constant displacement for 30 minutes. Cylinders were tested at 37°C, in PBS and scaffolds were tested at both 37°C, in PBS and room temperature in PBS.

The stress relaxation behavior was characterized using a quasi-linear viscoelastic model. The nonlinear elastic portion was modeled using a 1D model commonly used in biomechanics:

$$T = A\left(e^{B\varepsilon} - 1\right)$$

Where T is the 1st Piola-Kirchoff stress used for large deformation, e is the large strain, and A, B are model constants fit to experimental data. The reduced relaxation function was approximated using a three term Prony series of the form:

$$G(t) = c_0 + c_1 e^{-\frac{t}{\tau_1}} + c_2 e^{-\frac{t}{\tau_2}}$$

Where G represents the reduced relaxation function, t is time, and c_0, c_1, c_2, τ_1, and τ_2 are model constants fit to experimental data. The model constants c_0, c_1, and c_2 are further required to satisfy the constraint:

$$c_0 + c_1 + c_2 = 1$$

Using the reduced relaxation function and elastic response stress as a function of time is calculated as:

$$T(t) = \int_0^t \left(c_0 + c_1 e^{\frac{\tau - t}{\tau_1}} + c_2 e^{\frac{\tau - t}{\tau_2}} \right) ABe^{B\varepsilon} \frac{d\varepsilon}{d\tau} d\tau$$

Where $\frac{d\varepsilon}{d\tau}$ is the strain rate and the other parameters are as defined previously. The stress T(t) can be calculated for the ramp strain test. The model constants A, B c_0, c_1, c_2, τ_1, and τ_2 were fit to experimental data using a custom written MATLAB program that

utilizes the nonlinear programming algorithm fmincon. The aggregate modulus (H_A) is computed as the stress divided by strain at the end of the ramp.

Finite element analysis on scaffold designs

Complete anisotropic effective stiffness constants were calculated using the voxel-based homogenization software VOXELCON (Quint Corp, Tokyo, Japan), as described previously.[15] Briefly, voxel models were created of both the design input STL files of scaffold designs and the voxelized μCT scans of actual fabricated scaffolds for each design. STL files were first converted to .vox files, and then .jpeg files. Microview was used to select a repeating periodic region of interest (ROI) within the STL file, and the ROI was exported in .png format, and then converted to a .raw image. This .raw image was imported into VOXELCON for finite element analysis. The μCT scanned scaffold images were imported into Microview and a ROI was selected from the center point of the scaffold. This ROI was exported in .png format and the same sequence of routines was performed as were on the STL files. For the finite element analysis, PCL aggregate modulus values from mechanical testing results of solid cylinders were converted to elastic modulus values using the equation described by:

$$H_A = \frac{Ev}{(1+v)(1-2v)} + \frac{2E}{3(1-2v)}$$

Where E = elastic modulus, ν = Poisson's ratio. These elastic modulus values were input into VOXELCON, with a Poisson's ratio of 0.2, and run on scaffold designs. VOXELCON output an effective elastic modulus and effective Poisson's ratio for each design that was then input back into the equation to determine the effective aggregate

modulus (H_A) of each scaffold design for each molecular weight and curing temperature tested.

Measuring Contraction of PCL

Contraction of melt-cast PCL was measured for solid PCL cylinders and 3D-designed scaffolds. Cylinders and scaffolds were scanned dry using a MS-130 high resolution micro-computed tomography (μCT) scanner (GE Medical Systems, Toronto, CAN) at 16 μm voxel resolution, 75kV and 75mA. GEMS Microview software was used to analyze μCT data. 3D designed scaffolds (n=5) were scanned at three phases throughout processing: after the wax mold had been cast into PCL material and after removal of wax mold during a 30h EtOH soak. Changes in outer diameter and overall porosity are reported.

In Vitro Experiment

As proof that these scaffolds can be used for cartilage regeneration, scaffolds (n=4 for each of 3 designs) were seeded with fresh porcine chondrocytes, harvested from metacarpophalangeal joints of domestic pigs (Northwest Market, Northwest, MI). 3.2 x 10^6 chondrocytes were suspended in 50μl of type 1 rat tail collagen (stock concentration: 5.9 mg/ml, BD Biosciences, # 354236) and subsequently seeded into each PCL scaffold (cell density = 64 x 10^6 cells/ml). The collagen was gelled for 30 minutes at 37°C before scaffolds were removed from the custom Teflon seeding mold, and placed into wells of media (DMEM, 10%FBS, 1% P/S, 0.1mM Non-essential Amino Acids, 50 μg/ml 2-phospho-L-ascorbic acid, 0.4 mM proline, 5ug/ml insulin). Scaffold+collagen gel+cells

were grown in vitro (37°C, 5% CO_2) on an orbital shaker. After 2 weeks, scaffolds were removed, fixed in zinc formaldehyde (ZFIX, Anatech, Battle Creek, MI) overnight, dehydrated in EtOH washes, and paraffin embedded. Sections were stained with Safranin-O (with a Fast green counter stain) to illustrate GAG production.

Statistical Analysis

Statistical analysis, including 2-way ANOVA and student t-tests, were performed in SPSS software (SPSS for Windows, Rel 14.0. 2005 Chicago: SPSS Inc.).

5.3. Results

Mechanical Variations due to Melting Temperature and Molecular Weight

PCL solid cylinders and 3D-designed scaffolds both exhibited stress-relaxation profiles, as seen in Figure 5.1. In the ranges used for this study, variations in melting temperature (110°C - 150°C) and molecular weight (25kDa-50kDa) show no significant trends for altering the equilibrium aggregate modulus of bulk PCL (two-way ANOVA) (Table 5.1 and Figure 5.2). There were also no significant differences within melt temperature groups with regards to changes in molecular weight, or within molecular weight groups with regards to changes in melt temperature.

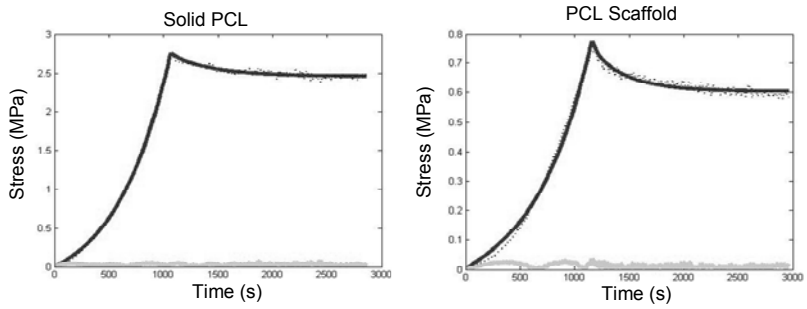

Figure 5.1. Solid PCL cylinders and 3D-designed PCL scaffolds both exhibit stress-relaxation profiles.

Table 5.1. Equilibrium aggregate modulus of solid melt-cast PCL (25, 37, 43 or 50 kDa)cylinders processed at various melting temperatures (110°C, 130°C, 150°C).

Aggregate Modulus (MPa)				
Melt Temperature (°C)	Solid Cylinder (n=7, n=6*)			
110	39.06 ± 12.83	43.99 ± 6.55*	39.05 ± 9.96	41.82 ± 6.18
130	42.78 ± 10.45	28.75 ± 7.45*	33.28 ± 8.34	33.56 ± 8.38*
150	41.99 ± 13.41*	32.78 ± 10.66	27.42 ± 7.11	32.39 ± 6.70
	25	37	43	50
	PCL Molecular Weight (kDa)			

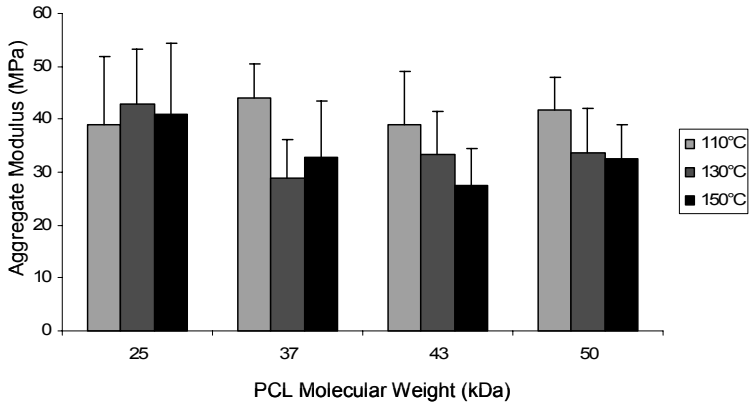

Figure 5.2. Variations in processing parameters (molecular weight or melting temperature) of melt-cast PCL show no significant trends for altering the aggregate modulus of the bulk material.

Mechanical variations between room temperature and 37°C testing

Significant increases in aggregate modulus (One way ANOVA, linear regression) are seen when scaffolds are tested in stress relaxation at room temperature (21°C) versus

testing done at a physiological temperature of 37°C (Figure 5.3). Changes in testing temperature from 21°C to 37°C cause a 3.1 MPa increase in aggregate modulus (0.2 MPa / °C) across all groups ($R^2 = 0.91$, $p \leq 0.01$). This demonstrates the importance of testing biomaterial scaffolds at a physiological temperature for in vivo applications.

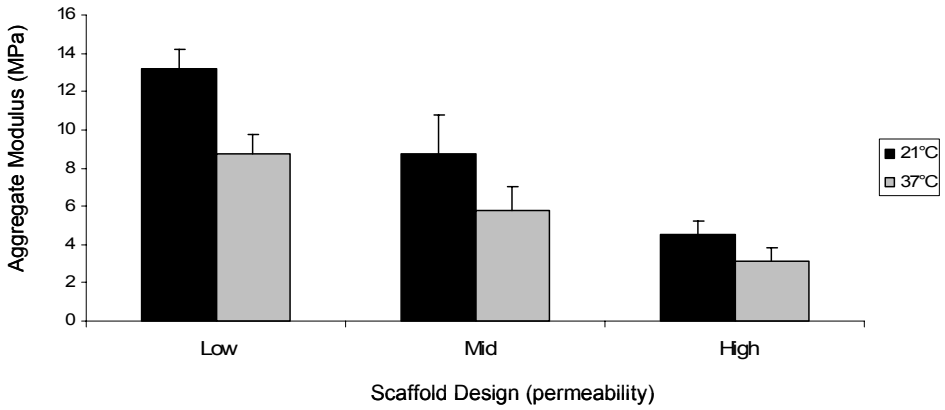

Figure 5.3. Stress-relaxation testing performed at room temperature causes significant increases in the aggregate modulus of PCL scaffolds (0.2 MPa/°C).

Contraction of PCL Scaffolds

Processing in ethanol (EtOH) causes PCL scaffolds to contract significantly. Figure 5.4 illustrates representative uCT images of a scaffold before and after EtOH soaking. Changes in scaffold outer diameter can be seen in Table 5.2. Interestingly, there was no contraction of solid cylinders as measured by calipers after ethanol soaking.

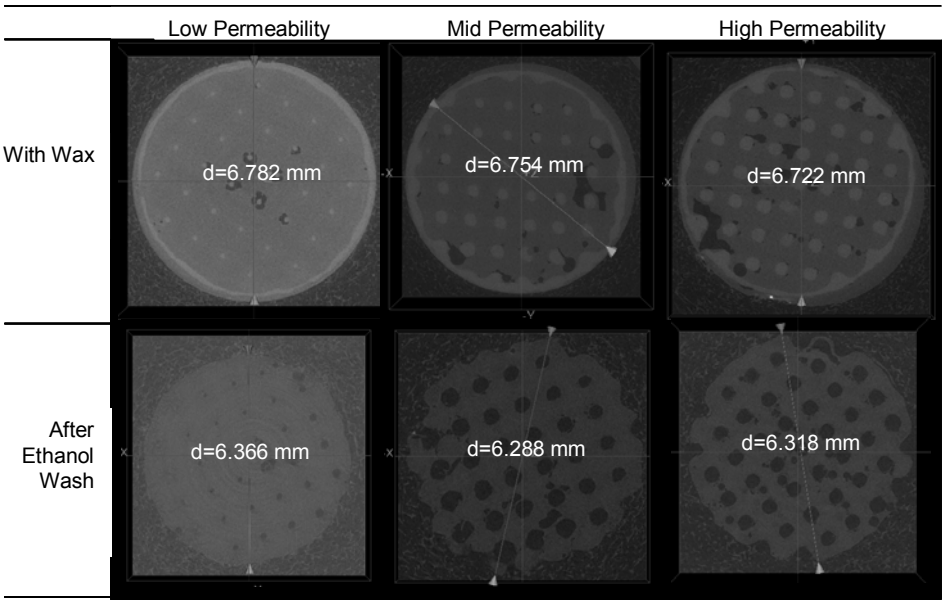

Figure 5.4. Contraction of PCL scaffolds after washing in 100% ethanol as measured by µCT.

Table 5.2. Contraction of PCL in ethanol causes changes in diameter and porosity of 3D scaffolds.

	37 kDa PCL Scaffolds (n=5)		
Scaffold Design	**Start diameter (mm)**	**Δ Outer diameter (mm)**	**Δ Outer diameter (%)**
Low	6.782 ± .03	.422 ± .05	6.222 ± .70
Mid	6.754 ± .06	.466 ± .08	6.910 ± 1.16
High	6.722 ± .07	.404 ± .05	6.01 ± .77
		Overall	
	6.753 ± .06	.431 ± .06	6.38 ± .96

Finite Element Analysis to predict aggregate modulus

FEA was used to calculate aggregate modulus values of scaffold design files and µCT images of actual scaffolds using a bulk material H_A determined through stress-relaxation tests performed on solid cylinders of PCL (17.21 MPa) Table 5.2 displays computational and experimental H_A values of the three PCL scaffolds used . Aggregate moduli computed by FEA on design files and on uCT images correlated well with the experimentally measured moduli (R^2 = 0.9764 , R^2 = 0.9811, respectively) (Figure 5.5). Image-based FEA models created directly from µCT scans matched experimental moduli values more closely, as these images accounted for the contraction of PCL, which

resulted in increased volume fraction. This verifies the ability of image-based FEA to compute scaffold stiffness without the need for destructive testing. Testing the actual PCL scaffolds both experimentally and computationally validates the computationally predicted aggregate modulus data relative to the experimentally determined compressive modulus data for both design files and μCT images.

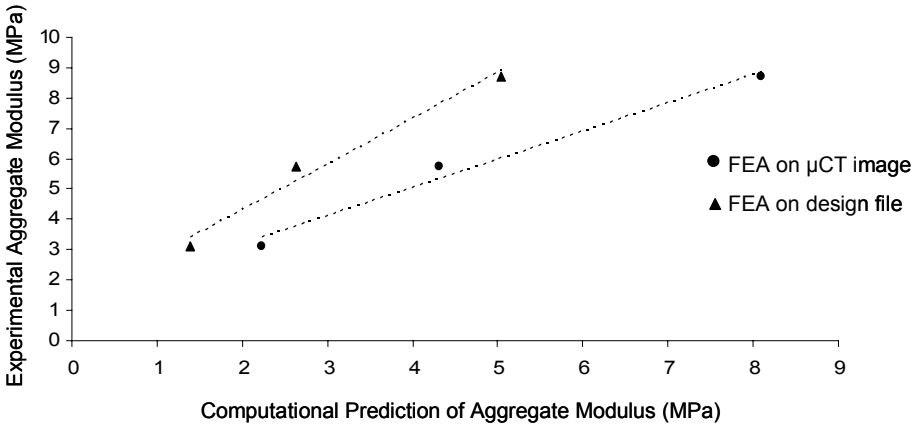

Figure 5.5. Correlations between experimentally measured aggregate modulus values and computational FEA predictions of design files (R^2 = 0.9764) and μCT images (R^2 = .9811) show that stiffness of scaffolds can be predicted without the use of destructive mechanical testing.

In Vitro Experiment

A histological image seen in Figure 5.6 confirms the presence of sGAG and other cartilage proteins after 2 weeks in vitro culture of scaffolds seeded with chondrocytes embedded in a collagen I hydrogel. Safranin O staining is present throughout the scaffold in varying intensities.

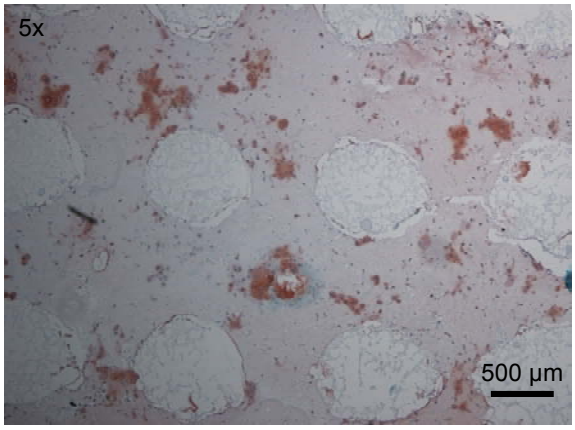

Figure 5.6. Chondrocytes seeded within collagen 1 hydrogel produce cartilaginous matrix on 3D designed, melt cast PCL scaffolds after 2 weeks in vitro.

5.4 Discussion and Conclusion

Synthetic materials offer increased control and variation over scaffold mechanical properties. Solid freeform fabrication (SFF) of scaffolds is an ideal fabrication choice that can exploit this control and variability. In terms of matching mechanical properties of scaffolds to native tissue properties, SFF grants the ability to accurately determine mechanical properties of scaffold designs through finite element analysis, simply by knowing the bulk material properties of the polymers that can be used for scaffold fabrication. SFF also provides many benefits specific to cartilage tissue engineering. On a global scale, it enables design and fabrication of anatomically shaped scaffolds. For osteochondral applications, it allows creation of biphasic scaffolds that incorporate multiple geometries into a single scaffold [26, 27] allowing for in-growth of multiple tissues into a single structure. Particularly beneficial for articular cartilage applications, it allows creation of zones of organization within a single tissue compartment.[28] Native cartilage exhibits a superficial zone (elongated and flattened chondrocytes arranged in fascicles parallel to the surface), an intermediate zone (round chondrocytes randomly distributed),

and a deep zone (chondrocytes arranged in short columns)[29] SFF allows the incorporation of distinctly designed architectural zones into a single scaffold, allowing recapitulation of this native organizational scheme. More locally, SFF allows for precise control of internal architectures, such as pore size, pore shape, interconnectivity and porosity. This increased control, over conventional methods, creates excellent reproducibility of intricate architectures, providing obvious benefits to basic science research and clinical applications. Within the field of tissue engineering research, it enables us to study how various scaffold architectures may affect cell infiltration, mass transport of nutrients and metabolic waste, and thereby influence tissue regeneration. Several authors have reviewed the advantages of SFF techniques currently in use for a wide array of applications. [1, 13, 30-40]

The repair strategy that this work aims to achieve using SFF is described by Hutmacher *et al*. as "strategy 1" in which "the physical scaffold structure supports the polymer/cell/tissue construct from the time of cell seeding up to the point where the tissue transplant is remodeled by the host tissue."[1] Although scaffold mechanical properties can be changed by altering porosities and pore sizes, these changes also affect tissue regeneration in complicated manners. The ability to match initial properties through changes in bulk material properties is an advantageous route to pursue.

Studies have demonstrated that, due to influences on setting behavior, both molecular weight and preparation temperatures have an effect on polymer mechanical properties. A study on poly(acrylic acid) shows that compressive and tensile mechanical properties are

increased with increasing additive molecular weight.[41] Nicholson *et al.* [42] show that the elastic properties, inelastic elongation behavior, and tensile strength of an advanced polymer (LaRC™-SI) are affected by processing temperature and molecular weight, where Young's modulus and tensile strength decrease with increasing temperatures, and tensile strength increases with increasing molecular weight. The ability to predict and vary the performance of PCL scaffolds based on intrinsic material properties is highly desirable. Unfortunately, aggregate modulus values of solid PCL cylinders are not significantly altered when the processing parameters of molecular weight and melting temperature are varied. Although even higher molecular weight PCL could be explored, for melt casting it is likely too viscous at 80°C to be successfully cast.

Accurate assessment of melt-cast PCL scaffolds is necessary in order to ensure that the scaffold properties are within the range of articular cartilage. Although it seems natural to mechanically test scaffolds for in vivo applications at physiological temperatures, it is not always done, probably due to the more intricate set-up involved. This work shows the importance of mechanically testing PCL at physiological temperatures for medical applications where the material will be implanted. An increase from 21°C to 37°C cause a significant change (3.1 MPa) in aggregate modulus that should not be overlooked.

Finite element analysis can be used to accurately predict the aggregate modulus of scaffolds based on known bulk material properties of melted PCL. When designing more intricate architectures or creating custom implants, prediction of scaffold properties

(whether on a design file or on a μCT image) through FEA will allow non-destructive mechanical analysis of a specific construct.

Ethanol is often used for processing of scaffolds, as shown here to dissolve wax, or in many instances to sterilize implants. Here, we find that EtOH causes significant contraction of 37 kDa PCL, due to molecular compaction of the carbon chain or a change in bond structure when placed in a polar solution. In separate work, it was found that 50kDa powder PCL exhibited the same contraction profile. When designing custom scaffolds it will be important to compensate for contraction of material seen in this study. Computational up scaling of the scaffold implant could be applied to fix this change, or a less polar solvent, that does not cause contraction, can be investigated for removal of wax (note: acetone was also investigated, but caused warping and deterioration of the PCL scaffolds before wax was dissolved out). Compensating for the contraction of PCL is also important in situations where the material will be placed in a polar in vivo environment. For instance, Yu *et al*.[43] document contraction of PCL in bladder applications, where the material is in contact with urine.

PCL has been shown to be compatible with a variety of cells types. Osteoblasts,[7, 44] smooth muscle cells,[45] fibroblasts,[3, 46, 47] bone marrow stromal cells,[14, 48] HGFs,[15] and chondrocytes[49-51] are among the cells that have been seeded onto PCL scaffolds for skeletal tissue engineering applications. Focusing specifically on cartilage applications, studies have shown encouraging cellular infiltration, redifferentiation, and proliferation of chondrocytes on PCL in vitro.[50, 52-55] Eyrich *et al.* found that seeding cells into PCL

scaffolds through encapsulating them in fibrin gel increased both the seeding efficiency and the homogenous matrix distribution.[56] Furthermore, both in vitro and in vivo studies have shown abundant proteoglycans and type II collagen expression on PCL scaffolds seeded with chondrocytes, embryonic stem cells, and bone marrow-derived mesenchymal stem cells (with the latter two induced to differentiate down a chondrogenic lineage by culture in specific differentiation medias).[51, 56-63] Oliveria *et al.* report better biocompatibility compared to PGA scaffolds where they see lack of tissue in center of scaffolds possibly due to acidic by products.[60] PCL scaffolds have also been applied for use in osteochondral sites where studies show promising results in terms of bone growth, cartilage growth and integration.[64, 65] Here we demonstrate that cartilaginous tissue can be produced throughout 3D-designed melt-cast PCL scaffolds when chondrocytes are seeded within collagen 1 hydrogel.

Melt-casting of PCL shows promise for use in cartilage tissue engineering research. Aside from its mentioned applications for regeneration of articular defects, it also provides a cheap, easy, organic-solvent-less fabrication method for studying the effects that scaffold architectures, mechanical properties, or surface modifications may have on tissue regeneration.

Acknowledgements

Funding for this project provided by the National Science Foundation (GSRF) and a Regenerative Medicine Training Grant (T90 DK070071) and NIH RO1 DE 13608. Thank you to Kristen Wolfe and Annie Mitsak for contraction studies on 50kDa PCL and

for investigation of acetone as an alternative solvent. Thank you to Jon Ong for preliminary work that eliminated use of 90°C cylinders.

References

1. Hutmacher DW. Scaffolds in tissue engineering bone and cartilage. Biomaterials 2000;21:2529-43.

2. Hutmacher DW. Scaffold design and fabrication technologies for engineering tissues--state of the art and future perspectives. J.Biomater.Sci.Polym.Ed. 2001;12:107-24.

3. Hutmacher DW, Schantz T, Zein I, Ng KW, Teoh SH, Tan KC. Mechanical properties and cell cultural response of polycaprolactone scaffolds designed and fabricated via fused deposition modeling. J.Biomed.Mater.Res. 2001;55:203-16.

4. Rohner D, Hutmacher DW, Cheng TK, Oberholzer M, Hammer B. In vivo efficacy of bone-marrow-coated polycaprolactone scaffolds for the reconstruction of orbital defects in the pig. J.Biomed.Mater.Res.B.Appl.Biomater. 2003;66:574-80.

5. Zein I, Hutmacher DW, Tan KC, Teoh SH. Fused deposition modeling of novel scaffold architectures for tissue engineering applications. Biomaterials 2002;23:1169-85.

6. Ramanath HS, Chua CK, Leong KF, Shah KD. Melt flow behaviour of poly-epsilon-caprolactone in fused deposition modelling. J.Mater.Sci.Mater.Med. 2008;19:2541-50.

7. Kweon H, Yoo MK, Park IK, Kim TH, Lee HC, Lee HS*, et al*. A novel degradable polycaprolactone networks for tissue engineering. Biomaterials 2003;24:801-8.

8. Hoque ME, Hutmacher DW, Feng W, Li S, Huang MH, Vert M*, et al*. Fabrication using a rapid prototyping system and in vitro characterization of PEG-PCL-PLA scaffolds for tissue engineering. J.Biomater.Sci.Polym.Ed. 2005;16:1595-610.

9. Wang F, Shor L, Darling A, Sun W, Guceri S, Lau A. Precision extruding deposition and characterization of cellular poly-e-caprolactone tissue scaffolds. 2003 Solid Freeform Fabrication Symposium.

10. Wu BM, Borland SW, Giordano RA, Cima LG, Sachs EM, Cima MJ. Solid free-form fabrication of drug delivery devices. J Controlled Release 1996;40:77,78-87.

11. Xiong Z, Yan Y, Wang S, Zhang R, Zhang C. Fabrication of porous scaffolds for bone tissue engineering via low-temperature deposition. Scripta Materialia 2002;46:771,772-776.

12. Sun W, Darling A, Starly B, Nam J. Computer-aided tissue engineering: overview, scope and challenges. Biotechnol.Appl.Biochem. 2004;39:29-47.

13. Sun W and Lal P. Recent development on computer aided tissue engineering--a review. Comput.Methods Programs Biomed. 2002;67:85-103.

14. Marra KG, Szem JW, Kumta PN, DiMilla PA, Weiss LE. In vitro analysis of biodegradable polymer blend/hydroxyapatite composites for bone tissue engineering. J.Biomed.Mater.Res. 1999;47:324-35.

15. Williams JM, Adewunmi A, Schek RM, Flanagan CL, Krebsbach PH, Feinberg SE*, et al*. Bone tissue engineering using polycaprolactone scaffolds fabricated via selective laser sintering. Biomaterials 2005;26:4817-27.

16. Wiria FE, Leong KF, Chua CK, Liu Y. Poly-epsilon-caprolactone/hydroxyapatite for tissue engineering scaffold fabrication via selective laser sintering. Acta Biomater. 2007;3:1-12.

17. Tan KH, Chua CK, Leong KF, Cheah CM, Gui WS, Tan WS*, et al*. Selective laser sintering of biocompatible polymers for applications in tissue engineering. Biomed.Mater.Eng. 2005;15:113-24.

18. Mondrinos MJ, Dembzynski R, Lu L, Byrapogu VK, Wootton DM, Lelkes PI*, et al*. Porogen-based solid freeform fabrication of polycaprolactone-calcium phosphate scaffolds for tissue engineering. Biomaterials 2006;27:4399-408.

19. Lu L, Zhu X, Valenzuela RG, Currier BL, Yaszemski MJ. Biodegradable polymer scaffolds for cartilage tissue engineering. Clin.Orthop.Relat.Res. 2001;(391 Suppl):S251-70.

20. Beaupre GS, Stevens SS, Carter DR. Mechanobiology in the development, maintenance, and degeneration of articular cartilage. J.Rehabil.Res.Dev. 2000;37:145-51.

21. Hollister SJ. Porous scaffold design for tissue engineering. Nat.Mater. 2005;4:518-24.

22. Mantila SM, Williams JM, Krebsbach PH, Hollister SJ. Pore size effects of polycaprolactone scaffolds on in vivo bone tissue engineering. 2006;52 Annual Meeting:Poster # 839.

23. Guilak F, Best BA, Ratcliffe A, Mow VC. Instrumentation for load and displacement controlled studies on soft connective tissues. 1989;AMD 98:113-6.

24. Soltz MA and Ateshian GA. Experimental verification and theoretical prediction of cartilage interstitial fluid pressurization at an impermeable contact interface in confined compression. J.Biomech. 1998;31:927-34.

25. Ateshian GA, Warden WH, Kim JJ, Grelsamer RP, Mow VC. Finite deformation biphasic material properties of bovine articular cartilage from confined compression experiments. J.Biomech. 1997;30:1157-64.

26. Schek RM, Taboas JM, Segvich SJ, Hollister SJ, Krebsbach PH. Engineered osteochondral grafts using biphasic composite solid free-form fabricated scaffolds. Tissue Eng. 2004;10:1376-85.

27. Taboas JM, Maddox RD, Krebsbach PH, Hollister SJ. Indirect solid free form fabrication of local and global porous, biomimetic and composite 3D polymer-ceramic scaffolds. Biomaterials 2003;24:181-94.

28. Woodfield TB, Van Blitterswijk CA, De Wijn J, Sims TJ, Hollander AP, Riesle J. Polymer scaffolds fabricated with pore-size gradients as a model for studying the zonal organization within tissue-engineered cartilage constructs. Tissue Eng. 2005;11:1297-311.

29. Ross MH and Pawlina W. Histology : a text and atlas : with correlated cell and molecular biology. Baltimore, MD: Lippincott Williams & Wilkins 2006.

30. He C, Xia L, Luo Y, Wang Y. The application and advancement of rapid prototyping technology in bone tissue engineering. Sheng Wu Yi Xue Gong Cheng Xue Za Zhi 2004;21:871-5.

31. Hutmacher DW, Sittinger M, Risbud MV. Scaffold-based tissue engineering: rationale for computer-aided design and solid free-form fabrication systems. Trends Biotechnol. 2004;22:354-62.

32. Leong KF, Cheah CM, Chua CK. Solid freeform fabrication of three-dimensional scaffolds for engineering replacement tissues and organs. Biomaterials 2003;24:2363-78.

33. Mironov V. Toward human organ printing: Charleston Bioprinting Symposium. ASAIO J. 2006;52:e27-30.

34. Moroni L, de Wijn JR, van Blitterswijk CA. Integrating novel technologies to fabricate smart scaffolds. J.Biomater.Sci.Polym.Ed. 2008;19:543-72.

35. Morsi YS, Birchall IE, Rosenfeldt FL. Artificial aortic valves: an overview. Int.J.Artif.Organs 2004;27:445-51.

36. Peltola SM, Melchels FP, Grijpma DW, Kellomaki M. A review of rapid prototyping techniques for tissue engineering purposes. Ann.Med. 2008;40:268-80.

37. Stevens B, Yang Y, Mohandas A, Stucker B, Nguyen KT. A review of materials, fabrication methods, and strategies used to enhance bone regeneration in engineered bone tissues. J.Biomed.Mater.Res.B.Appl.Biomater. 2008;85:573-82.

38. Weigel T, Schinkel G, Lendlein A. Design and preparation of polymeric scaffolds for tissue engineering. Expert Rev.Med.Devices 2006;3:835-51.

39. Yang S, Leong KF, Du Z, Chua CK. The design of scaffolds for use in tissue engineering. Part II. Rapid prototyping techniques. Tissue Eng. 2002;8:1-11.

40. Yeong WY, Chua CK, Leong KF, Chandrasekaran M. Rapid prototyping in tissue engineering: challenges and potential. Trends Biotechnol. 2004;22:643-52.

41. Majekodunmi AO, Deb S, Nicholson JW. Effect of molecular weight and concentration of poly(acrylic acid) on the formation of a polymeric calcium phosphate cement. 2003;14:747-52.

42. Nicholson LM, Whitley KS, Gates TS, Hinkley JA. Influence of molecular weight on the mechanical performance of a thermoplastic glassy polyimide. J.Mater.Sci. 2000;35:6111-21.

43. Yu DS, Lee CF, Chen HI, Chang SY. Bladder wall grafting in rats using salt-modified and collagen-coated polycaprolactone scaffolds: preliminary report. Int.J.Urol. 2007;14:939-44.

44. Coombes AG, Rizzi SC, Williamson M, Barralet JE, Downes S, Wallace WA. Precipitation casting of polycaprolactone for applications in tissue engineering and drug delivery. Biomaterials 2004;25:315-25.

45. Sung HJ, Meredith C, Johnson C, Galis ZS. The effect of scaffold degradation rate on three-dimensional cell growth and angiogenesis. Biomaterials 2004;25:5735-42.

46. Tang ZG and Hunt JA. The effect of PLGA doping of polycaprolactone films on the control of osteoblast adhesion and proliferation in vitro. Biomaterials 2006;27:4409-18.

47. Oh SH, Park IK, Kim JM, Lee JH. In vitro and in vivo characteristics of PCL scaffolds with pore size gradient fabricated by a centrifugation method. Biomaterials 2007;28:1664-71.

48. Li WJ, Tuli R, Okafor C, Derfoul A, Danielson KG, Hall DJ*, et al*. A three-dimensional nanofibrous scaffold for cartilage tissue engineering using human mesenchymal stem cells. Biomaterials 2005;26:599-609.

49. Izquierdo R, Garcia-Giralt N, Rodriguez MT, Caceres E, Garcia SJ, Gomez Ribelles JL*, et al*. Biodegradable PCL scaffolds with an interconnected spherical pore network for tissue engineering. J.Biomed.Mater.Res.A. 2008;85:25-35.

50. Garcia-Giralt N, Izquierdo R, Nogues X, Perez-Olmedilla M, Benito P, Gomez-Ribelles JL*, et al*. A porous PCL scaffold promotes the human chondrocytes redifferentiation and hyaline-specific extracellular matrix protein synthesis. J.Biomed.Mater.Res.A. 2008;85:1082-9.

51. Li WJ, Danielson KG, Alexander PG, Tuan RS. Biological response of chondrocytes cultured in three-dimensional nanofibrous poly(epsilon-caprolactone) scaffolds. J.Biomed.Mater.Res.A. 2003;67:1105-14.

52. Thorvaldsson A, Stenhamre H, Gatenholm P, Walkenstrom P. Electrospinning of highly porous scaffolds for cartilage regeneration. Biomacromolecules 2008;9:1044-9.

53. Li WJ, Cooper JA,Jr, Mauck RL, Tuan RS. Fabrication and characterization of six electrospun poly(alpha-hydroxy ester)-based fibrous scaffolds for tissue engineering applications. Acta Biomater. 2006;2:377-85.

54. Tsai WB and Wang MC. Effects of an avidin-biotin binding system on chondrocyte adhesion and growth on biodegradable polymers. Macromol.Biosci. 2005;5:214-21.

55. Lee JW, Kim YH, Park KD, Jee KS, Shin JW, Hahn SB. Importance of integrin beta1-mediated cell adhesion on biodegradable polymers under serum depletion in mesenchymal stem cells and chondrocytes. Biomaterials 2004;25:1901-9.

56. Eyrich D, Wiese H, Maier G, Skodacek D, Appel B, Sarhan H*, et al*. In vitro and in vivo cartilage engineering using a combination of chondrocyte-seeded long-term stable fibrin gels and polycaprolactone-based polyurethane scaffolds. Tissue Eng. 2007;13:2207-18.

57. Fecek C, Yao D, Kacorri A, Vasquez A, Iqbal S, Sheikh H*, et al*. Chondrogenic Derivatives of Embryonic Stem Cells Seeded into 3D Polycaprolactone Scaffolds Generated Cartilage Tissue In Vivo. Tissue Eng.Part A. 2008; May 7, Epub ahead of print.

58. Lin CH, Su JM, Hsu SH. Evaluation of type II collagen scaffolds reinforced by poly(epsilon-caprolactone) as tissue-engineered trachea. Tissue Eng.Part C.Methods 2008;14:69-77.

59. Mohan N and Nair PD. Polyvinyl alcohol-poly(caprolactone) semi IPN scaffold with implication for cartilage tissue engineering. J.Biomed.Mater.Res.B.Appl.Biomater. 2008;84:584-94.

60. Oliveira JM, Rodrigues MT, Silva SS, Malafaya PB, Gomes ME, Viegas CA*, et al*. Novel hydroxyapatite/chitosan bilayered scaffold for osteochondral tissue-engineering applications: Scaffold design and its performance when seeded with goat bone marrow stromal cells. Biomaterials 2006;27:6123-37.

61. Li WJ, Tuli R, Huang X, Laquerriere P, Tuan RS. Multilineage differentiation of human mesenchymal stem cells in a three-dimensional nanofibrous scaffold. Biomaterials 2005;26:5158-66.

62. Huang Q, Goh JC, Hutmacher DW, Lee EH. In vivo mesenchymal cell recruitment by a scaffold loaded with transforming growth factor beta1 and the potential for in situ chondrogenesis. Tissue Eng. 2002;8:469-82.

63. Bunaprasert T, Thongmarongsri N, Thanakit V, Ruangvejvorachai P, Buranapraditkul S, Maneesri S*, et al*. Tissue engineering of cartilage with porous polycarprolactone--alginate scaffold: the first report of tissue engineering in Thailand. J.Med.Assoc.Thai. 2006;89 Suppl 3:S108-14.

64. Shao X, Goh JC, Hutmacher DW, Lee EH, Zigang G. Repair of large articular osteochondral defects using hybrid scaffolds and bone marrow-derived mesenchymal stem cells in a rabbit model. Tissue Eng. 2006;12:1539-51.

65. Cao T, Ho KH, Teoh SH. Scaffold design and in vitro study of osteochondral coculture in a three-dimensional porous polycaprolactone scaffold fabricated by fused deposition modeling. Tissue Eng. 2003;9 Suppl 1:S103-12.

CHAPTER 6

TAILORING THE MECHANICAL PROPERTIES OF 3D-DESIGNED POLY(GLYCEROL SEBACATE) SCAFFOLDS FOR CARTILAGE APPLICATIONS

6.1 Introduction

Polymer scaffolds will play a key role in treating cartilage defects, deterioration, and damage caused by aging, disease and trauma. There are a number of synthetic materials and a wide range of fabrication methods being applied to make such scaffolds, with the general acceptance that these constructs should be biocompatible, biodegradable, and mechanically stable. Here, we focus on the requirement that a scaffold should have mechanical properties, particularly tangent modulus values, in the range of native cartilage values. There are two components that determine the final effective scaffold stiffness: 1) the base material stiffness and 2) the scaffold pore architecture. Since pore geometry may be restricted by tissue in-growth requirements, it would be advantageous to also alter effective scaffold stiffness by altering the base material stiffness. We show how the processing conditions of poly(glycerol sebacate) (PGS) can be varied to tailor the mechanical properties of three-dimensionally designed, solid-freeform fabricated (SFF) scaffolds for cartilage tissue engineering.

Poly(glycerol sebacate) has recently been applied for tissue engineering. Synthesis and characterization of the polymer, created through a polycondensation reaction of glycerol and sebacic acid, was first reported for use in biotechnology and bioengineering in 2002[1] to provide good mechanical properties and rubberlike elasticity, established degradation and crosslinking mechanisms optimal for soft tissue engineering applications. Along with being tougher, less expensive and more flexible than existing biodegradable elastomers, glycerol and polymers containing sebacic acid have been approved by the US Food and Drug Administration for medical applications. To date, PGS has been studied for applications in nerve guidance,[2] soft tissue regeneration,[3, 4] vascular and myocardial tissue regeneration,[5-9] blood vessel reconstruction,[10, 11] drug delivery,[12] and in the replacement of photoreceptor cells.[13] PGS is a biodegradable polymer with biocompatibility and mechanical properties that make it well suited for applications such as those mentioned above and, as we show here, for use in cartilage tissue engineering.

PGS is processed through first creating a prepolymer, and then curing the prepolymer at high temperatures to obtain a thermoset elastomeric polymer. Most studies have fabricated the polymer through conventional methods, creating films or porogen-leached sponges. The most advanced structures reported are tubular sheets and films developed as scaffolds for blood vessels renal tubules or various ducts.[10, 11] In this work, we demonstrate the ability to process PGS using SFF techniques in order to create scaffolds with designed pore shapes, pore sizes, porosities, and architectures. In the past, this fabrication has been widely used in our lab in order to make designed scaffolds from poly(l-lactide acid), poly(lactic-co-glycolic acid), poly(ε-caprolactone), hydroxyapatite,

poly(propylene-fumarate), and poly(propylene-fumarate)/tri-calcium phosphate blends.[14-23] for applications in bone regeneration, spinal cord reconstruction, and cartilage tissue engineering. Because most of these materials, when fabricated into 3D designed scaffolds, exhibit mechanical properties that are outside the ranges of cartilage, we have more recently applied this technology to more elastomeric materials, such as poly(glycerol sebacate) (PGS) and poly(1,8-octanedial-co-citrate) (POC) for cartilage tissue engineering applications.[24] We believe that the mechanical properties of these materials make them ideal for use in fabricating scaffolds for load bearing articular sites. Fabrication of PGS by this means is not yet reported.

One of the main advantages of using PGS for tissue engineering is that its mechanical properties can be tailored to match specific tissue properties through altering processing parameters during the prepolymer and/or curing steps. In 2008, Chen *et al.* demonstrated the ability to alter the mechanical properties of PGS for myocardial tissue applications through changing curing temperature, recording Young's modulus values of .056 MPa (110°C), .22MPa (120°C), and 1.2MPa (130°C).[7] In this work we evaluate how changing the molar ratios of glycerol: sebacic acid during pre-polymer synthesis and how changing the curing time causes variations in non-linear elastic mechanical properties.

The purpose of this chapter is to assess PGS as a scaffolding material for cartilage tissue engineering by determining how synthesis conditions affect both bulk PGS properties and those of PGS scaffolds with designed architecture. Since PGS applications for cartilage regeneration have not been previously reported, we further demonstrate that PGS

scaffolds support robust cartilage formation when seeded with porcine chondrocytes in vitro.

6.2 Materials and Methods

Fabrication of Solid Cylinders and 3D-designed scaffolds

Pre-polymer synthesis

PGS pre-polymer (pPGS) was synthesized following methods described by Gao *et al.*[4] For this research, three batches of pPGS were synthesized with various molar ratios of sebacic acid:glycerol (3:4, 1:1, 4:3). Sebacic acid and glycerol were reacted under N_2 at 120°C. After 24 hours, the N_2 was removed and a vacuum of 50mTorr was pulled for an additional 48 hours, with a condenser attached.

Polymer Curing

Curing of pre-polymer was done through a modified protocol[4] that enabled fabrication of designed architecture scaffolds from wax molds. To create solid cylinders for mechanical testing, the pre-polymer was poured into a Teflon mold, and cured for various time points (24h w/out vacuum plus 24h, 48h, or 72h with a 100mTorr vacuum). A three-dimensional (3D) scaffold (3mm height, 6.35mm diameter, 1mm spherical pores, 54% porosity) was designed using custom Interactive Data Language™ programs (IDL; Research Systems, Inc., Boulder, CO).[15, 16] To fabricate designed scaffolds, pPGS was poured into a Teflon mold, and an inverse hydroxyapatite (HA) mold was pressed into the pPGS. HA molds were fabricated following a protocol previously established in the lab, with inverse HA molds made on a SolidScape printer (SolidScape Inc., Merrimack,

NH). [25] The Teflon/pPGS/HA mold unit was placed within a vacuum oven to cure at 150°C. For the first 24 hours, no vacuum was pulled, in order to allow the prepolymer to begin to cure, preventing air bubbles from forming in the polymer when a vacuum is pulled. After 24 hours, a strong vacuum (100 mTorr) was pulled, and the temperature was maintained at 150°C for 24, 48 or 72 hours longer. The HA+PGS construct was removed from the cup, and the HA was dissolved out using a rapid decalcifying agent (RDO, Apex Engineering, Aurora, IL) to achieve the final PGS scaffold. The schematic of this process was shown in Figure 3.5. PGS scaffolds and cylinders were autoclaved and rinsed overnight in DMEM before mechanical testing or chondrocyte seeding. Note, curing times reported in the results section refer to the hours cured after a vacuum was pulled (24, 48 and 72).

Micro-computed tomography image analysis

In order to assess defects and create images for finite element analysis (FEA), solid cylinders and scaffolds were scanned using a MS-130 high resolution μCT scanner (GE Medical Systems, Toronto, CAN) at a 16 μm voxel resolution. Scans were performed in air at 75 kV and 75 mA. GEMS Microview software (GE Medical Systems, Toronto, CAN) was used to view reconstructed images.

Mechanical Testing

Solid cylinders and 3D-designed scaffolds were tested in compression using an MTS Alliance RT30 electromechanical test frame (MTS Systems Corp., MN).

Stress-Relaxation in Confined Compression

Stress-relaxation tests were performed in confined compression following a protocol established by Guilak *et al.* in 1989 [26] and used extensively in the field by others.[27, 28] Briefly, pre-soaked samples were loaded into a confining cylindrical chamber filled with a phosphate buffered saline solution controlled at 37°C. A porous indenter was lowered until a reading of .05lb was output on the computer, signifying that the indenter was in contact with the cylinder or scaffold. This load was held for 600s and assumed to be the 0% strain position. Under displacement control, stress-relaxation testing was performed with a single ramp of 20% strain applied at 0.25 μm/s or 5 μm/min. The crosshead was then held at constant displacement for 30 min to record relaxation.

Unconfined Compression

Unconfined compression tests were performed on solid cylinders (n = 5-10 for each group, with variation in sample size due to exclusion of poorly made cylinders) under displacement control. Samples were compressed to failure in the z-direction between two fixed steel platens at a rate of 2 mm/min after a preload of .05 lb was applied. A single set of 3D-designed scaffolds were fabricated (n=7) (1:1 molar ratio, 48h cure time) and tested in unconfined compression in order to validate FEA predictions.

Finite Element Analysis

Complete anisotropic effective stiffness constants were calculated using the voxel-based homogenization software VOXELCON (Quint Corp, Tokyo, Japan), as described previously in.[23] STL design files were converted to .vox files, and PGS modulus values

from mechanical testing of solid cylinders (3 molar ratios x 3 curing temperatures) were input into VOXELCON, with a Poisson's ratio of 0.3, and run on scaffold designs.

In Vitro Study

Chondrocyte harvest

Cartilage was harvested from fresh metacarpophalangeal joints of domestic pigs obtained from a local abattoir (Northwest Market, Northwest, MI). Cartilage pieces were digested in a digest solution [DMEM high glucose, serum free, 1 mg/ml collagenase II (Sigma # C1764), 2% Pen/strep, 2% kanamycin (Roche, 12728700), and .2% Fungizone (Invitrogen, 15290-018)] on a stir plate for 6 hours at 37°C, 5% CO_2. The solution was then filtered through sterile nylon. Cells were spun at 2000rpm for 8 minutes, and plated overnight on tissue culture polystyrene in DMEM + 10%FBS + 1% P/S + 50 µg/ml 2-phospho-L-ascorbic acid (BioChemika, 49752). The following day, cells were trypsinized and immediately suspended in collagen gel for scaffold seeding.

Cell seeding and in vitro culture

PGS scaffolds were sterilized in an autoclave and presoaked in DMEM for 24 hours prior to cell seeding. Chondrocytes were suspended in a composite 5% Hyaluronic Acid (HyA) (stock concentration: 2.7 mg/ml in 0.8M NaCl, MW: 3 x 10^6 Da: Hyalogic LLC, Edwardsville, KS) info)/collagen I gel (stock concentration: 5.9 mg/ml, BD Biosciences, #354236) at ~30 x 10^6 cells/ml. 4% v/v .5M sodium hydroxide with 220 mg/ml sodium bicarbonate was used to increase the pH of the collagen/HyA/cell suspension just before seeding into the scaffolds in order to create gelling at 37°C. Cells were evenly seeded into

scaffolds by using a custom designed Teflon mold. After gelling (~30 minutes), scaffolds were removed from the mold. Scaffold + Cells + Gel constructs were cultured in an incubator (37°C, 5% CO_2) in 24-well plates on an orbital shaker for 2 weeks. Media (DMEM, 10%FBS, 1% P/S, 0.1mM Non-essential Amino Acids, 50 µg/ml 2-phospho-L-ascorbic acid, 0.4 mM proline, 5ug/ml insulin) was changed every other day. After 2 weeks, scaffolds (n=2) were removed, fixed in 10% buffered formalin phosphate (Fisher, SF100-20) overnight, dehydrated in EtOH washes, and paraffin embedded. Sections were stained with Alcian Blue to illustrate GAG production.

sGAG quantification

At 2 weeks, scaffolds (n=3) were removed from culture, finely chopped, and placed immediately into 1 ml of papain solution (papain, 1X PBS, cysteine HCL, EDTA, pH=6.0; mixed for 3h at 37°C then filtered). Scaffolds were digested in papain for 24 hours and then immediately frozen at -20°C. A DMMB assay was run on digested scaffolds. Briefly, 20ul of sample was mixed with 200ul of dimethylmethylene blue reagent and absorbance was immediately read on a plate reader (MultiSkan Spectrum, Thermo, Waltham, MA) at 525 nm.[29] Readings were compared to a standard curve established from chondroitin 6-sulfate from shark (Sigma, C4384).

DNA Quantification

Papain digested scaffolds were also used to determine DNA content through a Hoechst 33258 Assay (Sigma, #861405). Briefly, 100ul digested sample was added to 100ul Hoechst and read with excitation: 355nm, emission: 460nm (Fluoroskan Ascent FL,

Thermo, Waltham, MA) in a 96 well plate. Readings were compared to standards made from calf thymus DNA (Sigma, #D0805).

Quantitative-PCR

qtPCR was used to determine the expression of cartilage specific genes (collagen II and aggrecan), a chondrocyte dedifferentiation marker (collagen I) and a house-keeping gene (GAPDH). Scaffolds were removed from culture, rinsed twice with PBS, cut into small pieces (~1mm^3), and placed immediately into RNAlater (Qiagen, D-40724). Scaffolds were incubated RNAlater at 4°C for 24 hours then transferred to -20°C for storage. For RNA extraction, scaffold + tissue were homogenized in Buffer RLT for approximately 60 seconds. Lysate was then centrifuged, and supernatant was removed. RNA was extracted using an RNeasy Mini Kit (Qiagen #74104), and samples were stored at -80°C. After measurement of RNA concentration for each sample, first-stand cDNA was synthesized using random primers (Superscript Kit #18064). Samples were prepared for qtPCR using a Taqman universal PCR master mix (Applied Biosystems, 4304437) and custom designed porcine primers. qtPCR was then performed using an ABI PRISM 7700 (Applied Biosystems, Foster City, CA 94404, U.S.A). As a control, prior to seeding, 5x10^6 chondrocytes were incubated in RNAlater and used for qtPCR.

Statistical Analysis

Multiple linear regression was performed using SPSS software (SPSS for Windows, Rel 14.0. 2005 Chicago: SPSS Inc.).

6.3 Results

Fabrication of cylinders and scaffolds

Micro-CT analysis of solid cylinders confirmed the absence of air bubble defects in these mechanical testing specimens. Successful fabrication of designed scaffolds can be seen in Figure 6.1, where μCT analysis of scaffolds, again, confirms the absence of defects (Figure 6.1 a/b). Volume fraction quantification done on μCT images reveals that the porosity of fabricated scaffolds (48.1 ± 4.24 %) is slightly less than that of the design file (54%), while scaffold pore diameters (1.04 ± .04 mm) are equal to designed pore sizes (1.0 mm). Decreased porosity of actual scaffolds is most likely due to small amount of PGS penetrating into pores.

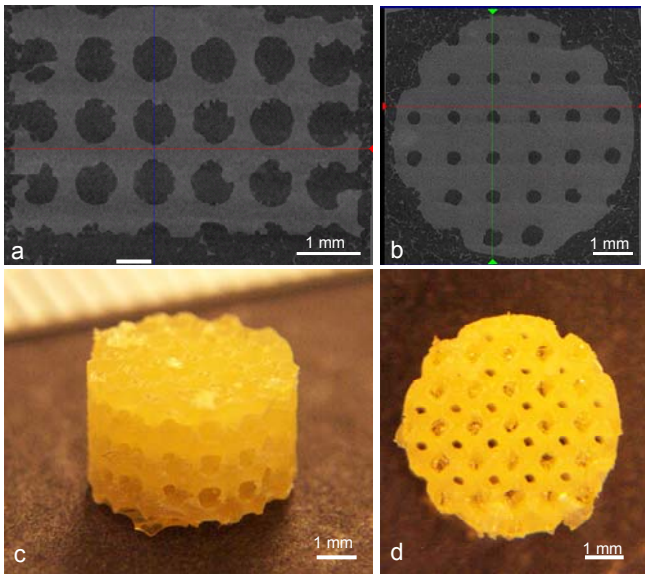

Figure 6. 1 Successfully fabricated 3D-designed PGS scaffolds illustrated through microCT images, side view (a) and top view (b) and digital images, side view (c) and top view (d).

Mechanical Property Variations

Stress-relaxation testing done on solid cylinders (n=2 for each molar ratio/cure time) revealed that PGS does not exhibit typical viscoelastic responses. Stress-relaxation

profiles were not dependent on strain rate (.25 um/sec v. 5 μm/sec), nor did they relax under constant displacement after loading (Figure 6.2), indicating that PGS exhibited predominantly elastic properties and therefore, PGS bulk and scaffolds were tested in unconfined compression and fit to a 1D nonlinear elastic model commonly used for biological soft tissues:

$$T = A\left(e^{B\varepsilon} - 1\right)$$

where T is the 1st Piola-Kirchoff stress, ε is the large strain, and A and B are model parameters fit to experimental data. The fit was performed using a specially written MATLAB program calling the optimization function fminunc. The tangent modulus at 10% strain was calculated as:

$$E^{\text{tangent}} = \frac{dT}{d\varepsilon} = ABe^{B\varepsilon}$$

Representative fits for solid cylinders and 3D scaffolds can be seen in Figure 6.3.

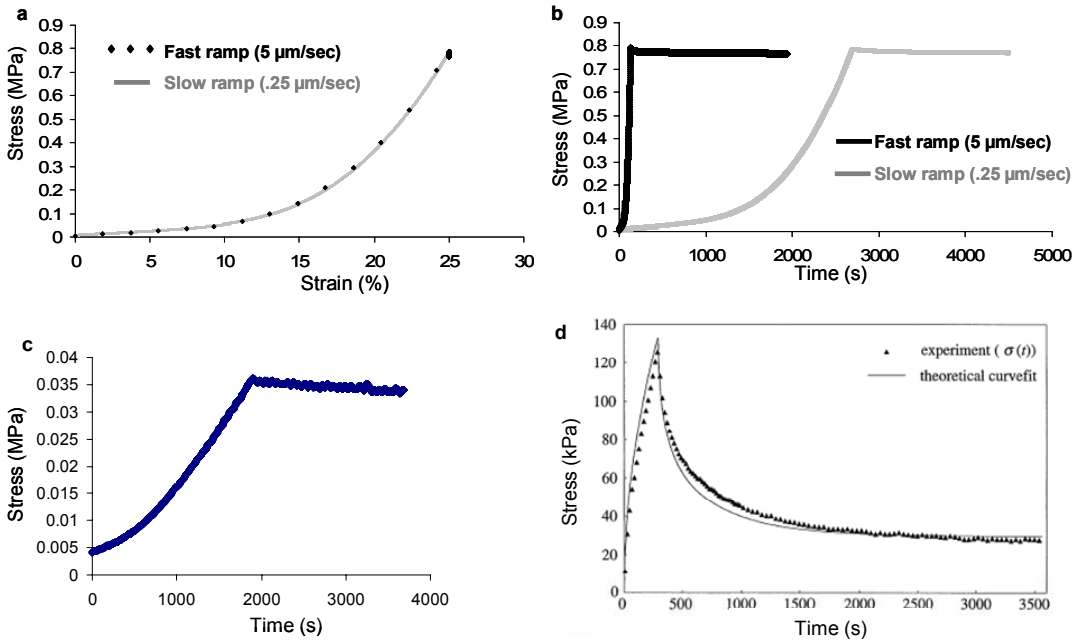

Figure 6.2. Stress vs. strain (a) and stress versus time (b) response of PGS cylinders and scaffolds (c) tested in stress relaxation demonstrates that they do not exhibit the typical viscoelastic response of cartilage (d) as shown by Soltz and Ateshian.[27]

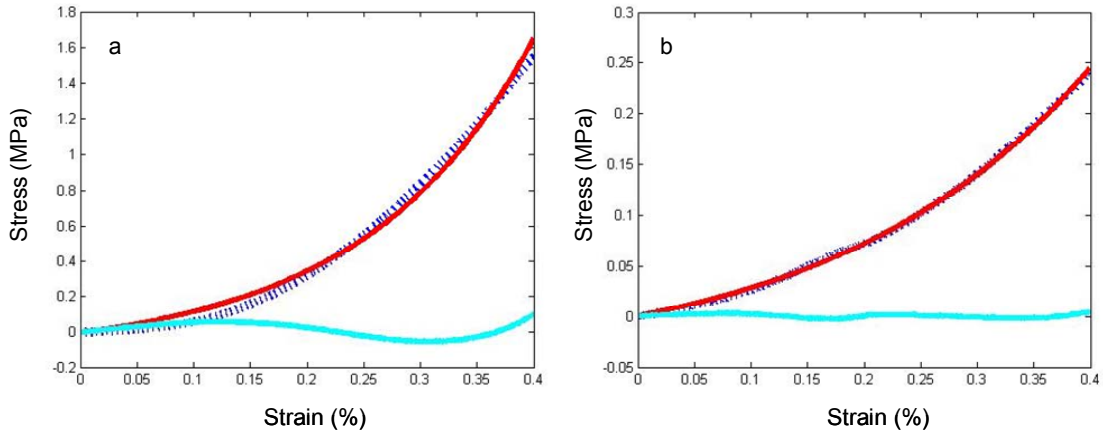

Figure 6.3. 1D nonlinear elastic model provides good fit for solid PGS cylinders (a) and 3D-designed scaffolds (b).

As seen in Figure 6.4, the tangent elastic modulus of PGS is significantly altered through variations in pre-polymer molar ratios and curing times. Multiple regression provided a powerful (adjusted R^2 = .70, predictive power = 70%) linear equation for tangent

modulus (at 10% strain) dependent on these two variables: y = 3.607 – 1.410 * (molar ratio of glycerol: sebacic acid) + 0.60 * (curing time in hours).

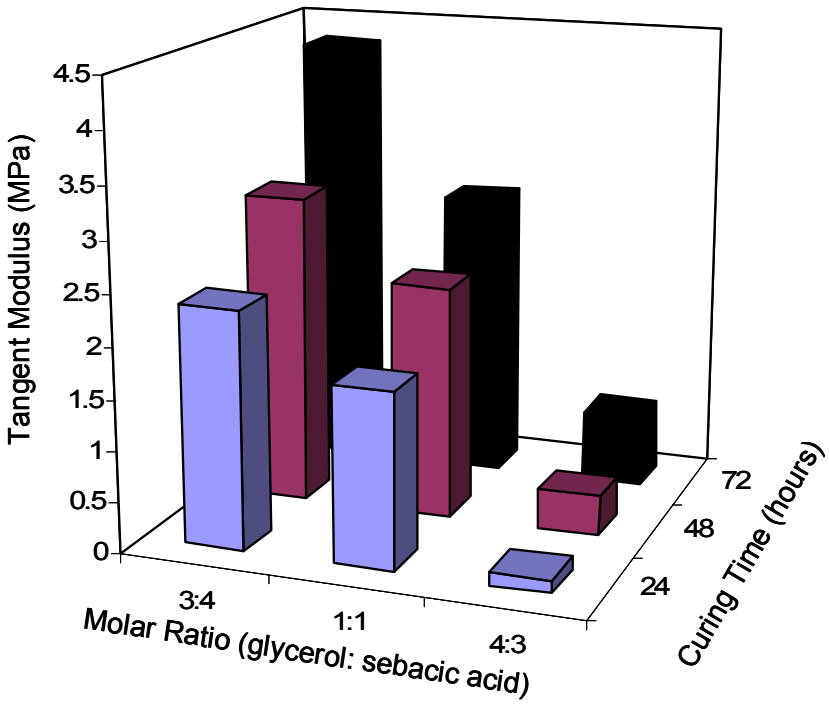

Figure 6. 4. Tangent Modulus (at 10% strain) values for PGS cylinders with various processing parameters. Linear regression can be used to predict the modulus (70% power) from these two variables: Modulus (MPa) = 3.607 – 1.410 * (ratio of glycerol: sebacic acid) + 0.60 * (vacuum curing time in hours).

Finite Element Analysis

FEA was used to calculate the tangent elastic modulus values of scaffold design files and μCT images of actual scaffolds using values of solid cylinder tangent modulus at 10% strain. Table 6.1 displays experimental modulus values of solid cylinders, FEA predictions of modulus values for a 3D scaffold from design files, and modulus values from experimentally tested scaffolds. The voxel model is able to accurately predict the tangent modulus of scaffolds from the design file (prediction = 0.60 MPa, actual = 0.57 ± 0.24).

Table 6.1. Modulus values of solid PGS cylinders made from varying glycerol:sebacic acid molar ratios and varying curing times were used in FEA to predict the modulus value of scaffolds that could be made using the same conditions. Scaffolds were tested experimentally to verify predictions.

	Tangent Modulus (MPa) (at 10% strain)								
cure time (hours)	Solid Cylinders (n=*)			Scaffold Design File (FEA)			Actual Scaffold (Experimental) (n=7)		
24	2.34 ± 0.83 [7]	1.73 ± 0.92 [10]	0.13 ± 0.12 [5]	0.62	0.46	0.03			
48	3.05 ± 0.71 [9]	2.29 ± 0.61 [10]	0.40 ± 0.17 [8]	0.81	0.60	0.11		0.57 ± 0.24	
72	4.28 ± 1.15 [8]	2.82 ± 0.49 [8]	0.71 ± 0.38 [7]	1.13	0.75	0.19			
	3:4	1:1	4:3	3:4	1:1	4:3	3:4	1:1	4:3
	Molar Ratio (glycerol: sebacic acid)								

*Sample size (n) is displayed in superscript for each group.

In Vitro Study

Chondrocytes suspended in collagen 1 hydrogel within 3D designed scaffolds maintained a rounded morphology and were able to produce a cartilaginous matrix as seen in digital images and through alcian blue staining in Figure 6.5. Sulfated-GAG concentrations were within the same ranges as chondrocytes cultured under identical conditions on poly(ε-caprolactone) (PCL) of the same architectural design (29.64 ± 11.87 vs. 33.00 ± 6.24 μg GAG/μg DNA, respectively) (n=3). Collagen 2: collagen 1 ratios were higher for chondrocytes cultured on PGS than those cultured under identical conditions on PCL (20.91 ± 3.25 vs. 8.69 ± 0.17), but were lower than mRNA expression by unseeded chondrocytes (267). Aggrecan expression by cells on PGS was similar to cells seeded on PCL (1.74 ± 0.68 vs. 1.67 ± 0.07), and both expression levels were higher than expressed by chondrocytes (0.37).

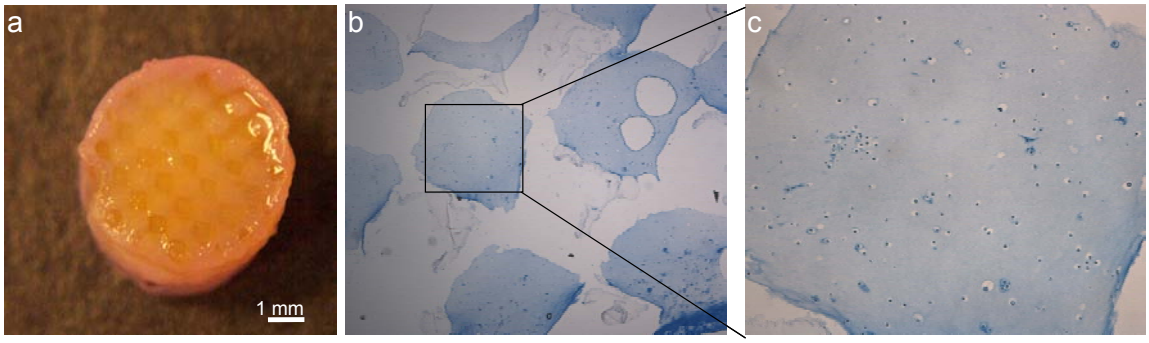

Figure 6.5. Digital images and histological sections (stained with alcian blue) show in vitro growth of cartilaginous tissue into PGS scaffolds.

6.4 Discussion and Conclusion

We have presented a novel PGS fabrication method. Actual scaffold pore sizes and porosities show no major deviations from design files, and there is no significant swelling of solid cylinders or scaffolds when they are soaked in DMEM or PBS.

It is highly desirable to be able to synchronize biomimetic mechanical properties of a scaffold with architectures designed for optimal tissue regeneration. Intuitively, one way in which the mechanical properties of a scaffold can be altered is through changing the structural features, such as pore size, porosity, interconnectivity, and pore shape.[15, 30] However, changing these features also has an effect on cartilage tissue regeneration. [31-36] Working with a material that's intrinsic elastic properties can be altered enables fabrication of scaffolds with a wide range of architectures (designed for optimal tissue regeneration) from one material, all of which will support in vivo loads. As shown here, PGS is beneficial in this respect, as its mechanical properties can be varied simply through changing the molar ratios of glycerol to sebacic acid during pre-polymer synthesis or varying the duration of curing.

After establishing a collection of bulk mechanical properties for nine processing combinations (3 molar ratios x 3 curing times), we used FEA to predict the elastic moduli of a 3D designed scaffold fabricated from these various batches of PGS. A single batch of scaffolds, fabricated from an intermediate of the nine processing combinations, verified that modulus values reported through FEA are reasonable estimates. This demonstrates the ability of image-based FEA to compute the effective stiffness of PGS scaffolds without the need for destructive testing.

Although PGS does not exhibit viscoelastic properties, the ability to match the elastic modulus of scaffolds to the elastic component of cartilage is a step in the right direction. There is no data that indicates how critical it is to match all cartilage properties exactly to achieve good mechanical support and regeneration. A current clinical treatment, autologous chondrocyte implantation, has shown success without *any* substantial mechanical support.[37] However, patients must be extremely careful not to overload the delicate periosteal flap which envelopes the repair site. This draws a thin line between the amount of post-operative mechanical loading shown to enhance tissue regeneration, and the amount that will damage the graft.[38] Furthermore, this data can be applied to other soft tissue engineering applications that PGS is being studied for, such as myocardial tissue[7] , where non-linear elastic properties are highly desirable.

The elastic component of experimental cartilage data can be separated out using the following equation:

$$H_A = \frac{Ev}{(1+v)(1-2v)} + \frac{2E}{3(1-2v)}$$

where, H_A is the aggregate modulus, E is the elastic component of this modulus, and v is the Poisson's ratio. Poisson's ratio was assumed to be 0.3, as experimentally measured by Cohen *et al*. With literature showing H_A values of healthy cartilage ranging from .089 MPa to 2.22 MPa,[27, 28, 39-47] the calculated elastic component ranges from 0.04 to 0.99 MPa. Elastic modulus values predicted for this particular scaffold design from the collection of PGS bulk properties, range from 0.03 to 1.13 MPa, completely encompassing the native tissue values that one might wish to match.

Furthermore, an in vitro experiment shows that PGS can indeed be used for cartilage tissue engineering applications where chondrocytes are seeded within a scaffold to produce a cartilaginous matrix. Aggrecan is expressed in higher levels on PGS scaffolds than in pre-seeded cells, showing favorable trends toward chondrogenesis. Collagen 2: collagen 1 ratio, commonly referred to as a "differentiation index" for chondrocytes,[48] where a larger values represents more chondrogenic gene expression and a lower value represents more fibroblastic gene expression, is higher on PGS than on identical studies done using PCL. Differences between expression levels on PGS versus PCL may be related to the hydrophilicity of PGS. Increased material hydrophilicity may enhance cell adhesion, retain more sGAG, and more closely mimic the native hydrophilic nature of cartilage ECM, however further studies need to be done in order to verify this hypothesis.

PGS is a good candidate for cartilage tissue engineering applications. As shown for the first time, it can be fabricated into 3D designed scaffolds using SFF techniques and is biocompatible with chondrocytes in vitro. Its bulk mechanical properties can be altered during synthesis and curing in order to match stiffness values of 3D-designed scaffolds to those of native cartilage. Furthermore, scaffold modulus values can be predicted using FEA, eliminating the need for destructive testing on custom scaffolds.

Acknowledgements

Funding for this project provided by the National Science Foundation (GSRF), a Regenerative Sciences Training Grant (T90 DK070071), and NIH RO1 DE 13608. Thank you to Claire Jeong for fabricating many of the wax and HA molds used in this study.

References

1. Wang Y, Ameer GA, Sheppard BJ, Langer R. A tough biodegradable elastomer. Nat.Biotechnol. 2002;20:602-6.

2. Sundback CA, Shyu JY, Wang Y, Faquin WC, Langer RS, Vacanti JP*, et al*. Biocompatibility analysis of poly(glycerol sebacate) as a nerve guide material. Biomaterials 2005;26:5454-64.

3. Wang Y, Kim YM, Langer R. In vivo degradation characteristics of poly(glycerol sebacate). J.Biomed.Mater.Res.A. 2003;66:192-7.

4. Gao J, Crapo PM, Wang Y. Macroporous elastomeric scaffolds with extensive micropores for soft tissue engineering. Tissue Eng. 2006;12:917-25.

5. Radisic M, Park H, Martens TP, Salazar-Lazaro JE, Geng W, Wang Y*, et al*. Pre-treatment of synthetic elastomeric scaffolds by cardiac fibroblasts improves engineered heart tissue. J.Biomed.Mater.Res.A. 2007;86(3):713-24.

6. Gao J, Ensley AE, Nerem RM, Wang Y. Poly(glycerol sebacate) supports the proliferation and phenotypic protein expression of primary baboon vascular cells. J.Biomed.Mater.Res.A. 2007;83:1070-5.

7. Chen QZ, Bismarck A, Hansen U, Junaid S, Tran MQ, Harding SE*, et al*. Characterisation of a soft elastomer poly(glycerol sebacate) designed to match the mechanical properties of myocardial tissue. Biomaterials 2008;29:47-57.

8. Sales VL, Engelmayr GC,Jr, Johnson JA,Jr, Gao J, Wang Y, Sacks MS*, et al*. Protein precoating of elastomeric tissue-engineering scaffolds increased cellularity, enhanced extracellular matrix protein production, and differentially regulated the phenotypes of circulating endothelial progenitor cells. Circulation 2007;116:I55-63.

9. Fidkowski C, Kaazempur-Mofrad MR, Borenstein J, Vacanti JP, Langer R, Wang Y. Endothelialized microvasculature based on a biodegradable elastomer. Tissue Eng. 2005;11:302-9.

10. Motlagh D, Yang J, Lui KY, Webb AR, Ameer GA. Hemocompatibility evaluation of poly(glycerol-sebacate) in vitro for vascular tissue engineering. Biomaterials 2006;27:4315-24.

11. Crapo PM, Gao J, Wang Y. Seamless tubular poly(glycerol sebacate) scaffolds: High-yield fabrication and potential applications. J.Biomed.Mater.Res.A. 2007; 86(2): 354-63.

12. Nijst CL, Bruggeman JP, Karp JM, Ferreira L, Zumbuehl A, Bettinger CJ*, et al*. Synthesis and characterization of photocurable elastomers from poly(glycerol-co-sebacate). Biomacromolecules 2007;8:3067-73.

13. Neeley WL, Redenti S, Klassen H, Tao S, Desai T, Young MJ*, et al*. A microfabricated scaffold for retinal progenitor cell grafting. Biomaterials 2008;29:418-26.

14. Chu TM, Hollister SJ, Halloran JW, Feinberg SE, Orton DG. Manufacturing and characterization of 3-d hydroxyapatite bone tissue engineering scaffolds. Ann.N.Y.Acad.Sci. 2002;961:114-7.

15. Hollister SJ. Porous scaffold design for tissue engineering. Nat.Mater. 2005;4:518-24.

16. Hollister SJ, Levy RA, Chu TM, Halloran JW, Feinberg SE. An image-based approach for designing and manufacturing craniofacial scaffolds. Int.J.Oral Maxillofac.Surg. 2000;29:67-71.

17. Lin CY, Hsiao CC, Chen PQ, Hollister SJ. Interbody fusion cage design using integrated global layout and local microstructure topology optimization. Spine 2004;29:1747-54.

18. Lin CY, Kikuchi N, Hollister SJ. A novel method for biomaterial scaffold internal architecture design to match bone elastic properties with desired porosity. J.Biomech. 2004;37:623-36.

19. Schek RM, Taboas JM, Hollister SJ, Krebsbach PH. Tissue engineering osteochondral implants for temporomandibular joint repair. Orthod.Craniofac.Res. 2005;8:313-9.

20. Schek RM, Taboas JM, Segvich SJ, Hollister SJ, Krebsbach PH. Engineered osteochondral grafts using biphasic composite solid free-form fabricated scaffolds. Tissue Eng. 2004;10:1376-85.

21. Schek RM, Wilke EN, Hollister SJ, Krebsbach PH. Combined use of designed scaffolds and adenoviral gene therapy for skeletal tissue engineering. Biomaterials 2006;27:1160-6.

22. Taboas JM, Maddox RD, Krebsbach PH, Hollister SJ. Indirect solid free form fabrication of local and global porous, biomimetic and composite 3D polymer-ceramic scaffolds. Biomaterials 2003;24:181-94.

23. Williams JM, Adewunmi A, Schek RM, Flanagan CL, Krebsbach PH, Feinberg SE*, et al*. Bone tissue engineering using polycaprolactone scaffolds fabricated via selective laser sintering. Biomaterials 2005;26:4817-27.

24. Kim K, Jeong CG, Hollister SJ. Non-invasive monitoring of tissue scaffold degradation using ultrasound elasticity imaging. Acta Biomater. 2008;4:783-90.

25. Chu TM, Orton DG, Hollister SJ, Feinberg SE, Halloran JW. Mechanical and in vivo performance of hydroxyapatite implants with controlled architectures. Biomaterials 2002;23:1283-93.

26. Guilak F, Best BA, Ratcliffe A, Mow VC. Instrumentation for load and displacement controlled studies on soft connective tissues. 1989;AMD 98:113-6.

27. Soltz MA and Ateshian GA. Experimental verification and theoretical prediction of cartilage interstitial fluid pressurization at an impermeable contact interface in confined compression. J.Biomech. 1998;31:927-34.

28. Ateshian GA, Warden WH, Kim JJ, Grelsamer RP, Mow VC. Finite deformation biphasic material properties of bovine articular cartilage from confined compression experiments. J.Biomech. 1997;30:1157-64.

29. Farndale RW, Buttle DJ, Barrett AJ. Improved quantitation and discrimination of sulphated glycosaminoglycans by use of dimethylmethylene blue. Biochim.Biophys.Acta 1986;883:173-7.

30. Hollister SJ and Lin CY. Computational design of tissue engineering scaffolds. Comput.Methods Appl.Mech.Eng. 2007;196:2991-8.

31. Miot S, Woodfield T, Daniels AU, Suetterlin R, Peterschmitt I, Heberer M*, et al*. Effects of scaffold composition and architecture on human nasal chondrocyte redifferentiation and cartilaginous matrix deposition. Biomaterials 2005;26:2479-89.

32. Freed LE, Marquis JC, Nohria A, Emmanual J, Mikos AG, Langer R. Neocartilage formation in vitro and in vivo using cells cultured on synthetic biodegradable polymers. J.Biomed.Mater.Res. 1993;27:11-23.

33. Malda J, Woodfield TB, van der Vloodt F, Wilson C, Martens DE, Tramper J*, et al*. The effect of PEGT/PBT scaffold architecture on the composition of tissue engineered cartilage. Biomaterials 2005;26:63-72.

34. Bhardwaj T, Pilliar RM, Grynpas MD, Kandel RA. Effect of material geometry on cartilagenous tissue formation in vitro. J.Biomed.Mater.Res. 2001;57:190-9.

35. Kuboki Y, Jin Q, Kikuchi M, Mamood J, Takita H. Geometry of artificial ECM: sizes of pores controlling phenotype expression in BMP-induced osteogenesis and chondrogenesis. Connect.Tissue Res. 2002;43:529-34.

36. Griffon DJ, Sedighi MR, Schaeffer DV, Eurell JA, Johnson AL. Chitosan scaffolds: interconnective pore size and cartilage engineering. Acta Biomater. 2006;2:313-20.

37. Peterson L, Minas T, Brittberg M, Nilsson A, Sjogren-Jansson E, Lindahl A. Two- to 9-year outcome after autologous chondrocyte transplantation of the knee. Clin.Orthop.Relat.Res. 2000;(374):212-34.

38. Lewis PB, McCarty LP,3rd, Kang RW, Cole BJ. Basic science and treatment options for articular cartilage injuries. J.Orthop.Sports Phys.Ther. 2006;36:717-27.

39. Williamson AK, Chen AC, Sah RL. Compressive properties and function-composition relationships of developing bovine articular cartilage. J.Orthop.Res. 2001;19:1113-21.

40. Klein TJ, Chaudhry M, Bae WC, Sah RL. Depth-dependent biomechanical and biochemical properties of fetal, newborn, and tissue-engineered articular cartilage. J.Biomech. 2005; 40(1): 182-90.

41. Bursac PM, Obitz TW, Eisenberg SR, Stamenovic D. Confined and unconfined stress relaxation of cartilage: appropriateness of a transversely isotropic analysis. J.Biomech. 1999;32:1125-30.

42. Soltz MA and Ateshian GA. Interstitial fluid pressurization during confined compression cyclical loading of articular cartilage. Ann.Biomed.Eng. 2000;28:150-9.

43. Moroni L, de Wijn JR, van Blitterswijk CA. 3D fiber-deposited scaffolds for tissue engineering: Influence of pores geometry and architecture on dynamic mechanical properties. Biomaterials 2005; 27(7): 974-85.

44. Schinagl RM, Gurskis D, Chen AC, Sah RL. Depth-dependent confined compression modulus of full-thickness bovine articular cartilage. J.Orthop.Res. 1997;15:499-506.

45. Schwartz CJ and Bahadur S. Investigation of articular cartilage and counterface compliance in multi-directional sliding as in orthopedic implants. Wear 2007;262:1315-20.

46. Armstrong CG and Mow VC. Variations in the intrinsic mechanical properties of human articular cartilage with age, degeneration, and water content. J.Bone Joint Surg.Am. 1982;64:88-94.

47. Athanasiou KA, Agarwal A, Dzida FJ. Comparative study of the intrinsic mechanical properties of the human acetabular and femoral head cartilage. J.Orthop.Res. 1994;12:340-9.

48. Martin I, Jakob M, Schafer D, Dick W, Spagnoli G, Heberer M. Quantitative analysis of gene expression in human articular cartilage from normal and osteoarthritic joints. Osteoarthritis Cartilage 2001;9:112-8.

CHAPTER 7

THE EFFECTS OF SCAFFOLD PERMEABILITY ON CHONDROGENESIS USING CHONDROCYTES OR BONE MARROW STROMAL CELLS

7.1 Introduction

Advancements in cartilage tissue engineering are being made through the use of biodegradable scaffolds. In order for this field to progress, it is important to characterize structural and physical scaffold properties that affect the enhancement and maintenance of new cartilage formation. It is widely proposed that scaffold permeability influences chondrogenesis. However, there is no definitive conclusion as to how permeability affects cartilage regeneration, as it has not been rigorously controlled. Here, we investigate the in vitro effects of scaffold permeability on matrix production and cellular differentiation of chondrocytes and bone marrow stromal cells (BMSCs) using designed poly(e-caprolactone) (PCL) scaffolds with rigorously controlled permeability.

It has been proven that permeability is a physical design parameter that can be used to describe the impact that complicated structural properties such as pore size, pore shape, interconnectivity, pore distribution, fenestration size and distribution, and orientation of pores have on mass transport within a scaffold.[1] Particularly for cartilage tissue engineering, this is an interesting design parameter to study. In more metabolically active tissues, such as bone, it is generally accepted that an increase in permeability

correlates with an increase in tissue growth. However, this contradicts a number of findings for cartilage. Clinically, native articular cartilage exhibits relatively low permeability in comparison to bone, increases in permeability are correlated with disease and deterioration, and decreases in permeability with tissue depth correlates with a rise in proteoglycan content.[2] Knowing that oxygen and nutrient diffusion are governed by scaffold permeability[3], there is further evidence that scaffolds designed with decreased permeability may enhance cartilage tissue regeneration: First, native chondrocytes live in a low oxygen environment[21-23], and it is proposed that increases in oxygen may result in disturbance to chondrocyte metabolism through production of abnormal levels of reactive oxygen species (ROS). This is evidenced in osteoarthritic tissue, where ROS are produced in greater amounts resulting in oxidative stresses that cause deterioration of tissue.[4] Secondly, in tissue engineering studies, cartilage grows in anaerobic conditions where oxygen diffusion is *low*.[5-7] And finally, imposing a low oxygen level in *in vitro* conditions has been shown to significantly influence the regenerative potential of chondrocytes and BMSCs in monolayer and 3D culture.[8-25]

In this chapter, we examine how the physical property of permeability, as described by Darcy's law, affects chondrocytes or bone marrow stromal cells seeded onto PCL scaffolds and cultured *in vitro*, with the hypothesis that this parameter can be used to more accurately predict the effects of scaffold architecture on chondrogenesis. We believe that because scaffold permeability affects diffusion, oxygen tension, and nutrient exchange it will impact cellular differentiation and cartilaginous tissue production on biodegradable scaffold, and should be regarded as an independent design consideration.

In order to pursue this hypothesis, we use SFF techniques to create 3D-designed poly(ε-caprolactone) scaffolds with significantly different permeability values. Because structural properties such as pore size, pore shape, and interconnectivity have been shown to affect chondrogenesis, these properties were kept consistent in our designs. Variations in permeability were created through changing the diameter of the interconnection between pores. Scaffolds were seeded with bone marrow stromal cells or chondrocytes and cultured in vitro for up to 6 weeks in order to examine the effects that permeability has on cellular differentiation and matrix production of these cells.

7.2 Materials and Methods

Scaffold Design, Fabrication, and Characterization

Scaffold Design

Three-dimensional (3D)-designed scaffolds (3mm height, 6.35mm diameter, 1mm spherical pores) were designed using custom Interactive Data Language™ programs (IDL; Research Systems, Inc., Boulder, CO). Scaffolds were designed such that the throat size between pores was the only structural difference between scaffolds, creating "low", "mid" and "high" permeable designs.

Scaffold Fabrication

Inverse wax molds of designs were processed on a Solidscape MM2 3D printer (SolidScape Inc., Merrimack, NH). Scaffolds were made by pressing these wax molds directly into melted 37kDa polycaprolactone (CAPA 6400, Solvay Caprolactones, Warrington, Cheshire, UK). Briefly, PCL pellets were placed into a Teflon mold, and

melted (115°C, 1 Torr, 120 minutes). After melting and air bubble removal, the Teflon mold was pulled from the oven, and allowed to cool for 270 seconds at room temperature, reaching 80°C (just below the melting temperature of the wax molds). At this time, inverse wax molds were pressed into the melted PCL, and the entire construct was cooled overnight. Wax was dissolved from the PCL using 100% EtOH. A schematic of this process was shown in Figure 3.3.

Computational Permeability Measurement

An image based homogenization theory program, that combines Darcy's Law and the Navier-Stokes equation, was used in order to compute permeability, K, as defined by: $K_{ij}=1/\mu\ [v^j_i]$ ($m^3/N\cdot s$), where μ=fluid viscosity and v=velocity field.[26]

Experimental Permeability Measurement

A custom permeability chamber was designed (Appendix B) to exert a constant hydraulic pressure on a scaffold. Water flow through the chamber and into a secondary container placed atop a scale (Ohaus Scout Pro) connected to a PC was continually recorded. Within LabView (National Instruments, Austin, TX), an equation derived from Bernoulli's equation (with a frictional loss correctional term) and Darcy's Law, as described by Li and Mak,[27] was used to compute permeability:

$$k = \frac{\Delta x}{A \cdot M_{B2}} \cdot \frac{2\pi^2 r^4}{(M_{B1}/M_{B2})^2 - 1}$$

where k=permeability ($m^4/N \cdot s$), Δx = length of scaffold (m), A = cross-sectional area of scaffold (m), M_{B1}=Mass flow rate without scaffold (g/s), M_{B2}=Mass flow rate with scaffold (g/s), r = radius of water outlet (m). Labview recorded 3 readings per second, giving a continuous output of permeability. Permeability data was plotted to validate that the permeability level was constant throughout the experiment. The data was then averaged to obtain experimental scaffold permeability. Scaffolds were tested in the chamber with and without collagen gel incorporated.

Porosity, Pore Size, Interconnection Size Measurement

Fabricated scaffolds were scanned dry using a MS-130 high resolution micro-computed tomography (μCT) scanner (GE Medical Systems, Toronto, CAN) at 16 μm voxel resolution, 75kV and 75mA. GEMS Microview software was used to analyze the images for porosity, pore diameter and interconnection (throat) diameter. Results can be seen in Table 7.1.

Mechanical Properties

Stress-relaxation tests were performed in confined compression following a protocol established by Guilak *et al.* in 1989 [28] and used extensively in the field by others.[29, 30] Briefly, pre-soaked samples were loaded into a confining cylindrical chamber filled with a physiological saline solution controlled at 37°C. A porous indenter was lowered until a reading of .15 lb was output on the computer, signifying that the indenter was in contact with the scaffold. This load was held for 600s and assumed to be the 0% strain position. Under displacement control, stress-relaxation testing was performed with a single ramp

of 10% strain applied at 0.25 μm/s, followed by a 30 min relaxation. Data obtained from stress relaxation testing was fit to a two-term prony series program in MATLAB to determine relaxation parameters and equilibrium aggregate modulus.

In Vitro Experimentation

Chondrocyte Harvest

Cartilage was harvested from fresh metacarpophalangeal joints of domestic pigs obtained from a local abattoir (Northwest Market, Northwest, MI). Cartilage pieces were stirred in a digest solution [DMEM high glucose, serum free, 1 mg/ml collagenase II (Sigma # C1764), 2% Pen/strep, 2% kanamycin (Roche, 12728700), and .2% Fungizone (Invitrogen, 15290-018)] for 6 hours at 37°C, 5% CO_2. The solution was then filtered through sterile nylon. Cells were spun at 2000 rpm for 8 minutes, and plated overnight on tissue culture polystyrene in DMEM + 10%FBS + 1% P/S + 50 μg/ml 2-phospho-L-ascorbic acid (BioChemika, 49752). The following day, cells were trypsinized and immediately suspended in collagen gel for scaffold seeding.

Bone Marrow Stromal Cell Harvest

Bone marrow was harvested at the Seguin Animal Hospital (Seguin, TX) from the hip of a Yucatan Mini Pig (Lone Star Laboratory Swine) and placed into media (DMEM+10%FBS+2% P/S+.2%Fungizone + .1% Gentamycin + 200 units/ml Heparin) for overnight shipment on ice to the University of Michigan. Bone marrow aspirate was placed into tissue culture flasks upon arrival. Half of the media (DMEM + 2% P/S + .2% Fungizone + 10% FBS) was changed on day 7 and day 11. On day 14, cells were

passaged and then grown to 80% confluence, at which point they were frozen in liquid nitrogen for later use.

Cell Seeding

Scaffolds were sterilized in 100% Ethanol for 24 hours, followed by rinses in sterile water (12 hours) and DMEM (4 hours) prior to seeding. Chondrocytes or BMSCs were suspended in a composite 5% Hyaluronic Acid (HyA) (stock concentration: 2.7 mg/ml in 0.8M NaCl, MW: 3 x 10^6 Da: Hyalogic LLC, Edwardsville, KS) info)/collagen I gel (stock concentration: 5.9 mg/ml, BD Biosciences, #354236) at ~30 x 10^6 cells/ml. Cells were evenly seeded into scaffolds using a custom designed Teflon mold. Due to variances in the porosity, a different volume of collagen gel (calculated from void area) and a different cell number was seeded into each design in order to maintain a consistent cell seeding density (Low: 1.25 x 10^6 cells/scaffold, 47µl gel; Mid: 1.93 x 10^6 cells/scaffold, 59µl gel; High: 2.2 x 10^6 cells/scaffold, 71µl gel). 4% v/v .5M sodium hydroxide with 220 mg/ml sodium bicarbonate was used to increase the pH of the collagen/HyA/cell suspension just prior to scaffold in order to create gelling at 37°C. After gelling (~30 minutes), scaffolds were removed from the mold.

In Vitro Culture

Scaffold + Cells + Gel constructs were cultured in an incubator (37°C, 5% CO_2) in 24-well plates on an orbital shaker for up to 6 weeks. Media (Chondrocyte Scaffolds: DMEM, 10%FBS, 1% P/S, 0.1mM Non-essential Amino Acids, 50 µg/ml 2-phospho-L-ascorbic acid, 0.4 mM proline, 5ug/ml insulin or BMSC Scaffolds: DMEM, 10%FBS,

1% P/S, 0.1mM Non-essential Amino Acids, 50 μg/ml 2-phospho-L-ascorbic acid, 0.4 mM proline, 5ug/ml insulin, 10ng/ml TGF-β, and .1 μM dexamethasone) was changed every other day. At each time point, scaffolds were extracted for DMMB and Hoechst (Chon: n=5, BMSC: n=4), qtPCR (Chon: n=2, BMSC: n=4) and histology (Chon: n=2, BMSC: n=2).

sGAG Quantification

At 2, 4 or 6 weeks, scaffolds were removed from culture, finely chopped, and placed immediately into 1 ml of papain solution (papain, 1X PBS, cysteine HCL, EDTA, pH=6.0; mixed for 3h at 37°C then filtered). Scaffolds were digested in papain for 24 hours and then immediately frozen at -20°C. A DMMB assay was run on digested scaffolds. Briefly, 20ul of sample was mixed with 200ul of dimethylmethylene blue reagent and absorbances were immediately read on a plate reader (MultiSkan Spectrum, Thermo, Waltham, MA) at 525 nm.[31] Readings were compared to a standard curve established from chondroitan 6-sulfate from shark (Sigma, C4384).

DNA Quantification

Papain digested scaffolds were used to determine DNA content through a Hoechst 33258 Assay (Sigma, #861405). Briefly, 100ul digested sample was added to 100ul Hoechst and read with excitation: 355nm, emission: 460nm (Fluoroskan Ascent FL, Thermo, Waltham, MA) in a 96 well plate. Readings were compared to standards made from calf thymus DNA (Sigma, #D0805).

Quantitative-Polymerase Chain Reaction (qtPCR)

qtPCR was used to determine the expression of cartilage specific genes (collagen II and aggrecan), a chondrocyte dedifferentiation marker (collagen I) and a house-keeping gene (GAPDH). Scaffolds were removed from culture, rinsed twice with PBS, cut into small pieces (~1mm^3), and placed immediately into RNAlater (Qiagen, D-40724). Scaffolds were incubated (4°C for 24 hours) and then stored (20°C) in RNAlater. For RNA extraction, scaffold + tissue were homogenized in Buffer RLT for approximately 60 seconds. Lysate was then centrifuged, and supernatant was removed. RNA was extracted using an RNeasy Mini Kit (Qiagen #74104), and samples were stored at -80°C. After measuring RNA concentration for each sample, first-stand cDNA was synthesized using random primers (Superscript Kit #18064). Samples were prepared for qtPCR using a Taqman universal PCR master mix (Applied Biosystems, 4304437) and custom designed porcine primers. qtPCR was then performed on an ABI PRISM 7700 (Applied Biosystems, Foster City, CA 94404, U.S.A). As a control, 5x10^6 chondrocytes and 5x10^6 BMSCs were also used for qtPCR. Just before the scaffold seeding step, these cells were instead placed into RNAlater and incubated at 4°C for 24 hours, and then stored at -80°C until analysis.

Histology

Paraffin embedded histological sections were stained with Alcian Blue (chondrocyte scaffold) or Safranin-O/Fast Green (BMSC scaffolds).

Statistical Analysis

Statistical analysis, including one-way ANOVA, linear regression, and fixed-effect modeling, was performed using SPSS software (SPSS for Windows, Rel 14.0. 2005 Chicago: SPSS Inc.).

7.3 Results

Scaffold Design, Fabrication, and Characterization

Scaffolds were fabricated from polycaprolactone. As discussed in chapter 3, PCL degrades very slowly, making it an ideal choice for studies where changes in scaffold architecture caused by degradation would alter mass transport properties throughout the study. Because parameters such as interconnectivity, pore size, and pore shape have all been shown to have an effect on cartilage regeneration, scaffolds for this study were designed with a consistent pore size (diameter = 1mm), a consistent pore shape (spherical) and 100% interconnectivity. Spherical pore shape was chosen for this study because previous work in the lab shows that cells (chondrocytes and BMSCs) cultured in these pores produce more robust ECM with higher sGAG concentrations in comparison to cubical pores. These finding were attributed to increased local cell densities (chondrocytes) or induction of cellular condensations (BMSCs). Variations in permeability were created through altering the throat diameter (0.31, 0.46, 0.55 mm) between pores, as seen in Figure 7.1.

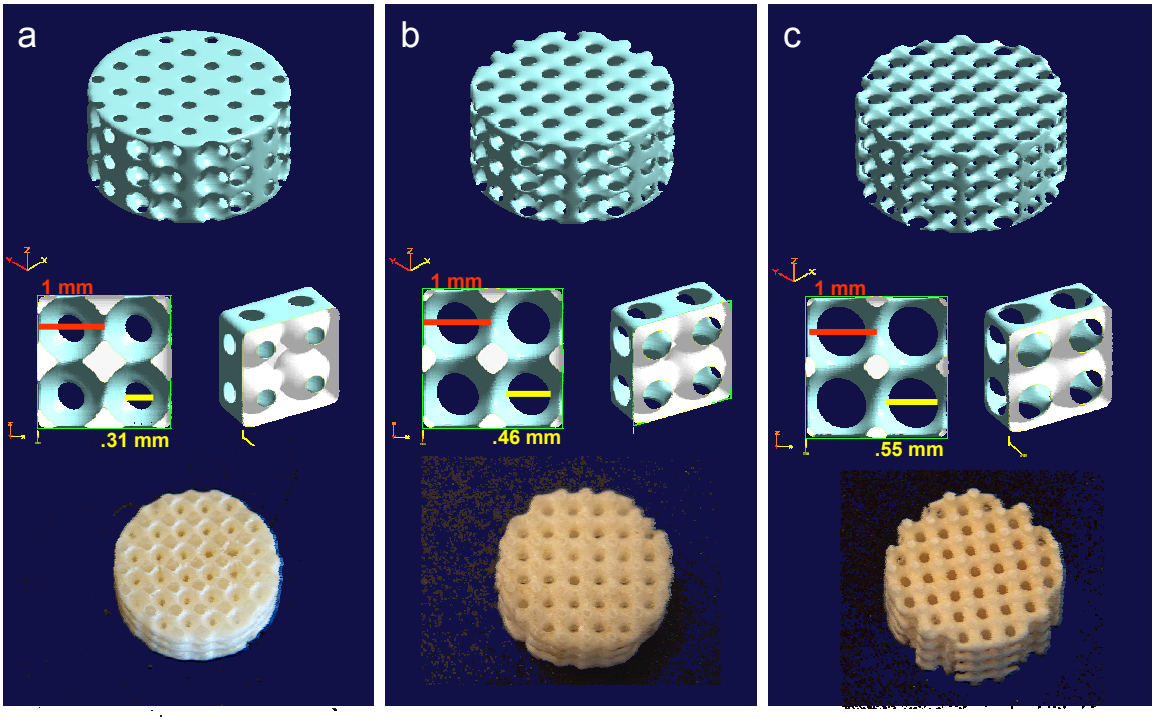

Figure 7.1. Surface rendering of scaffold design (top) and 2x2 unit cells (middle) and digital images of fabricated scaffolds for low (a), mid (b), and high (c) permeable designs.

Computationally and experimentally measured structural scaffold properties can be seen in Table 7.1. Actual scaffold porosity, pore size, and interconnective size were lower than designed sizes due to contraction of the PCL material in ethanol (see Chapter 5).

Table 7.1. Computationally designed and experimentally measured (μCT) structural scaffold properties.

StructuralScaffold Properties	Low Permeability	Mid Permeability	High Permeability
Porosity (designed)	53%	63%	70%
Porosity (actual) (n=5)	30% ± 0.89	47% ± 3.41	59% ± 1.75
Pore size (designed) (mm)	1.00	1.00	1.00
Pore size (actual) (mm) (n=5)	0.75 ± .02	0.80 ± .02	0.86 ± .02
Interconnection size (designed) (mm)	0.39	0.54	0.61
Interconnection size (actual) (mm) (n=5)	0.22 ± 0.03	0.30 ± 0.03	0.38 ± 0.03

Computational permeability measurements confirmed differences between scaffold designs, labeled as “low”, “mid” and “high” in reference to design permeability. Next, difference in permeability was experimentally verified in a permeability chamber. After

determining that fabricated scaffolds were significantly different between designs (one-way ANOVA, $p \leq .05$), collagen 1 hydrogel was incorporated into scaffolds to recapitulate the in vitro seeding protocol. With gel, scaffold permeability values dropped to ~20% of the original scaffold experimental value and continued to exhibit significant differences (one-way ANOVA, $p \leq .05$) between designs, with experimental permeability now matching closely with computationally predicted values (Table 7.2 and Figure 7.2). Furthermore, linear correlations between computationally predicted permeability values and experimental values (with and without collagen gel incorporation) allow for more accurate prediction of actual scaffold permeability from computational design files in the future (Figure 7.3).

Table 7.2. Computational and experimental permeability measurements on design files, scaffolds, and scaffolds with gel show significant differences between designs.

	Permeability (x 10^{-7} m^3/N·s)		
Design	Computational	Experimental (n=6)	Experimental (with gel) (n=5)
Low	0.69 (Low)	2.93 ± 0.73 (Low)	0.66 ± 0.24 (Low)
Mid	2.34 (3.4 x Low)	7.40 ± 1.40 (2.5 x Low)	1.11 ± 0.33 (1.7 x Low)
High	3.99 (5.8 x Low)	15.37 ± 2.81 (5.25 x Low	3.60 ± 2.23 (5.5 x Low)

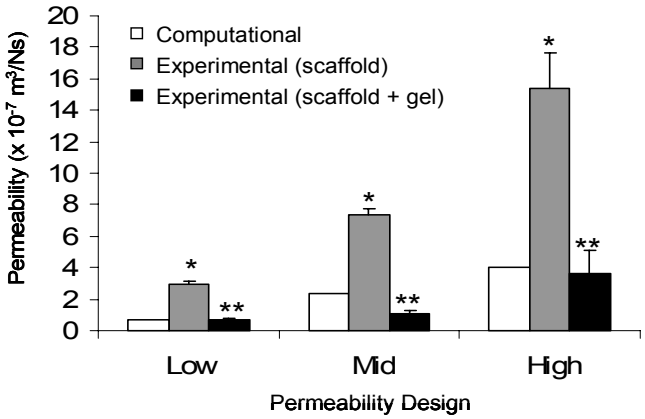

Figure 7.2 Experimental permeability of scaffold designs (Low, Mid, High) were significantly different (one-way ANOVA, $p \leq 0.05$) with and without collagen gel incorporation.

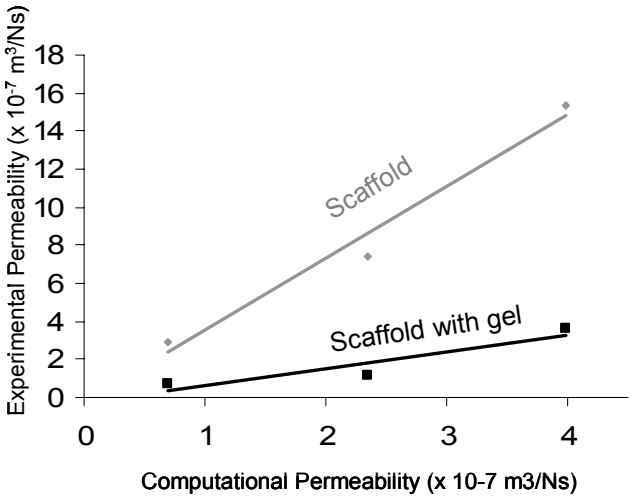

Figure 7.3 Linear correlation between computationally predicted permeability (y = 3.77x – 0.25, R^2 = 0.97) and experimental permeability (y = 0.89x – 0.29, R^2 = 0.86) allows computational design of scaffolds that meet target experimental permeability values.

Mechanical Properties

The importance of mechanically testing PCL at 37°C is described in Chapter 5, where it is also demonstrated that PCL exhibits a viscoelastic mechanical response. Here, we find that the aggregate modulus of low (8.71 ± 1.06 MPa), mid (5.76 ± 1.24 MPa) and high (3.09 ± 0.77 MPa) scaffold designs are higher than the generally accepted ranges of articular cartilage (0.5 – 1.0 MPa).

In vitro experimentation

Chondrocyte Study

Chondrocytes proliferated and produced cartilaginous matrix during the 4 week in vitro culture period (Figure 7.4). Live cell numbers increased from (.53 to 1.5 x 10^6, 283%), (.50 to 1.49 x 10^6, 310%), (.49 to 1.18 x 10^6, 254%) for low, mid and high designs respectively over 4 weeks (Figure 7. 5).

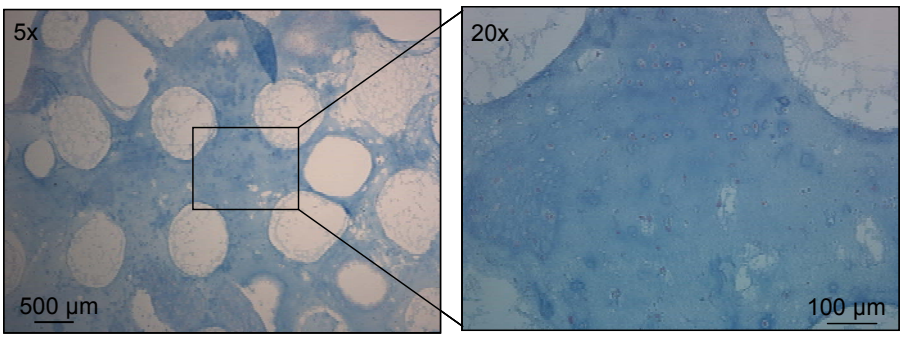

Figure 7.4. Alcian blue stains proteoglycans produced by chondrocytes after 4 weeks of in vitro culture.

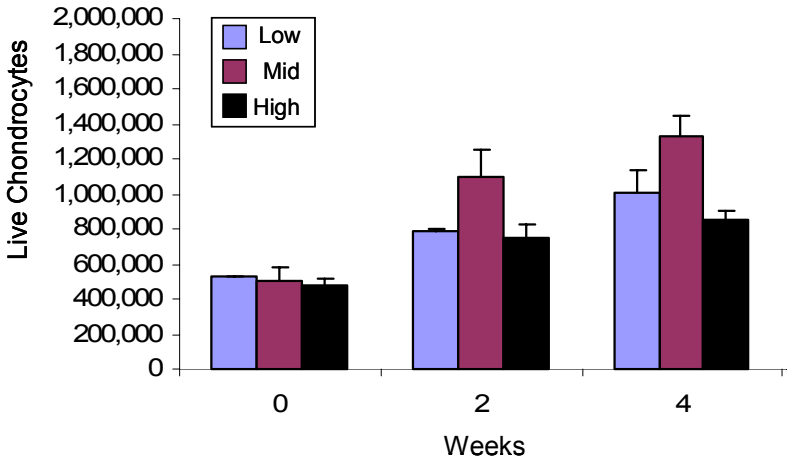

Figure 7.5. Chondrocyte proliferation on 3D designed scaffolds over 4 weeks of in vitro culture.

Sulfated-glycosaminoglycan (sGAG) content, measured through a DMMB assay, is used to quantify cartilaginous matrix production by chondrocytes. At 2 weeks, there is a trend of decreasing sGAG content as scaffold permeability increases. At 4 weeks, the lowest permeable scaffold displays a significant increase in GAG content, measured in regards to sample or DNA content, versus the mid and high permeable designs (one way ANOVA, $*p \leq 0.05$) (Figure 7.6). These data suggest that a lower permeable scaffold design is favorable for cartilaginous matrix production by chondrocytes.

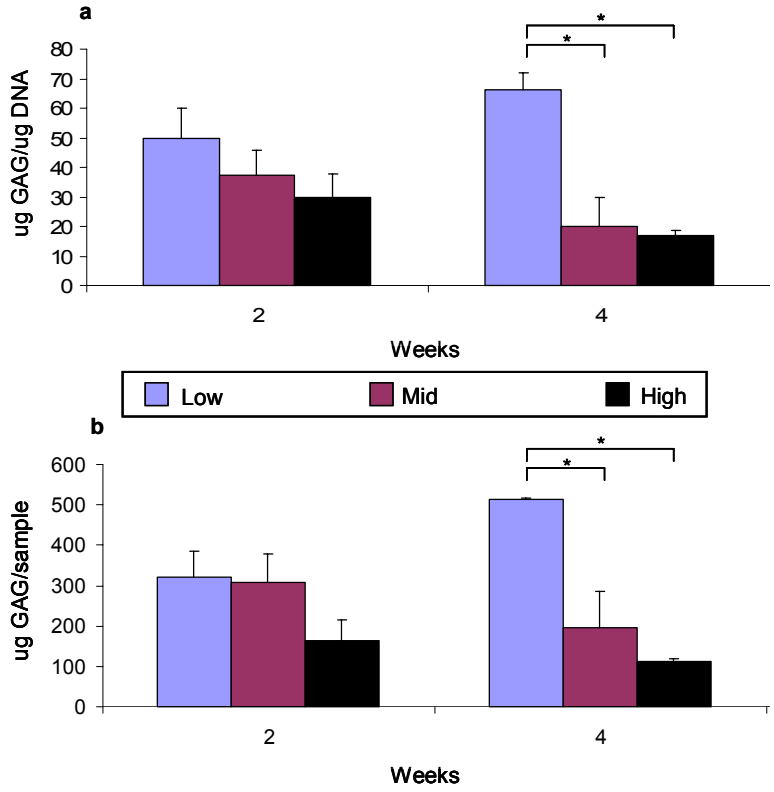

Figure 7.6. GAG content, a) per DNA content and b) per sample, measured on low, mid, and high permeable scaffolds seeded with chondrocytes after 2 and 4 weeks of in vitro culture (One Way ANOVA, *p ≤ 0.05).

Quantitative-PCR can be used to measure the messenger RNA expression for proteins found in cartilage. It is assumed that mRNA expression correlates with downstream cellular protein expression. First, we use this method to quantify the amount of aggrecan that chondrocytes seeded with our scaffolds express. Aggrecan is the main proteoglycan found in cartilage, and is a typical marker of differentiated chondrocytes. As seen in Figure 7.7, aggrecan is expressed by chondrocytes cultured within scaffolds, but there is no significant difference between scaffold design groups at both the 2 week and 4 week time point. For comparison, pre-seeded chondrocyte expression normalized to GAPDH levels was 0.37, and is represented in Figure 7.7 with a dotted line.

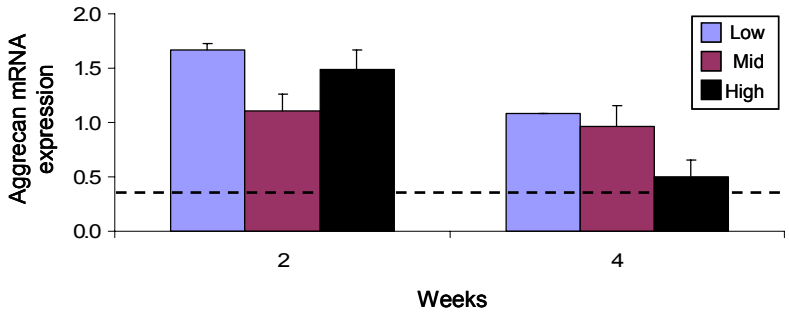

Figure 7.7. Aggrecan expression by chondrocytes within 3D designed scaffolds is higher than that expressed by pre-seeded chondrocytes (dotted line), but is not significantly different between designs.

Quantitative-PCR was also used to measure collagen expression by cells. Type two collagen is the major fibrillar collagen of articular cartilage, accounting for 90-95% of the overall collagen content.[32] This gene is localized to cartilage, the vitreous of the eye, the nucleus pulposus of intervertebral discs and the embryonic chick primary corneal stroma. It provides cartilage with its tensile strength and immobilizes proteoglycans within its matrix. Collagen 1, generally associated with bone, tendons, and ligaments, is found in small amounts in human articular cartilage and increasing amounts in fibrocartilages, presumably contributing to the functional requirements of the tissues. Its level of expression is commonly used as a marker of chondrocyte dedifferentiation. As a ratio, the expression of collagen 2: collagen 1 is termed the "differentiation index" with a larger value correlating with a more chondrocytic genotype, and a lower values correlating with more fibroblastic gene expression.[33] From 2 to 4 weeks, both the low and mid permeable designs show an increase in collagen 2: collagen 1 expression (Figure 7.8). At 4 weeks, there appears to be a linear relation (linear regression, $p = .02$) between permeability and collagen 2: collagen 1 expression, where a decrease in scaffold

permeability correlates with an increase in the chondrogenic differentiation index. For comparison, collagen 2: collagen 1 expression by pre-seeded chondrocytes normalized to GAPDH was 266.

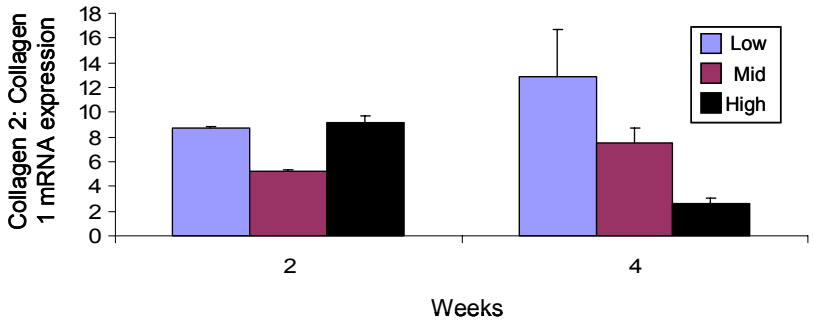

Figure 7.8 Low and mid permeable designs show an increase in collagen 2: collagen 1 expression between 2 and 4 weeks. At 4 weeks there appears to be a linear relation between increasing scaffold permeability and decreasing "differentiation index".

Bone Marrow Stromal Cell Study

Bone marrow stromal cells, mesenchymal stem cells derived form the bone marrow, are a precursor to chondrocytes. They can be "pulsed" down a chondrogenic lineage through the use of specific nutrients in culture media.[5] Their use on cartilage tissue engineering scaffolds would eliminate the need to harvest chondrocytes from a healthy joint surface. They are also unproblematic in monolayer culture and have a higher mitotic potential at increased age than chondrocytes. Figure 7.9 illustrates the rounded morphology of BMSCs pulsed in chondrogenic media on 3D scaffolds, suggesting successful pulsing of these cells down a chondrogenic lineage.

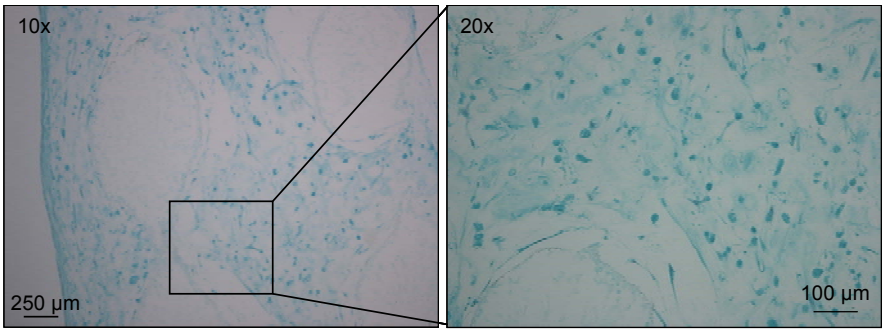

Figure 7.9. Fast green staining of BMSCs after 2 weeks in vitro culture in chondrogenic media shows a more rounded, chondrogenic morphology on 3D scaffolds.

In contrast to chondrocytes, BMSCs encapsulated in collagen 1 hydrogel and seeded into 3D designed scaffolds show a decrease in live cell numbers between 0 and 2 weeks (Figure 7.10). Because these cells naturally have a higher metabolic requirement than chondrocytes it is likely that cell death as quantified between 0 and 2 weeks (40%, average of all designs), occurred within the first couple of days after seeding. After this initial period, cells proliferated, with cell increases of (.37 to .64 x 10^6, 173%), (.40 to .63 x 10^6, 156%), (.53 to .83 x 10^6, 157%) between 2 weeks and 6 weeks for low, mid and high designs respectively.

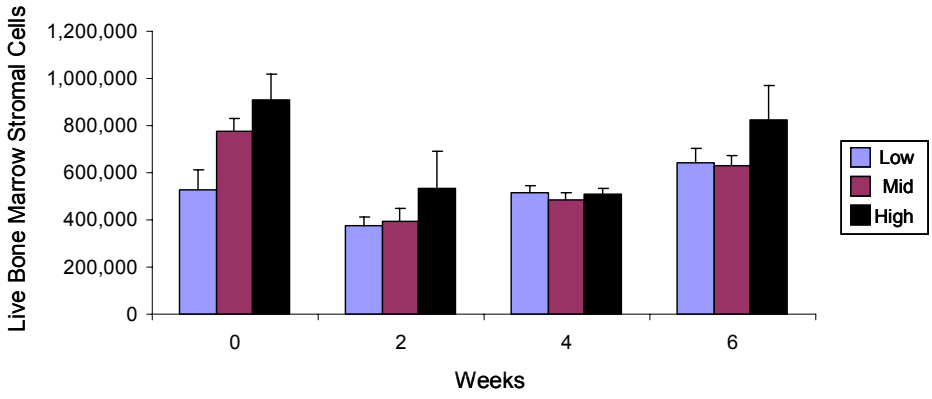

Figure 7.10. BMSCs are less robust than chondrocytes when seeded into PCL scaffolds, showing 40% cell death between 0 and 2 weeks.

Production of cartilaginous matrix by BMSCs, as quantified by sGAG content in scaffolds or and sGAG content normalized to DNA content, increases over time, but there is no significant differences between groups (Figure 7.11). This suggests that BMSCs have differentiated down the chondrogenic lineage, but that there is no relation between scaffold permeability and the amount of sGAG production by the cells.

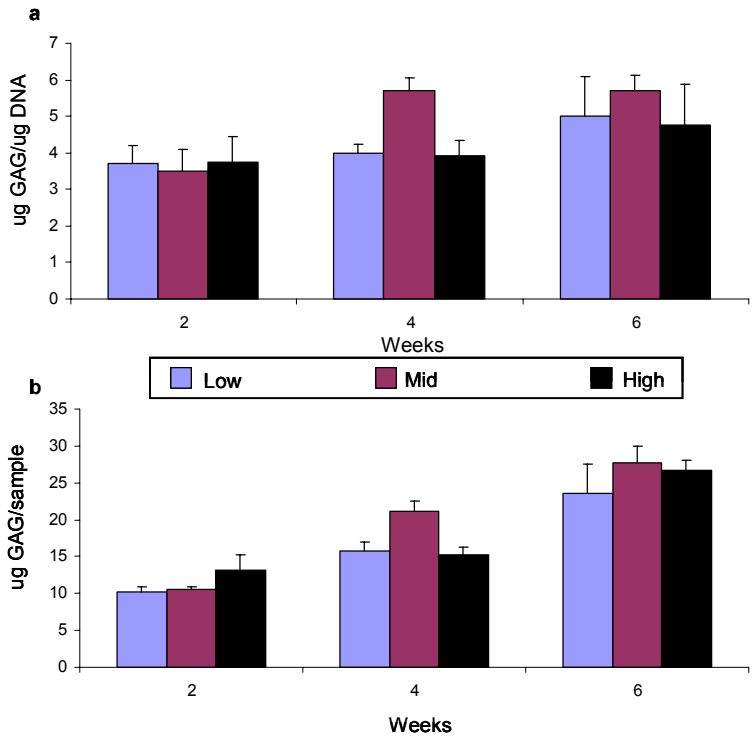

Figure 7.11. BMSCs produce cartilaginous matrix on scaffolds, as evidenced by sGAG production, but there is no significant difference in regards to scaffold permeability.

Expression of aggrecan by BMSCs further demonstrates their differentiated state. As seen in Figure 7.12, aggrecan expression increases for all designs from 2 to 4 weeks, where thereafter it remains the same or decreases slightly. For comparison, aggrecan expression by pre-seeded BMSCs normalized to GAPDH was .0006.

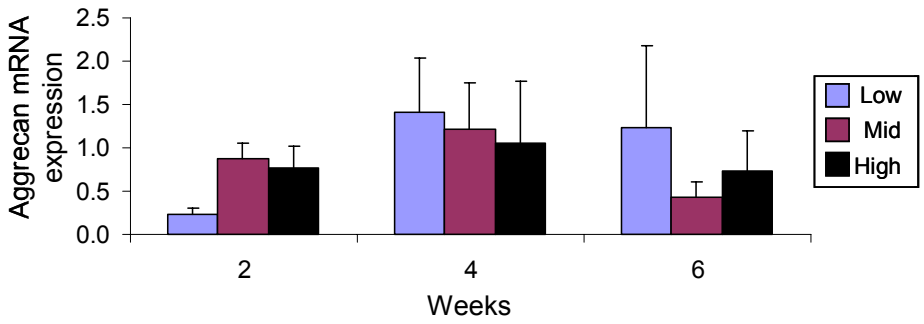

Figure 7.12. Aggrecan expression by BMSCs is higher than pre-seeded BMSCs and further confirms their chondrogenic differentiation.

Collagen type two expression can be used as a sensitive marker for chondrogenic differentiation of precursor cells, and may coincide with an irreversible commitment to chondrogenesis.[34] In this study, we looked at the differentiation index (ratio of collagen 2: collagen 1 expression) of BMSCs between low, mid and high permeable scaffolds at 2, 4, and 6 weeks. Using a fixed effect statistical model, overall design effects reveal that an increase in permeability (as correlated to each design), results in a 1.1 increase in the chondrogenic index (Figure 7.13a). This same model reveals that over time, the low permeability design shows no significant increase in, but rather a trend for decrease in collagen 2: collagen 1 ratio (Δ -0.2, $p = 0.8$). The mid permeable design shows a non-significant trend towards increases in differentiation index (Δ 1.33, $p = 0.32$) over time. And finally, the high permeability design shows a significant increase in the differentiation index over time (Δ 2.7, $p \leq 0.05$) (Figure 7.13b). This data suggests that BMSCs favor a higher permeable scaffold environment when cultured in 3D designed scaffolds in vitro in chondrogenic media.

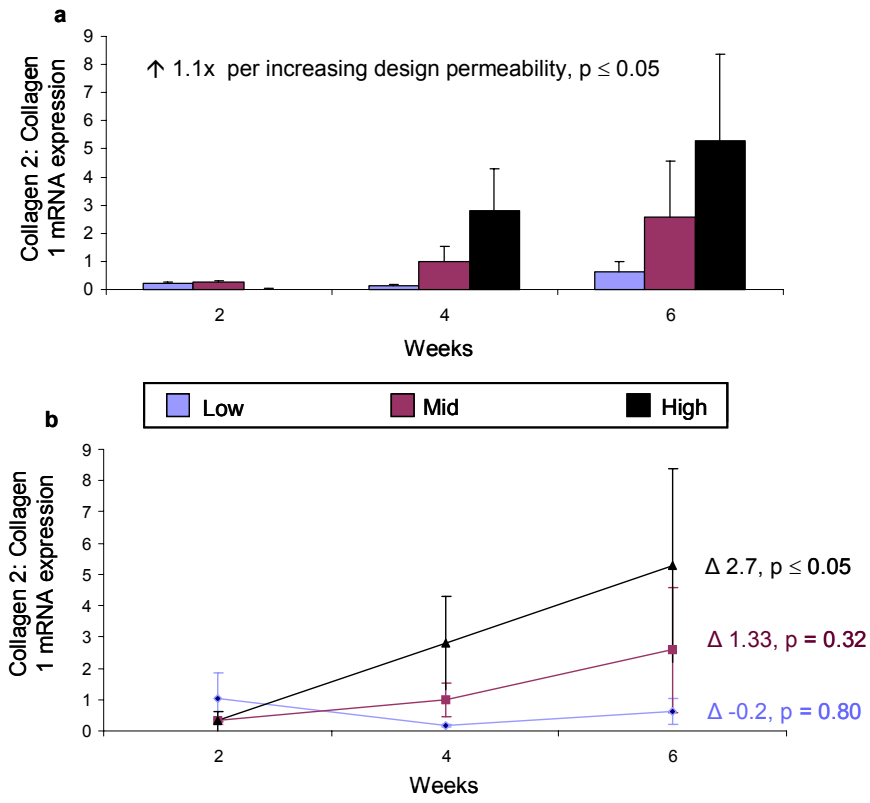

Figure 7.13. Collagen 2: collagen 1 expression by BMSCs shows that they favor a more permeable scaffold design, as evidenced by fixed effects of design (a) and time (b).

7.4. DISCUSSION AND CONCLUSIONS

The aim of this study was to evaluate the effects of permeability on chondrogenesis in 3D-designed scaffolds using chondrocytes or bone marrow stromal cells. The first step was to design and fabricate scaffolds with controlled, reproducible, and significantly different permeability both alone and when infiltrated with collagen 1 hydrogel. This ensured that throughout the study, whether the gel is present, or has degraded (as is suspected over time), there is a significant difference in the parameter we are evaluating. We were able to accomplish this goal by designing scaffolds with 1mm, spherical pores and 100% interconnectivity. Experimental permeability measurements confirmed

computational permeability predictions for these designs: that significant difference exists between low, mid and high designs.

3D-designed scaffolds were mechanically tested in stress-relaxation to evaluate their biphasic nature and load-bearing capacity. Scaffolds showed the viscoelastic response inherent of native articular cartilage (see Chapter 5), but aggregate modulus values of these designs were higher than native tissue values. Increased stiffness between implanted matrices and native tissue may cause fibrous tissue formation, elevated levels of strain in the adjacent cartilage, and acceleration of degeneration of the tissue.[35] This suggests that another, less stiff material may be more suited for fabrication of these particular scaffold designs. However, fabrication of scaffold designs with higher permeability would have continually lower aggregate moduli. In this case, or for altogether different architectural design, PCL may provide aggregate modulus values within the range of cartilage. Furthermore, for studying the effects of permeability, PCL is the ideal choice, as it does not degrade as quickly as other synthetic materials, such that permeability of the scaffold design does not change over time in culture.

The effects of scaffold permeability on cell proliferation, cartilaginous matrix production, and expression of cartilage-specific genes were assessed for chondrocytes and bone marrow stromal cells. Chondrocytes are a natural choice for cartilage tissue engineering, as they are the only cells present in native tissue. However, harvesting of chondrocytes requires sacrifice of a healthy joint surface. The cells are also difficult to culture, as they tend to dedifferentiate in monolayer. For those reasons, other cell types, such as bone

marrow stromal cells and adipocyte-derived stem cells are continually explored for cartilage tissue engineering purposes.[5, 36-43]

Chondrocytes encapsulated in collagen 1 hydrogel, seeded onto 3D scaffolds, and cultured in vitro appear more robust than BMSCs seeded under the same conditions. This research shows a steady increase in chondrocyte proliferation as measured at 0, 2, and 4 weeks, while there is a decrease in BMSC numbers between the zero time point and the 2 week time point. Further studies would show a more detailed timeline for cell death. For chondrocytes, although there is an overall increase in cell number between the zero time point and 2 weeks, this doesn't prove that all cells seeded survived, but rather that over two weeks cell proliferation was greater than any initial cell death. For BMSCs, it could be possible that all cell death occurred during the first 24 hours or less, where after that, cell proliferation began. Further work would provide further details into the robustness of these cell types in this environment, allowing clinicians to compensate for cell death when implanting such matrices.

Results suggest that scaffold permeability affects the two cell types in opposite ways. Chondrocytes favor a lower permeable environment, that more closely mimics native cartilage conditions, when cultured in vitro on 3D scaffolds. The lowest permeable design shows significant increases in cartilaginous matrix production at 4 weeks over higher permeable designs (66 μg sGAG/μg DNA and 513 μg sGAG/scaffold on low designs versus 17 μg sGAG/μg DNA and 112 μg sGAG/scaffold on high designs). This data is also supported by an increase in aggrecan expression and an increase in the

"differentiation index" (collagen 2: collagen 1 expression) in correlation with decreased scaffold permeability. One explanation for these results is described by the correlation between permeability and oxygen tension. These changes can be attributed to decreases in oxygen tension (as reviewed in Chapter 4) in lower permeable designs that may induce production of cartilage specific components and structure of extracellular matrix.[7]

Bone marrow stromal cells favor a higher permeable environment when cultured on 3D designed scaffolds in vitro in chondrogenic media. This work shows an increase in cellular differentiation, as measured by the collagen 2: collagen 1 ratios, of 1.1 for each increasingly permeable scaffold design. We also show that over time, BMSCs cultured on low and mid permeable scaffolds show no significant increase in differentiation index, whereas on the highest permeable scaffold collagen 2: collagen 1 mRNA expression significantly increased by a factor of 2.7 every 2 weeks. These findings can be explained by the fact that BMSCs rely on nutrients from the media in order to differentiate. This implies that in this model, cells relied on the diffusion of nutrients into the scaffold more than the desire to be in a low permeable environment that more closely mimics native tissue, for chondrogenic differentiation.

Clinically, these findings have significant impact. When filling a defect site, a scaffold is automatically subjected to a lower permeable environment than is seen in vitro, as its radial edges and bottom surface will be confined between native cartilage tissue and subchondral bone. This data suggests that chondrocytes will be more suited for this type of repair system. When replacing an entire articular surface, this data favors the use of a

less permeable design when using chondrocytes or a more permeable design when using bone marrow stromal cells.

In conclusion, scaffold permeability has been shown to affect cartilaginous matrix production of chondrocytes and chondrogenic differentiation of bone marrow stromal cells on 3D scaffolds cultured in vitro. This physical parameter is used as a quantitative description of mass transport variations caused by structural properties such as pore size, porosity, pore shape, and interconnectivity. Although further studies should assess the effect of permeability in an in vivo orthotopic site, it should be deemed an important design consideration for scaffold tissue engineering.

Acknowledgements

Funding for this study provided by the National Science Foundation GRFP and a Regenerative Medicine Training Grant (T90 DK070071) (JMK). Thank you to Annie Mitsak and Brandon Busuito for help with media changes and to Huina Zhang and Tao Jincong for assistance with qtPCR.

References

1. Li SH, de Wijn JR, Layrolle P, de Groot K. Accurate geometric characterization of macroporous scaffold of tissue engineering. 2003;240-2:541-5.

2. Maroudas . Permeability of articular cartilage. 1968;219:1260.

3. Karande TS, Ong JL, Agrawal CM. Diffusion in musculoskeletal tissue engineering scaffolds: design issues related to porosity, permeability, architecture, and nutrient mixing. Ann.Biomed.Eng. 2004;32:1728-43.

4. Henrotin YE, Bruckner P, Pujol JP. The role of reactive oxygen species in homeostasis and degradation of cartilage. Osteoarthritis Cartilage 2003;11:747-55.

5. Yoo JU, Barthel TS, Nishimura K, Solchaga L, Caplan AI, Goldberg VM*, et al*. The chondrogenic potential of human bone-marrow-derived mesenchymal progenitor cells. J.Bone Joint Surg.Am. 1998;80:1745-57.

6. Bhardwaj T, Pilliar RM, Grynpas MD, Kandel RA. Effect of material geometry on cartilagenous tissue formation in vitro. J.Biomed.Mater.Res. 2001;57:190-9.

7. Malda J, Martens DE, Tramper J, van Blitterswijk CA, Riesle J. Cartilage tissue engineering: controversy in the effect of oxygen. Crit.Rev.Biotechnol. 2003;23:175-94.

8. Malda J, van Blitterswijk CA, van Geffen M, Martens DE, Tramper J, Riesle J. Low oxygen tension stimulates the redifferentiation of dedifferentiated adult human nasal chondrocytes. Osteoarthritis Cartilage 2004;12:306-13.

9. Kurz B, Domm C, Jin M, Sellckau R, Schunke M. Tissue engineering of articular cartilage under the influence of collagen I/III membranes and low oxygen tension. Tissue Eng. 2004;10:1277-86.

10. Murphy CL and Sambanis A. Effect of oxygen tension and alginate encapsulation on restoration of the differentiated phenotype of passaged chondrocytes. Tissue Eng. 2001;7:791-803.

11. Murphy CL and Sambanis A. Effect of oxygen tension on chondrocyte extracellular matrix accumulation. Connect.Tissue Res. 2001;42:87-96.

12. Domm C, Schunke M, Christesen K, Kurz B. Redifferentiation of dedifferentiated bovine articular chondrocytes in alginate culture under low oxygen tension. Osteoarthritis Cartilage 2002;10:13-22.

13. Hansen U, Schunke M, Domm C, Ioannidis N, Hassenpflug J, Gehrke T*, et al*. Combination of reduced oxygen tension and intermittent hydrostatic pressure: a useful tool in articular cartilage tissue engineering. J.Biomech. 2001;34:941-9.

14. Nagel-Heyer S, Goepfert C, Adamietz P, Meenen NM, Portner R. Cultivation of three-dimensional cartilage-carrier-constructs under reduced oxygen tension. J.Biotechnol. 2006;121:486-97.

15. Saini S and Wick TM. Effect of low oxygen tension on tissue-engineered cartilage construct development in the concentric cylinder bioreactor. Tissue Eng. 2004;10:825-32.

16. Schneider N, Lejeune JP, Deby C, Deby-Dupont GP, Serteyn D. Viability of equine articular chondrocytes in alginate beads exposed to different oxygen tensions. Vet.J. 2004;168:167-73.

17. Wernike E, Li Z, Alini M, Grad S. Effect of reduced oxygen tension and long-term mechanical stimulation on chondrocyte-polymer constructs. Cell Tissue Res. 2008;331:473-83.

18. Pawelek JM. Effects of thyroxine and low oxygen tension on chondrogenic expression in cell culture. Dev.Biol. 1969;19:52-72.

19. Grimshaw MJ and Mason RM. Modulation of bovine articular chondrocyte gene expression in vitro by oxygen tension. Osteoarthritis Cartilage 2001;9:357-64.

20. Grimshaw MJ and Mason RM. Bovine articular chondrocyte function in vitro depends upon oxygen tension. Osteoarthritis Cartilage 2000;8:386-92.

21. Clark CC, Tolin BS, Brighton CT. The effect of oxygen tension on proteoglycan synthesis and aggregation in mammalian growth plate chondrocytes. J.Orthop.Res. 1991;9:477-84.

22. Malda J, van den Brink P, Meeuwse P, Grojec M, Martens DE, Tramper J*, et al*. Effect of oxygen tension on adult articular chondrocytes in microcarrier bioreactor culture. Tissue Eng. 2004;10:987-94.

23. Schneider N, Mouithys-Mickalad A, Lejeune JP, Duyckaerts C, Sluse F, Deby-Dupont G*, et al*. Oxygen consumption of equine articular chondrocytes: Influence of applied oxygen tension and glucose concentration during culture. Cell Biol.Int. 2007;31:878-86.

24. Kanichai M, Ferguson D, Prendergast PJ, Campbell VA. Hypoxia promotes chondrogenesis in rat mesenchymal stem cells: a role for AKT and hypoxia-inducible factor (HIF)-1alpha. J.Cell.Physiol. 2008;216:708-15.

25. Robins JC, Akeno N, Mukherjee A, Dalal RR, Aronow BJ, Koopman P*, et al*. Hypoxia induces chondrocyte-specific gene expression in mesenchymal cells in association with transcriptional activation of Sox9. Bone 2005;37:313-22.

26. Hollister SJ and Lin CY. Computational design of tissue engineering scaffolds. Comput.Methods Appl.Mech.Eng. 2007;196:2991-8.

27. Li J and Mak AF. Hydraulic permeability of polyglycolic acid scaffolds as a function of biomaterial degradation. J.Biomater.Appl. 2005;19:253-66.

28. Guilak F, Best BA, Ratcliffe A, Mow VC. Instrumentation for load and displacement controlled studies on soft connective tissues. 1989;AMD 98:113-6.

29. Soltz MA and Ateshian GA. Experimental verification and theoretical prediction of cartilage interstitial fluid pressurization at an impermeable contact interface in confined compression. J.Biomech. 1998;31:927-34.

30. Ateshian GA, Warden WH, Kim JJ, Grelsamer RP, Mow VC. Finite deformation biphasic material properties of bovine articular cartilage from confined compression experiments. J.Biomech. 1997;30:1157-64.

31. Farndale RW, Buttle DJ, Barrett AJ. Improved quantitation and discrimination of sulphated glycosaminoglycans by use of dimethylmethylene blue. Biochim.Biophys.Acta 1986;883:173-7.

32. Goldberg VM and Caplan AI. Orthopedic tissue engineering : basic science and practice. New York: Marcel Dekker 2004.

33. Martin I, Jakob M, Schafer D, Dick W, Spagnoli G, Heberer M. Quantitative analysis of gene expression in human articular cartilage from normal and osteoarthritic joints. Osteoarthritis Cartilage 2001;9:112-8.

34. Hall BK. Bones and cartilage : developmental and evolutionary skeletal biology. Australia ; San Diego, Calif.: Elsevier Academic Press 2005.

35. Beaupre GS, Stevens SS, Carter DR. Mechanobiology in the development, maintenance, and degeneration of articular cartilage. J.Rehabil.Res.Dev. 2000;37:145-51.

36. Caplan AI and Bruder SP. Mesenchymal stem cells: building blocks for molecular medicine in the 21st century. Trends Mol.Med. 2001;7:259-64.

37. Heng BC, Cao T, Lee EH. Directing stem cell differentiation into the chondrogenic lineage in vitro. Stem Cells 2004;22:1152-67.

38. Martin I, Padera RF, Vunjak-Novakovic G, Freed LE. In vitro differentiation of chick embryo bone marrow stromal cells into cartilaginous and bone-like tissues. J.Orthop.Res. 1998;16:181-9.

39. Erickson GR, Gimble JM, Franklin DM, Rice HE, Awad H, Guilak F. Chondrogenic potential of adipose tissue-derived stromal cells in vitro and in vivo. Biochem. Biophys. Res. Commun. 2002;290:763-9.

40. Im GI, Shin YW, Lee KB. Do adipose tissue-derived mesenchymal stem cells have the same osteogenic and chondrogenic potential as bone marrow-derived cells? Osteoarthritis Cartilage 2005;13:845-53.

41. Nathan S, Das De S, Thambyah A, Fen C, Goh J, Lee EH. Cell-based therapy in the repair of osteochondral defects: a novel use for adipose tissue. Tissue Eng. 2003;9:733-44.

42. Zuk PA, Zhu M, Ashjian P, De Ugarte DA, Huang JI, Mizuno H*, et al*. Human adipose tissue is a source of multipotent stem cells. Mol.Biol.Cell 2002;13:4279-95.

43. Zuk PA, Zhu M, Mizuno H, Huang J, Futrell JW, Katz AJ*, et al*. Multilineage cells from human adipose tissue: implications for cell-based therapies. Tissue Eng. 2001;7:211-28.

CHAPTER 8

SUMMARY AND FUTURE DIRECTIONS

8.1 Summary

Clinical treatment options to repair articular cartilage damage and deterioration are progressing to the incorporation of synthetic matrices alongside autologous chondrocyte implantation. This work explores the mechanical properties and physical design considerations of potential matrices (scaffolds). Solid freeform fabrication is used throughout this work to create highly reproducible scaffolds with precise structural features in order to explore the mechanical potential of 3D designed poly(ε-caprolactone) (PCL) and poly(glycerol sebacate) (PGS) scaffolds, and to examine the effects that a designed physical property, permeability, may have on cartilage tissue regeneration.

The first part of this thesis explored the potential of PCL and PGS scaffolds to provide temporary mechanical function within a tissue defect by mimicking the stiffness of native cartilage. We found that PCL mimics the viscoelastic nature of cartilage, however its stiffness properties cannot be significantly changed through changes in molecular weight (25 kDA – 50 kDa) or changes in melting temperature (110°C - 150°C). Fabricated into the architectures explored in chapter 7, it has aggregate modulus (H_A) values (low: 8.71 ±

1.06, mid: 5.76 ± 1.24, high: 3.09 ± 0.77) within the correct magnitude, but higher than the desired ranges of cartilage (0.5-1.0 MPa). Future scaffolds made with a higher permeability or higher porosity design will have continually lower aggregate modulus values, and in such cases PCL could be used to match H_A values to native cartilage. We also quantified the differences in aggregate modulus of PCL mechanically tested at physiological temperatures versus room temperature, with increase of 150% (.2 MPa/°C) in modulus values for scaffolds tested at room temperature, demonstrating the importance of mimicking the in vivo environment during mechanical characterization for clinical applications. Furthermore, we discovered that PCL contracts significantly in ethanol, due to compaction of the carbon chain or a change in bond structure when placed in a polar environment. When designing custom scaffolds as mentioned earlier, it will be important to compensate for contraction of material seen in this study. Computational up scaling of the scaffold implant could be applied to fix this change, or a less polar solvent, that does not cause contraction, can be investigated for removal of wax. Compensating for the contraction of PCL is also important in situations where the material will be placed in a polar in vivo environment. For instance, Yu *et al.*[1] document contraction of PCL in bladder applications, where the material is in contact with urine.

Poly(glycerol sebacate) has never been used for cartilage tissue engineering applications. In this work we characterized the changes in stiffness that can be created through variations in the molar ratio of glycerol: sebacic acid during polymer synthesis and through variations in the duration of curing. Working with a material that's intrinsic elastic properties can be altered enables fabrication of scaffolds with a wide range of

architectures (designed for optimal tissue regeneration) from one material, all of which will support in vivo loads. We showed that although it does not mimic the viscoelastic properties of cartilage, the elastic component of PGS scaffolds, no matter what the architecture can be made to match generally accepted values for the elastic component of native cartilage (0.22 MPa – 0.45 MPa, corresponding to H_A = 0.5 – 1.0 MPa, ν = 0.3) (Table 8.1). Furthermore, we showed that chondrocytes seeded onto PGS produce sGAG quantities (29.64 ug sGAG/ug DNA vs. 33.00 ug sGAG/ug DNA on PCL) and cartilage specific gene expression (aggrecan: 1.67 vs. 1.74 on PCL and collagen 2: collagen 1 20.91 vs 8.69 on PCL) similar to or better than that of cells cultured on PCL under the same conditions, proving their biocompatibility with the material for the first time.

Throughout this work, we verify that finite element analysis can be used to predict the stiffness values of scaffold designs when bulk material properties are known. As seen in Table 8.1, it can be used to predict modulus values of scaffold designs from a database of bulk material properties (such as PGS). This technology can be used in the future to predict stiffness values of potential scaffold architectures or custom implant designs.

Table 8.1. Predicted tangent modulus values for low, mid and high permeable scaffold designs used in chapter 7 made from PGS characterized in chapter 6. Highlighted cells are those scaffolds which fall within the ranges of native tissue elastic properties.

	Predicted Tangent Modulus (MPa) (at 10% strain)								
cure time (hours)	Low Permeable Design			Mid Permeable Design			High Permeable Design		
24	0.62	0.46	0.03	0.36	0.27	0.02	0.21	0.16	0.01
48	0.81	0.60	0.11	0.47	0.35	0.06	0.28	0.21	0.04
72	1.13	0.75	0.19	0.66	0.43	0.11	0.39	0.26	0.06
	3:4	1:1	4:3	3:4	1:1	4:3	3:4	1:1	4:3
	Molar Ratio (glycerol: sebacic acid)								

The second goal of this work was to enhance cartilage tissue regeneration through providing optimal mass transport properties within the scaffold. We found that scaffold permeability affects chondrogenesis of chondrocytes and bone marrow stromal cells in different ways. Chondrocytes appear to prefer a less permeable scaffold environment, producing significantly more sGAG and increased expression of cartilage specific markers. At 2 weeks, there is a strong linear correlation between increasing permeability and decreasing sGAG content, and at 4 weeks, the lowest permeable design shows significant increases in sGAG content over both mid and high permeable designs (low: 66.4 ug sGAG/ug DNA, mid: 19.8 ug sGAG/ug DNA, high: 17.1 ug sGAG/ug DNA). This is supported by collagen 2: collagen 1 ratios at 4 weeks (low: 12.9, mid: 7.5, high: 2.6 normalized to GAPDH). A lower permeable scaffold environment mimics the natural environment of native cartilage, where increases in permeability are correlated with disease and deterioration, and decreases in permeability with tissue depth correlate with a rise in proteoglycan content.{{343 Maroudas, 1968; }} In tissue engineering, increases in scaffold permeability cause increases in oxygen levels, which have been shown to disturb the equilibrium of reactive oxygen species within the tissue, leading to deterioration of cartilage. In support of decreased scaffold permeability enhancing chondrogenesis by chondrocytes, Malda *et al.* state that "low oxygen induces production of cartilage specific components and structure of the extracellular matrix."[2]

Bone marrow stromal cells (BMSCs) display the opposite trend, favoring a higher permeable environment for chondrogenic differentiation, as displayed through collagen 2: collagen 1 expression. With increasing permeability, there is an increase of 1.1 in the

differentiation index for each scaffold design. Over time the highest permeable design shows a significant increase of 2.7 in the differentiation index every two weeks, with the low design actually showing a decrease in collagen 2: collagen 1 expression. Unlike chondrocytes, which are already differentiated when they are seeded onto the scaffolds, BMSCs rely on nutrients and growth factors from the media in order to induce them down the chondrogenic lineage. Therefore, this study shows that increased access to these induction factors is more important to these cells than mimicking the low permeable environment of native tissue.

Previous studies demonstrate that there is no consensus on how structural design parameters affect cartilage tissue regeneration on 3D scaffolds. In this work, we use the parameter of permeability to physically characterize the scaffold environment created by such structural properties. It is our hope that this parameter and other physical parameters such as diffusivity can be used to better understand how scaffold environments affect tissue regeneration. We believe that permeability may be the key to understanding differences seen in other studies.

Combining the two goals presented in this work has significant impact from a design perspective. It allows us to design scaffold architectures based solely on tissue in growth requirements, and then to choose processing parameters for a selected material that, when used to fabricate the chosen architecture, will create a scaffold effective stiffness that matches that of native tissue. An overview of the results found in this work is illustrated in Figure 8.1.

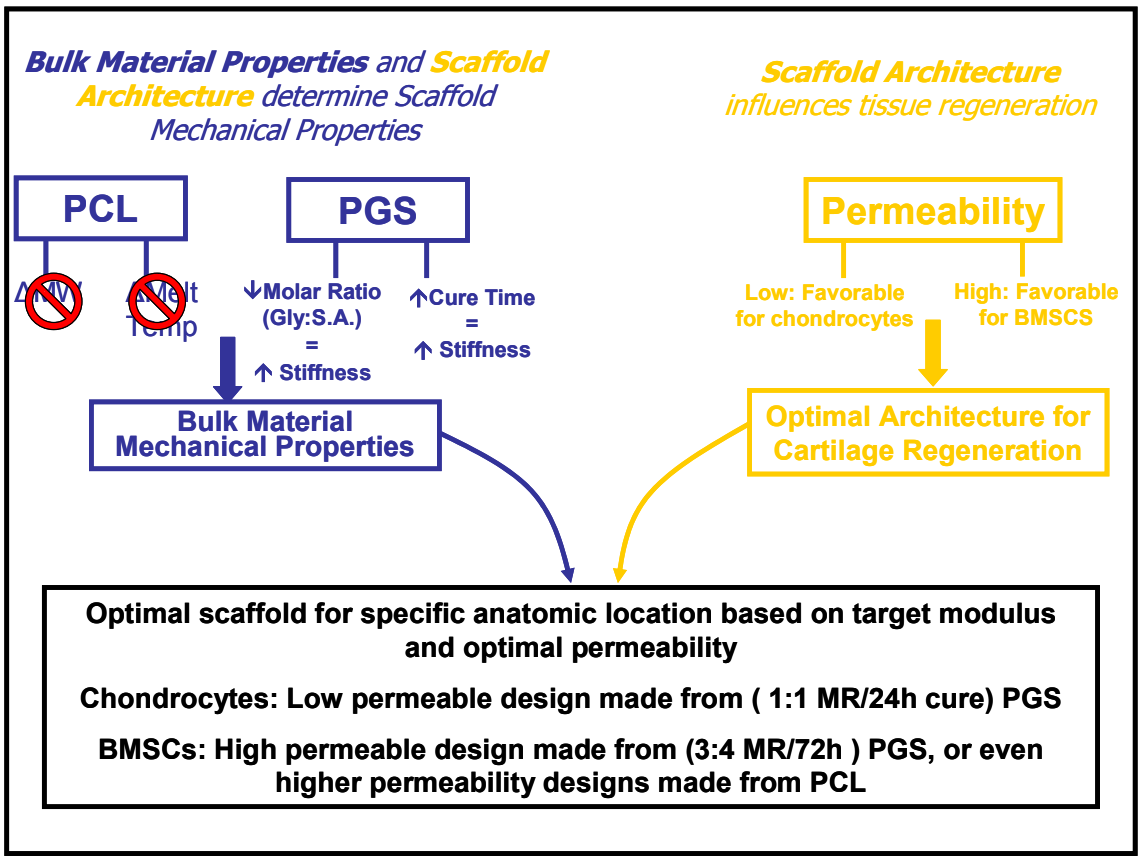

Figure 8.1 Flowchart showing major conclusions of this dissertation (MR=molar ratio).

8.2 Future Directions

8.2.1 Exploiting the differences between PCL and PGS

In the material characterization portion of this work, we discovered a number of interesting material differences between PCL and PGS. Because both of these materials can be used to make identical 3D scaffolds through SFF, their material differences could be used in order to study the effects of these properties on cartilage tissue regeneration. A comparative study between PGS and PCL scaffolds could reveal the influence that hydrophobicity has on cellular interactions, and therefore, cartilage tissue regeneration. Scaffolds made out of these two materials could also be used to explore the importance of

mimicking viscoelasticity in a load bearing model, revealing the extent to which this unique property should be pursued for optimal tissue regeneration and integration.

8.2.2 Osteochondral Scaffold from PCL and PGS

Previous work not included in this dissertation developed the use of selective laser sintered (SLS) PCL for bone applications.[3] With SLS PCL mechanical properties that fall within the lower ranges of trabecular bone, and PGS elastic properties that can be made to match those of native cartilage, these two materials could be combined to create an osteochondral scaffold. Further work in this area could assess the effects of closed or open interfaces between the two polymer sections, which would presumable influence cell-cell contacts between osteoblasts (or other bone-producing cells) and chondrocytes (or other cartilage-producing cells).

8.2.3 Permeability effects in other models

Now that low, mid, and high permeable designs can be fabricated and have been fully characterized to show significant difference between groups, these designs can be extended to study the effects of permeability on other cells for cartilage tissue engineering or for other tissue types all together. Preliminary studies have already begun using adipocyte-derived stem cells for cartilage purposes. Pre-adipocytes seeded onto the high permeable scaffold designs differentiated into morphologically rounded cells and produced some sGAG when cultured in media containing BMP6 (essential for differentiation in this study). Xu et al.[4] show that lower oxygen tensions (2%) promotes

early chondrogenesis in mouse pre-adipocytes. Further work to explore the effects of scaffold permeability on these cell types would be a logical next step.

Work has also begun exploring the effects of permeability on bone tissue regeneration using the low and high permeable designs created in this work. Preliminary work done by Annie Mitsak shows that bone is formed within the pores of all scaffold designs, and an outer bone shell surrounds the exterior of the scaffolds. Total bone produced on high permeability designs is greater than that produced on low permeability designs, but once total bone volume is normalized to the total amount of pore space available, significant differences are not present. Because higher permeability designs do allow for more bone growth overall, they may be a better choice for bone tissue engineering, however, increased permeability correlates with decreased initial mechanical properties, so further analysis that explores initial mechanical properties, rate of bone regeneration (and mechanical properties of the regenerated bone), and rate of scaffold degradation, all with regards to permeability can be explored.

8.2.4 Effects of permeability in more complex in vitro and in vivo environments

Permeability has an effect on the loading environment of scaffolds, which has been shown to have an effect on cartilage regeneration.[5-7] Further studies on the effects of permeability on tissue regeneration should extend into in vitro systems that generate load on the scaffolds. Permeability, as demonstrated, affects diffusion of growth factors into scaffolds. The complex cocktail of growth factors expressed in a synovial environment is not recapitulated in vitro. Testing of these scaffolds in an orthotopic site would provide

further impacts that designed scaffold permeability has on cartilage tissue engineering. Implantation in an orthotopic site would also take into account confinement of the radial edges and bottom of the scaffold as occurs in a clinical setting.

8.2.5 Exploring oxygen tension hypothesis

As hypothesized, chondrocyte favoritism of a low permeable environment may be due to lower oxygen levels created within the scaffold. In order to confirm this, work should be done to experimentally measure the differences in oxygen tension between scaffold designs. Although mathematical programs have been established to predict oxygen tensions within a scaffold, to the best of our knowledge, actual oxygen tensions within scaffolds has not been measured. Perhaps a device could be modeled after the device used by Woodhouse that measures the oxygen tension inside of bone.[8] This hypothesis can be further explored through quantitative assessment of histology through histomorphometric analysis, which would enable measurement of sGAG production at different areas of a scaffold, with the assumption that oxygen levels in the interior are lower than oxygen levels around the periphery of the scaffold.

References

1. Yu DS, Lee CF, Chen HI, Chang SY. Bladder wall grafting in rats using salt-modified and collagen-coated polycaprolactone scaffolds: preliminary report. Int.J.Urol. 2007;14:939-44.

2. Malda J, Martens DE, Tramper J, van Blitterswijk CA, Riesle J. Cartilage tissue engineering: controversy in the effect of oxygen. Crit.Rev.Biotechnol. 2003;23:175-94.

3. Williams JM, Adewunmi A, Schek RM, Flanagan CL, Krebsbach PH, Feinberg SE*, et al*. Bone tissue engineering using polycaprolactone scaffolds fabricated via selective laser sintering. Biomaterials 2005;26:4817-27.

4. Xu Y, Malladi P, Chiou M, Bekerman E, Giaccia AJ, Longaker MT. In vitro expansion of adipose-derived adult stromal cells in hypoxia enhances early chondrogenesis. Tissue Eng. 2007;13:2981-93.

5. Hung CT, Mauck RL, Wang CC, Lima EG, Ateshian GA. A paradigm for functional tissue engineering of articular cartilage via applied physiologic deformational loading. Ann.Biomed.Eng. 2004;32:35-49.

6. Abousleiman RI and Sikavitsas VI. Bioreactors for tissues of the musculoskeletal system. Adv.Exp.Med.Biol. 2006;585:243-59.

7. Kuo CK, Li WJ, Mauck RL, Tuan RS. Cartilage tissue engineering: its potential and uses. Curr.Opin.Rheumatol. 2006;18:64-73.

8. Woodhouse CF. An Instrument for the Measurement of Oxygen Tension in Bone - a Preliminary Report. 1961;43:819-28.

APPENDICES

APPENDIX A: POLY(ε-CAPROLACTONE) MELT CASTING PROTOCOL

Name of Procedure: Melt-Casting PCL scaffolds
Prepared by: Jessica Kemppainen
Location: This procedure is performed in LBME 2420
Hazards: none
Engineering Controls: none
Protective equipment: Use latex gloves when working with Ethanol, or to keep your hands protected from hot PCL.
Waste disposal: regular trash

Melt-Cast PCL Scaffold Fabrication

1. Assemble Teflon Mold
   You will periodically need to replace the Teflon tape on the screws. This assures that air won't be pulled into the PCL during high vacuum.

2. Place 6 pellets of PCL (CAPA6400) into each Teflon mold hole.
3. Coat outer cracks of mold with vacuum grease. Again, this assures that air won't be pulled into the polymer.
4. Place mold + PCL into the oven at 115°C. Close door, close vent and gas knobs, completely open vacuum knob.
5. Turn on vacuum pump. Assure that swagelock arrow is pointed toward the tube leading to the oven.
6. Leave in for 2 hours.
7. After 2 hours, close the vacuum knob, and turn off the vacuum pump. Open the vent knob, and slowly release the vacuum from the oven.
8. Remove mold+PCL from oven and let sit on cool countertop for 4m30s
9. Carefully press green wax mold into PCL.
10. Let sit overnight to cool and cure. (storage: on counter in Teflon mold)

Scaffold Processing

1. Disassemble Teflon mold
2. Press green wax+PCL out using alan wrench.
3. Trim excess PCL from the top and bottom of the green wax mold, using a razor blade.
4. Place green wax+PCL into a 50ml conical tube with ~40ml 100% EtOH.
5. Place on vortex for ~2hours (until all or most of the green wax is dissolved)
6. Drain green EtOH into waste bottle, and dump scaffolds onto a paper towel.
7. While the scaffolds are still damp, carefully remove the outer layer of excess PCL with your hands.
8. Place the scaffolds back on the vortex in 100% EtOH to remove anymore green wax (should take ~30min-1 hour depending on how much wax remains)
9. Remove scaffolds from EtOH, and place on paper towel (label the paper towel with the design name)
10. After scaffolds completely dry, use a fresh razor blade to trim them to a height of 3 unit cells (storage after step 10: in appropriately labeled weight dish on counter)

The following also serve as my "quality control" elimination steps.

11. Clean pores of scaffolds with cleaning wire.
12. Place scaffolds in 100% EtOH on spinner overnight.
13. Place scaffolds into plastic storage container

APPENDIX B: PERMEABILITY CHAMBER PROTOCOL

Name of Procedure: Permeability Chamber Measurements
Prepared by: Jessica Kemppainen
Location: This procedure is performed in LBME 2411C using the permeability chamber beside the sink
Hazards: none
Engineering Controls: none
Protective equipment: none
Waste disposal: regular trash

Please read protocol entirely and then see Jessica before using this for the first time.

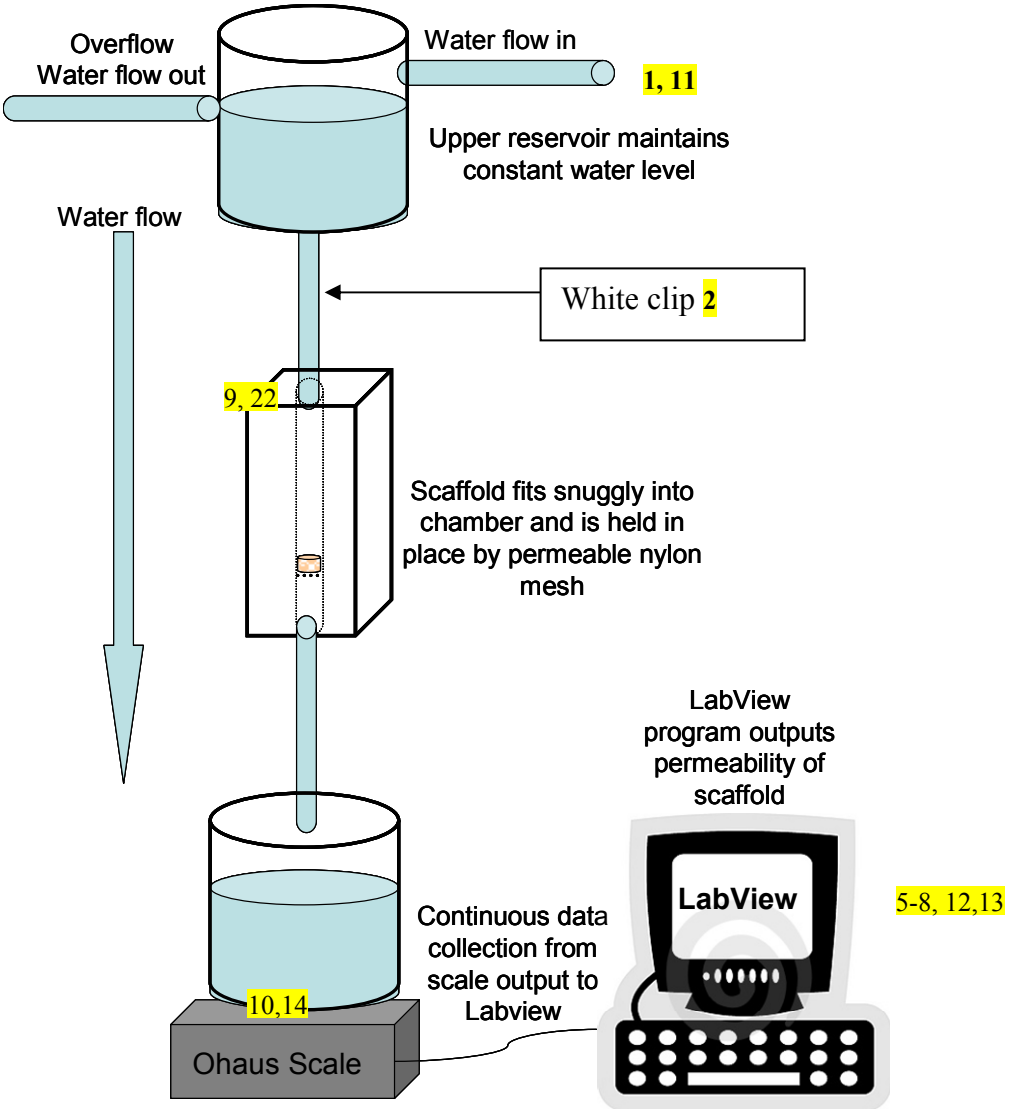

4

One hour prior to testing

1. Hook up "water flow in" hose to the sink faucet.
2. Make sure that white clip on hose is CLOSED.
3. Turn on cold water so that flow meets sharpie dot on reservoir (see Jessica).

Testing-Setup & Calibrated Mass Flow

4. Turn on scale.
5. On SEG-IMAGING, open Labview, File=permeability_meters.
6. Change OPERATION to "replace or create"
7. In FILE PATH click on the folder and create a new folder for your experiments
8. In FILE PATH, change the file name (now being saved in your folder) to MASSFLOW1
9. Hook up permeability chamber to reservoir-use needle nose pliers to tighten.
10. Set 500 ml plastic bottle on scale with tube from chamber centered into bottle.
11. Unclip white clip so that water begins flowing through the chamber.
12. Immediately after water begins flowing into bottle, click on the → in lab view (top left corner) to RUN.

Note:on the first flow, you will want to pinch out any air bubbles you see in the tubes before taking a measurement)

13. Watch weight on scale or in labview-once it reaches 350g-immediately hit the **red octagon stop** (NOT THE "STOP" button), then immediately reclip the white clip.**Do not let the scale see a load of more than 400g**.
14. Empty the plastic bottle into the sink.
15. Repeat starting at step 8, renaming now as MASSFLOW2
16. Repeat mass flow 5 times.
17. Average your results in excel, column 3: average the entire column, then average the averages of all five runs.
18. Type your average mass flow into the "Cal Mass Flow" box in labview.

Testing your samples

19. Measure height of sample: input into "sample length" box in labview
20. For Jessica's chamber, input .000032 into the "x-sec area" box. This is the cross sectional area of the chamber, which should also be the cross sectional area of your scaffold.
21. Rename file in "File Path" as specimen name
22. Unscrew chamber from reservoir using needle nosed pliers
23. Place sample into top of chamber carefully. There is a nylon filter (see diagram) that is glued to the edges, and WILL come out if you press too hard. I usually get the specimen situated and level within the tunnel and then tap it in using the chopsticks sitting beside the apparatus.
24. Tighten the chamber back onto the hose using needle nosed pliers
25. Place plastic bottle back on scale underneath hose.
26. Unclip the white clip
27. Just after water begins flowing into bottle, click on the → in lab view (top left corner) to RUN.
28. Watch weight on scale or in labview-once it reaches 350g-immediately hit the **red octagon stop** (NOT THE "STOP" button), then immediately reclip the white clip.**Do not let the scale see a load of more than 400g**.
29. Empty the plastic bottle into the sink.
30. Remove your specimen from the chamber by unscrewing the chamber from the hose, placing chamber upside down on paper towel, and then blowing a short/light blast of air (using the DUSTOFF canister) into the tubing. This should blow your scaffold out. **Do not stick anything into the chamber to get your scaffold out, as you will puncture the filter.**
31. Repeat for rest of specimens: start at step 19.

Afterwards

Drain water from upper reservoir and disconnect tubing from faucet.

APPENDIX C: PROTOCOL FOR CONFINED COMPRESSION (STRESS-RELAXATION)

Name of Procedure: Stress-relaxation confined compression testing
Prepared by: Jessica Kemppainen
Location: This procedure is performed in LBME 2420
Hazards: Load cells used in this procedure are extremely fragile. Do NOT overload them.
Engineering Controls: none
Protective equipment: safety glasses, close-toed shoes
Waste disposal: none

**** Do not bump or lean on the table that the MTS sits on during testing****

30 minutes prior to testing

1. Unscrew the red safety button on the MTS machine.
2. Turn on the MTS machine with the keypad by pressing the '| ' button. The program will not work correctly unless the machine is turned on **before** TestWorks4 is opened.
3. Open TestWorks4.
4. Enter the appropriate user login name.
5. Make sure the appropriate load cell is attached – we have 4 load cells (10N, 50N, 30kN and 500N). This will depend on the material that your scaffold is made from. (Note:I have used the 500N load cell for PCL and the 50N load cell for PGS with the acrylic chamber. If you think your sample will exert high enough loads to switch to the 30kN load cell, you may want to consider machining a stainless steel chamber.)
6. Setup the device: attach the porous indenter to the top load cell, and attach the fixed lower platen. Calibrate and Print General History:
    a. Select Tools → Calibrate and click the Calibrate button to calibrate the machine. Note: If a device error occurs, shut down the MTS machine and the computer. Turn the MTS machine on, and then turn the computer on and open TestWorks4. This should resolve the error.
    b. Select Tools → Calibrate → History → Print General History for the 500N load cell. Paste the General History in the MTS logbook.
7. Soak porous part of porous indenter in media for 30 minutes prior to testing by filling the chamber with media (or the solution you will use during tests) and lowering the indenter into the chamber.
8. (For thermal-controlled environment) Plug the thermal-controlling HyWatt (surrounding the exterior of the acrylic chamber) into the thermo-controller, and set it to 42°C. This will maintain the liquid you put within the chamber at 37°C.

Testing

9. Select Method → Open Method → "creep, relaxation and one cycle hysterisis package"→"compression"→"relaxation"→"JMK MTS Relax Compress 2 (1 ramp)"
10. Change the platen separation value in test inputs to 25 mm (or to the height of your chamber if you have designed your own)
11. Change test Procedue to 1. Set Platen Separation
12. Hit the large green arrow (RUN)
13. Enter Sample ID: date_intials_title of project (A "Sample" = all specimens tested this day), OK
14. Enter Specimen ID: name of specimen to test (A "specimen" = one scaffold), OK
15. Follow on screen instructions on how to align confined chamber with indenter
16. **Hit OK: at this point the indenter will lower** and find the bottom of the chamber and then raise 25mm up. Watch for double green arrows in lower right corner to change to a red square to signify the end of "platen separation".
17. You can now move the confined chamber to place your specimen gently into the bottom. Remember that in stress relaxation, load history is important, so avoid unnecessary loads on your specimen. Consider using the plunger of an insulin syringe.

18. Change the preload value. I suggest using .25 for materials such as PCL or .02 for materials such as POC or PGS. Essentially, you want the preload to just find the top of your specimen without placing any extra load onto it.
19. Change test procedure to 0: Test
20. *Hit the large green arrow to run the test
21. Follow onscreen instructions: again, these instructions inform you how to align the porous indenter with the confined compression chamber. OK.
22. "TEST IS ABOUT TO BEGIN"-hit OK on this screen to begin test. Note: test will take about 1 h.

After Test Completes

23. Hit OK on screen that appears. This will raise the crosshead.
24. File→save sample-When naming the data, use the following format 'date_user initials_sample description'. For example, 05102005_CLF_4wkPCLsubq. This saves the batch of specimens as a .msm file, which can only be read by Testworks. Save your data after each specimen. It is very important to do this after EVERY specimen tested. If you don't do this, and the computer crashes or the power goes out, you will lose all of your data.
25. To start next specimen go back up to *. You do not need to do a platen separation for each specimen. You must do it for each new day of testing.

At the end of the day

26. Export each Specimen Data: On Review tab, select specimen 1 by highlighting it in the upper left hand box. Select File → Export → Specimen. This file contains the raw data for each specimen-should be exported as a .txt file. It will be named as the "sample name" so you must go in and change this name before exporting the next specimen, or it will be written over. Go to jessmw folder, Export, sort by date and it will appear at the top. Add the specimen ID to the end of the file name. Repeat for each specimen.
27. Export Sample Data: Select File → Export → Sample. This file contains height data for all specimens tested under one sample name (one day), should be exported as a .txt file. You only need to do this once.
28. Raise crosshead on MTS
29. Clean out porous indenter with RO H2O followed by blowing air through it to completely dry out the indenter. Unscrew indenter from crosshead and wrap in kimwipe to store in the sample box it belongs in.
30. Close out of testworks
31. Power down the MTS, and engage the red safety button.

Data Analysis

32. Open .txt files in Excel. Select 'delimited', select 'comma' separation, and hit okay. DO NOT USE THE STRESS COLUMN. Calculate the stress yourself.

APPENDIX D: PROTOCOL FOR MEASURING DNA CONTENT

Name of Procedure: Hoechst 33258 protocol for measuring DNA content
Prepared by: Jessica Kemppainen
Location: This procedure is performed in LBME 2420
Hazards: Hoechst 33258 is toxic. Please read MSDS carefully before use.
Engineering Controls: none
Protective equipment: safety glasses, gloves
Waste disposal: Hoechst waste bottle

1. Make 1X TNE working solution
   5 mls 10X TNE + 45 mls dH_2O

2. Dilute Hoechst
   a. 495 ul 1X TNE + 5 ul 10mg/ml stock in 1.5 ml tube (= 0.1mg/ml)
   b. 4.99 mls 1X TNE + 10 ul a in 15 ml tube wrapped in aluminum foil (= 2X solution, 100 ng/ml, make fresh)

3. Make standards
   Calf thymus DNA (CT DNA) = 250 ul 1X TNE to vial shipped (as stated in directions from company, Sigma, #D0805) = 1 mg/ml solution (can store at 4°C for 3 months)

   Dilute 1mg/ml CT DNA to 100 µg/ml stock:
   100 ul CT DNA from 3 + 900 ul 1X TNE, filter

   Standards: For 10 – 500 ng/ml
   Start with 10 ul of CT DNA (100 µg/ml) in 990 ul 1X TNE (= 100 ng in 100 ul)
   Dilute 2X in 1X TNE 6 times, getting standards down to 1.562 ng (in 100 ul)

4. Measuring DNA content of samples and standards
   Add 100 ul/standard and 100 ul/sample to wells in a 96 well plate (duplicates or triplicates suggested)

   Add 100 ul diluted Hoechst (from 3)

   Incubate at room temperature for 5 minutes

   Read: excitation: 355nm, emission: 460nm (Fluoroskan Ascent FL, Thermo, Waltham, MA)

APPENDIX E: PROTOCOL FOR MEASURING S-GAG CONTENT

Name of Procedure: Dimethylmethylene Blue (DMMB) Assay for measuring s-GAG content
Prepared by: Jessica Kemppainen (modified from Elly Liao)
Location: This procedure is performed in LBME 2420
Hazards: none.
Engineering Controls: none
Protective equipment: gloves
Waste disposal: DMMB waste bottle

---

1. Mix DMMB reagent:
   16 mg 1,9 dimethyl-methylene blue dye (Sigma, # 341088)
   3.04 g Glycine
   2.37 g NaCl
   95 ml 0.1M HCl
   In 1 liter of diH_2O
   Bring to pH of 3.0

2. Make standards from shark chondroitan-6-sulfate (Sigma, # C4384)
   Starting with a stock concentration of 1 µg/ul
   Add 100 ul stock + 900 ul Millipore H_2) (= .1 µg/ul)
   Dilute 2X 6 times down to .0015 µg/ul

3. Measuring sGAG content of samples and standards
   Add 20 ul of standards or sample (well-mixed, centrifuged at 14,000, 10 min, 4°C if you need to remove polymer residue)

   Turn off most of the lights in your working environment, as DMMB is extremely light sensitive.

   Add 200ul DMMB to each well using multi-channel pipettor.

   Read immediately on a plate reader (MultiSkan Spectrum, Thermo, Waltham, MA) at 525 nm.
